NAVAL POSTGRADUATE SCHOOL
Monterey, California

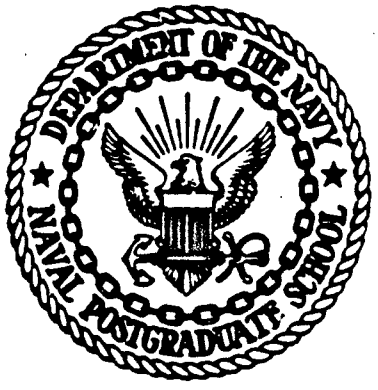

THESIS

SUB-BOTTOM HIGH RESOLUTION SONAR
UTILIZING NON-LINEAR ACOUSTIC PULSE
SELF-DEMODULATION

by

Roy Lance Eyman
Peter John LeStrange
Axel Harry Seemann

December 1982

Thesis Advisor: G. L. Sackman

Approved for public release,
distribution unlimited

Unclassified

SECURITY CLASSIFICATION OF THIS PAGE (When Data Entered)

REPORT DOCUMENTATION PAGE	READ INSTRUCTIONS BEFORE COMPLETING FORM
1. REPORT NUMBER	2. GOVT ACCESSION NO. AD-A127551	3. RECIPIENT'S CATALOG NUMBER
4. TITLE (and Subtitle) Sub-Bottom High Resolution Sonar Utilizing Non-Linear Acoustic Pulse Self-Demodulation	5. TYPE OF REPORT & PERIOD COVERED Master's Thesis December 1982
	6. PERFORMING ORG. REPORT NUMBER
7. AUTHOR(s) Roy Lance Eyman Peter John LeStrange Axel Harry Seemann	8. CONTRACT OR GRANT NUMBER(s)
9. PERFORMING ORGANIZATION NAME AND ADDRESS Naval Postgraduate School Monterey, California 93940	10. PROGRAM ELEMENT, PROJECT, TASK AREA & WORK UNIT NUMBERS
11. CONTROLLING OFFICE NAME AND ADDRESS Naval Postgraduate School Monterey, California 93940	12. REPORT DATE December 1982 13. NUMBER OF PAGES 146
14. MONITORING AGENCY NAME & ADDRESS(if different from Controlling Office)	15. SECURITY CLASS. (of this report) Unclassified 15a. DECLASSIFICATION/DOWNGRADING SCHEDULE

16. DISTRIBUTION STATEMENT (of this Report)

Approved for Public Release, Distribution Unlimited.

17. DISTRIBUTION STATEMENT (of the abstract entered in Block 20, if different from Report)

18. SUPPLEMENTARY NOTES

19. KEY WORDS (Continue on reverse side if necessary and identify by block number)

Parametric end-fire array, sediment penetration, target localization, resolution and classification, line-in-cone, shock excitation, independent propagation

20. ABSTRACT (Continue on reverse side if necessary and identify by block number)

An experiment involving the design and construction of a prototype sub-bottom high resolution sonar system utilizing non-linear pulse self-demodulation and suitable for deep water use is described. It is possible to generate a low frequency wave using the self-demodulation of a short, high frequency, finite amplitude pulse produced by the non-linear properties of the medium. The generated low frequency wave will theoretically

DD FORM 1 JAN 73 1473 EDITION OF 1 NOV 65 IS OBSOLETE S/N 0102-014-6601

Unclassified

SECURITY CLASSIFICATION OF THIS PAGE (When Data Entered)

have the high directivity of the primary wave while simultaneously possessing the bottom penetrating characteristics of the lower frequency. Measurements demonstrate that the pulse self-demodulation occurs as theoretically predicted, and the results are successfully applied to the design of the sonar system. Shallow water tests demonstrating the potential effectiveness of the sonar system for detection and classification of target objects in bottom sediments are also described.

Approved for public release, distribution unlimited.

Sub-Bottom High Resolution Sonar Utilizing Non-Linear Acoustic Pulse Self Demodulation

by

Roy Lance Eyman
Lieutenant, United States Navy
B.S., University of New Mexico, 1975

Peter John LeStrange
Lieutenant, United States Navy
B.S., Purdue University, 1977

Submitted in partial fulfillment of the
requirements for the degree of

MASTER OF SCIENCE IN ENGINEERING ACOUSTICS

and by

Axel Harry Seemann
Kapitänleutnant, Federal German Navy
Graduate, Federal German Naval Academy, 1974

Submitted in partial fulfillment of the
requirements for the degree of

MASTER OF SCIENCE IN PHYSICS

from the

NAVAL POSTGRADUATE SCHOOL
December, 1982

Authors: P. J. LeStrange, A. H. Seemann, Roy L. Eyman

Approved by: Leo L. Beranek
Thesis Advisor

Glenn B. Gilpen
Co-advisor

James V. Sanders
Chairman, Engineering Acoustic Academic Committee

William M. Tolles
Dean of Science and Engineering

ABSTRACT

An experiment involving the design and construction of a prototype sub-bottom high resolution sonar system utilizing non-linear pulse self-demodulation and suitable for deep water use is described. It is possible to generate a low frequency wave using the self-demodulation of a short, high frequency, finite amplitude pulse produced by the non-linear properties of the medium. The generated low frequency wave will theoretically have the high directivity of the primary wave while simultaneously possessing the bottom penetrating characteristics of the lower frequency. Measurements demonstrate that the pulse self-demodulation occurs as theoretically predicted, and the results are successfully applied to the design of the sonar system. Shallow water tests demonstrating the potential effectiveness of the sonar system for detection and classification of target objects in bottom sediments are also described.

TABLE OF CONTENTS

LIST OF TABLES

LIST OF FIGURES

ACKNOWLEDGEMENT

As is true for almost any endeavor of this magnitude, many individuals play significant roles in its accomplishment which are not readily discernible by the reader. These individuals deserve some small measure of recognition for their efforts.

It is our great pleasure to acknowledge the immeasurable contributions made by our thesis advisors, Professors George Sackman and Al Coppens. Their overall knowledge of and enthusiasm for the project and their understanding of the frustration inherent in the completion of an experimental thesis continually inspired us to "keep at it" with the result that the end product is something we can all be proud of. Further, we would like to thank Tom Muir of ARL, Austin, Texas for the initial "seed" idea for this project.

We would also like to acknowledge the contributions of Professor Steve Garrett. His expert knowledge in non-linear acoustics and his skills in experimental technique and error analysis made him an ideal sounding board for many of our questions and ideas. Though not directly involved in this thesis, Steve could always be counted on to take time from his busy schedule to assist us and teach us a little while he was at it. Much of our experimental success is probably directly attributable to Steve's assistance and knowledge

of current test equipment. We would also like to thank Professors Gary Ewing, Larry Ziomek and George Morris. Gary taught us all we ever wanted to know (and more) about pulse transformers. Gary also provided the transformer cores used in our experiments. Larry provided detailed instruction in general array theory. George "Coach" Morris provided assistance in developing computer algorithms for the simulation sections.

Thanks also to Bob Smith of the Electrical Engineering Technical Laboratory and Bob Moeller and Tom Maris of the Physics Department Machine Shop. Bob Smith spent many hours assembling and making several modifications to the transducer pulse circuit. Bob Moeller and Tom Maris also spent much time machining and assembling components for the four prototype transducers and the hardware used in the Liberty Bay tests.

Special thanks go out to Bill Anderson and Dick Evans of the Applied Research Division and Mel Case of the Acoustic Test Facility at Keyport, Washington. Bill possessed enough faith in the feasibility of the project and in us to secure the funding. Dick saw to the elimination of all logistics problems involved in the Liberty Bay tests including procurement of the MK. 46 dummy torpedo and the target sphere. Mel provided local expertise on the care and feeding of experiments conducted at the ATF.

To our colleagues and friends we owe a debt of gratitude for their many discussions, suggestions and efforts on our behalf. We would therefore like to acknowledge the contributions of LCDR Leslie Skowronek, LT Don Conte, Ken Smith, Kerry Yarber, and Gene Walls.

Finally, we are especially grateful to Pat Fatchett for her patience and skill in the preparation of this thesis. We would also like to thank the other members of the Physics and Electrical Engineering Departments who have contributed their time and expertise: Bryan Wilson, Jim Sanders, Paul Moose and Orestes Baycura.

I. INTRODUCTION

A. SCATTERING OF SOUND BY SOUND IN CLASSICAL FLUIDS

The generation of a propagating sound wave through the non-linear interaction of two other sound waves in classical fluids has been the subject of many theoretical and experimental investigations over the past twenty years. The application of this non-linear acoustic process, commonly called the "scattering of sound by sound" [Refs. 1,2], to the production of long range highly directional sonar signal transmissions has engendered a great deal of interest.

The consideration of finite amplitude or non-linear effects in acoustics requires the abandonment of two of the most fundamental and useful principles of linear acoustics: linear superposition and wave form stability. The principle of linear superposition is obviously violated when the interaction of two waves produces a third independent wave. The distortion of a wave can also be understood as a consequence of the scattering of sound by sound if the distortion is considered as a self scattering process.

The general thrust of investigations concerning these effects in fluids has been along the direction set by Westervelt [Ref. 3]. His analysis of the transmission of a "difference frequency" signal considers it to be radiated from an array of sources, driven by the non-linear terms in

the hydrodynamic equations and the equation of state, distributed continuously throughout the volume of interaction of the two primary waves. This virtual source array is analogous to an end-fire array and for this reason is frequently called a parametric end-fire array.

Westervelt [Ref. 4] established theoretically that the difference frequency wave resulting from the interaction of two collimated, co-linear plane waves whose frequencies were nearly equal would be highly directional. A subsequent paper by Bellen, Westervelt and Beyer [Ref. 5] presented an experimental verification of this result. As previously stated, the possibility of exploiting this difference frequency radiation in sonar systems to achieve highly directional, low frequency beams from small apertures has stimulated considerable interest in the applications of non-linear acoustics [Ref. 6]. In particular, Muir [Ref. 7] has obtained considerable data on penetration of parametric beams in sediment.

B. SELF-DEMODULATION OF A PULSED ACOUSTIC CARRIER WAVE

One of the first difficulties encountered in attempts to utilize practically finite amplitude effects has its root in the characteristics of the fluid itself. A classical fluid can support only longitudinal sound modes and, in the absence of dispersion, the non-linear production of a propagating wave can only take place if the primary waves

are co-linear [Ref. 8]. Maintaining colinearity of sources in a practical sonar system is not an easy task.

In 1965, Berktay presented a paper describing a "pulse produced by the self-demodulation of a pulsed carrier" [Ref. 6]. It has been established that the radiation pressure of a pulsed carrier propagating in a homogeneous fluid follows the envelope of the carrier [Ref. 9]. Because of the non-linearity of the acoustic propagation, the primary wave will interact with itself. According to Berktay, the interaction will produce two components; a band-limited signal at twice the carrier frequency which will be relatively rapidly attenuated by the medium, and a lower frequency signal whose bandwidth is a direct function of the carrier envelope and is the component of interest. The medium essentially plays the role of an acoustic demodulator and low pass filter.

Besides the elimination of the difficulties associated with colinear beams, this approach has some other distinct advantages. The propagated energy is contained within a short pulse, thus facilitating signal processing. Further, the beam width is quite narrow and without sidelobes because of the end fire array effect. Since the carrier is relatively high with short pulse duration the transmitted power density can be quite high without causing cavitation.

Berktay's theory has been accurately confirmed by experiments conducted in carbon tetrachloride by Moffet, Westervelt and Beyer [Refs. 10,11].

C. A NAVAL APPLICATION OF THE PULSE SELF-DEMODULATION PHENOMENON

One of the potential applications for finite amplitude acoustics involves locating objects buried in ocean sediments. By using the self-demodulation effect, and an appropriate choice of carrier frequency, the carrier will be attenuated by the water-sediment interface while the much lower frequency envelope function produced by the non-linear interaction will penetrate the interface and be reflected by the buried object, which is assumed to have a density different from that of the surrounding sediment. This phenomenon, in conjunction with the narrow projector beamwidth derived from the carrier frequency and coupled with a suitable position-fixing system, would facilitate locating the object with a high degree of accuracy in three dimensions. Further, by suitable choice of pulse length, a significant degree of target discrimination can be achieved.

The potential naval applications for such a technique are numerous. It is the purpose of this thesis to examine the theory inherent in this technique and to present a design experiment involving one application of this technique.

II. NATURE OF THE PROBLEM

A. SYSTEM DESCRIPTION

A system has been designed using this phenomenon to assist in locating and recovering research and development torpedoes buried in the silty marine sediment of the Nanoose Torpedo Test Range in the Straits of Georgia Basin near Canada's southwest coast. Water depth in this region ranges between 300 and 500 meters. Sediment depths in the area range between 10 to 15 meters on the slopes of the basin and 260 meters on the basin floor. The sediment has a gradually varying density between 1250 kilograms per cubic meter to 1360 kilograms per cubic meter [Ref. 12].

The present intention is to mount the system on existing platforms which include: (a) a submersible vehicle that is towed along the basin floor at approximately 10 meters or less above the sediment and, (b) a tethered "free swimmer" type vehicle operating with approximately the same altitude above the sediment as the towed vehicle. In either case, vehicle position is monitored via a combination of a fathometer on the vehicle and a three dimensional acoustic tracking range permanently installed in the basin.

B. CONSTRAINTS AND REQUIREMENTS

To date, very little study of pulse self-demodulation effects in the ocean medium appears in the literature.

Previous experiments demonstrating the effect have been performed with primary frequencies in the megahertz range in mediums such as carbon tetrachloride, and in water tanks over short ranges. In order to utilize the pulse self-demodulation effect in an ocean/sediment environment, the existing theory and experimental results must be extended and modified by the system and environmental constraints inherent in this application. Therefore, these constraints will dictate system design requirements.

First, the pulse self-demodulation must be generated in the ocean medium. This requires a high source level without causing cavitation. A design goal of 230 dB re 1 micropascal was selected while pulse length was to be restricted to less than 200 microseconds for cavitation avoidance and range resolution. The projector size and weight were also to be limited such that the source could be installed in existing search vehicles. A primary frequency of 100 kHz was chosen to produce the desired narrow source beamwidth with suitable attenuation in the medium.

Since the search vehicle is only several meters from the sediment surface, electrical power to the projector must be transmitted down several hundred meters of cable. Because of the difficulties involved in transmitting a high power tone burst over a very long cable, the decision was made to shock excite the projector by charging a capacitor on the search vehicle to a high DC potential via the cable

and then triggering the projector by discharging the capacitor through a pulse transformer. In this manner, most of the heavy weight electronics can be retained on the support vessel. This method dictates that the projector transducer must also have a low Q so that the short pulse requirement is achieved.

The resultant acoustic pulse must be as pure a sinusoid as possible with an envelope which will produce a secondary pulse whose spectral energy is confined to frequencies between 3 kHz and 15 kHz to facilitate sediment penetration. Since the shock excited source "rings" at its natural frequency, pulse purity and envelope shape depend on the transient response of the transducer.

Another design consideration dictated by the proximity of the search vehicle to the bottom involves detection of the pulse self-demodulation at ranges much shorter than theoretically required for the medium to attenuate the primary frequency. Therefore, a low pass filter was designed for the "front end" of the receiver electronics with the intention that the filter would simulate the attenuation of several hundred meters of ocean/sediment. The attenuation exhibited by the sediment at this location is on the order of 10 dB/m at 100 kHz to 2 dB/m at 9 kHz [Refs. 13,14].

This application requires target discrimination for cylindrical objects approximately 30 cemtimeters or more in

diameter and 2.5 meters or more in length with good resolution of target depth and orientation in the sediment. Doppler is not expected to affect the design since the target is stationary, the search vessel is operated at low speeds (generally 5 knots or less), and the bandwidth is quite wide.

A pulse repetition rate of 25 Hz to 30 Hz was desired corresponding to the two-way time delay to a maximum range of about 50 meters. This rate was anticipated to be rapid enough for target detection and definition if the projector is mechanically scanned from side to side.

The final constraints on the system involved the transmitter and receiver electronics. First, the receiver must detect both the primary pulse reflection from the sediment surface and the secondary pulse reflection from the target/hard bottom. The secondary pulse amplitude is expected to be on the order of 50 dB to 60 dB below that of the primary pulse. Second, because of the high source levels involved, it was expected that the receiver hydrophone would be separated from the projector by some finite distance. Finally, and most significantly, the receiver electronics must respond to signals in a linear fashion to avoid electronic non-linear effects which might be confused with the desired acoustic non-linear effects.

III. EXPERIMENTAL PROCEDURE

A. TRANSDUCER DEVELOPMENT

Two approaches were chosen to obtain a projector that would meet the stated design requirements. The first approach involved the local design and construction of a low Q, high power projector. The second approach was to order a commercially built projector from International Transducer Corporation (ITC) of Goleta, California. This second approach was taken to ensure that the basic premise of investigating the self-demodulation effect in a practical system would not be jeopardized by the lack of a suitable source. Further, the locally designed and constructed projector would have a different source geometry than that of the ITC projector. This would permit comparison of the two source geometries.

1. Ceramic Selection and Element Configuration

The first stage in the local design and construction approach was to obtain suitable piezoelectric ceramic elements. Eighteen lead titanate zirconate ceramic disks produced by Channel Industries, Incorporated, of Santa Barbara, California were obtained from production over-run stock in order to secure fast delivery. This particular ceramic, "CHANNEL 5400," exhibited the properties desired

for a low Q, high power projector [Ref. 15]. Disks 3 inches in diameter, 0.25 inches thick and polarized in the thickness mode were used for individual elements. The elements were to operate in pairs, such that the positive polarity faces of the ceramics are together in physical and electrical contact, [Fig. 3-1(a)], and would radiate in the thickness mode from both faces to lower the Q. An advantage to this construction is that it approximates a rigidly backed piston for each element; i.e., a velocity node on the plane of contact of the elements. This method also reduces the size, weight and complexity of the projector by eliminating the air-backing and tail mass usually associated with high power projectors. A planar array of these element pairs would then be placed in a corner reflector to provide a transmit aperture radiating in one direction.

2. First Prototype

The first prototype projector consisted of a single pair of elements. This prototype was constructed primarily to examine what types of adhesives and electrical contacts could be utilized to facilitate construction and ensure structural robustness. The adhesive chosen was an industrial epoxy, PR-420, and the electrical contact was "EXMET", a fine mesh copper screen. This choice of adhesive and contact material worked well but the resonant frequency of the pair, approximately 66 kHz, was considerably lower than predicted by the given characteristics of the

ceramics [Ref. 15]. It is believed this was due to the added compliance of the epoxy between the elements.

3. Second Prototype

The second prototype also consisted of a single pair of elements. The adhesive used for this prototype was EASTMAN KODAK CYANOLATE ADHESIVE (super glue) and the electrical contact was "EXMET". A brass plate 0.125 inches thick was cemented to the radiating surfaces with a layer of "EXMET" between the plate and the radiating surface, [Fig. 3-1(b)], for electrical contact on the return or negative side. The pair was then embedded in a sandwich of 0.25 inch thick plexiglass (lucite) to provide a simple and rugged structure that would facilitate sealing and mounting in a corner reflector. Fig. 3-2 shows details of this prototype.

The characteristics of this second prototype that were of particular interest were the electrical capacitance exhibited by the parallel combination of the two ceramic disks and the beamwidth and sidelobe levels presented by the 90 degree corner reflector. These parameters were needed to predict the electromechanical behavior of the full scale prototype projector and to determine the best shape for the corner reflector. The capacitance, as measured using an HP-4261A LCR meter, was approximately 12 nanofarads for the pair in parallel. The admittance exhibited by this prototype in air and water is shown in

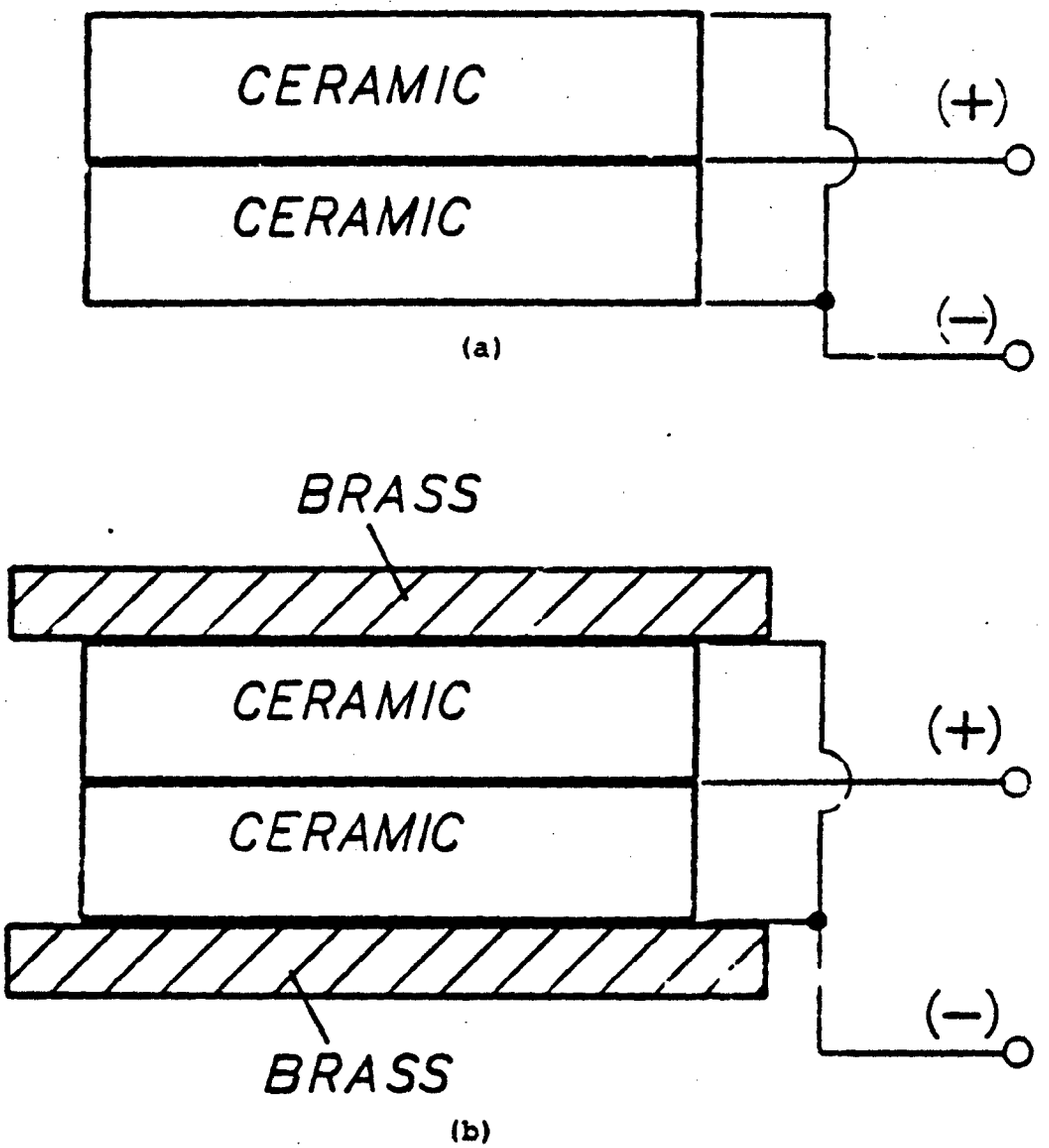

Fig. 3-1
Diagram of source element construction techniques for (a) first and (b) second prototype transducers.

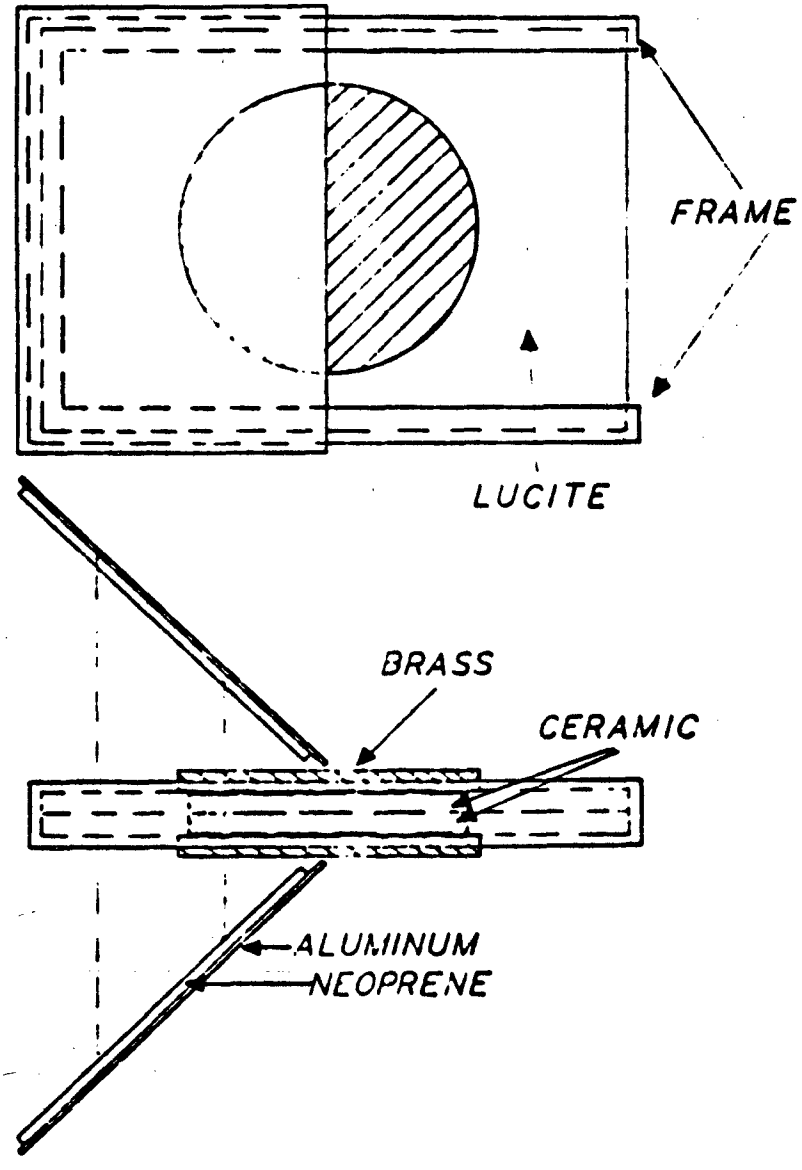

Fig. 3-2
Second prototype transducer construction diagram.

Fig. 3-3. The resonance at 75 kHz was a marked improvement over the first prototype. There was an additional resonance at approximately 33 kHz, not shown in Fig. 3-3, that corresponds to the radial mode of vibration.

Beam patterns for the second prototype were taken at 3 meters distance in an anechoic tank. The prototype was excited with a tone burst because the shock excitation transmit system had not been completed at this stage. The tone burst used was at 75 kHz and had a pulse duration of 100 microseconds. The corner reflector was a rectangular piece of 0.0625 inch thick aluminum covered with a layer of 0.375 inch thick cell-tite neoprene rubber (wetsuit material) to provide a pressure release surface. Fig. 3-2 shows details of the corner reflector. Figs. 3-4 and 3-5 show the beam patterns without and with the corner reflector, respectively. The pattern in Fig. 3-4 was taken by examining the transmission from only one side of the pair. It shows a pattern typical of that produced by a circular piston. Fig. 3-5 shows the pattern with the transducer mounted in the corner reflector. Significant narrowing of the on axis beam was observed, along with a strong increase in the sidelobe levels. This caused some consternation as the initial assumption was that the corner reflector would image both radiating surfaces as circular pistons. Upon further examination, the pattern in Fig. 3-5 was seen to be typical of that radiated from a rectangular piston with

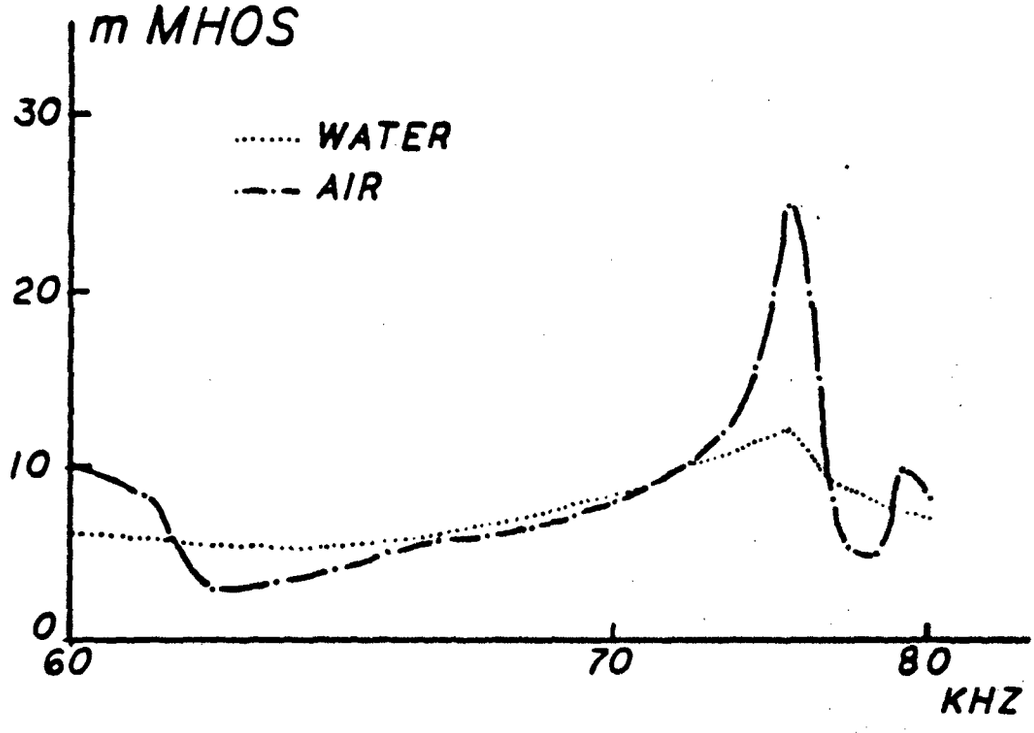

Fig. 3-3
Plot of admittance versus frequency for second prototype transducer.

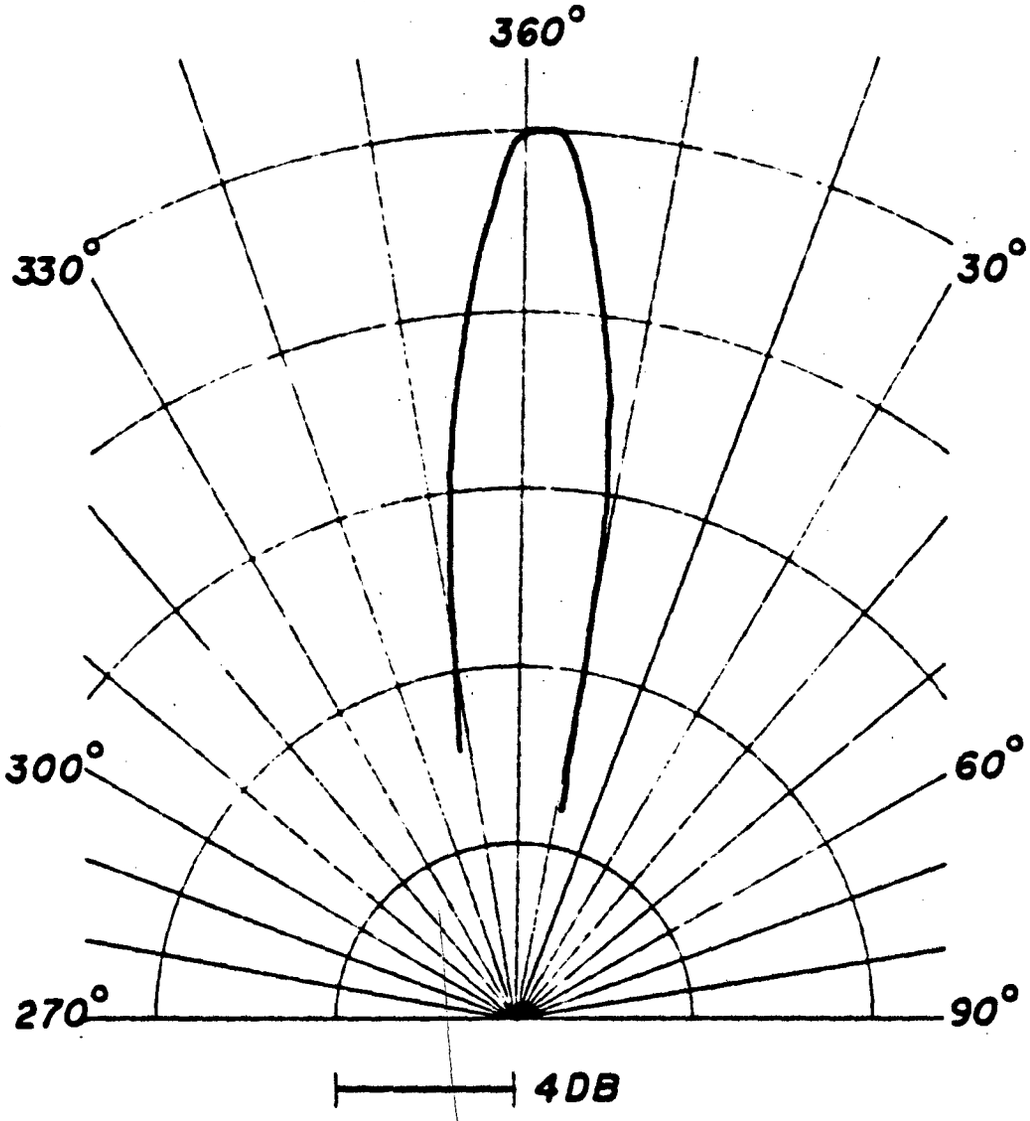

Fig. 3-4
Beam pattern of second prototype transducer at 79 kHz. (Mirrors removed)

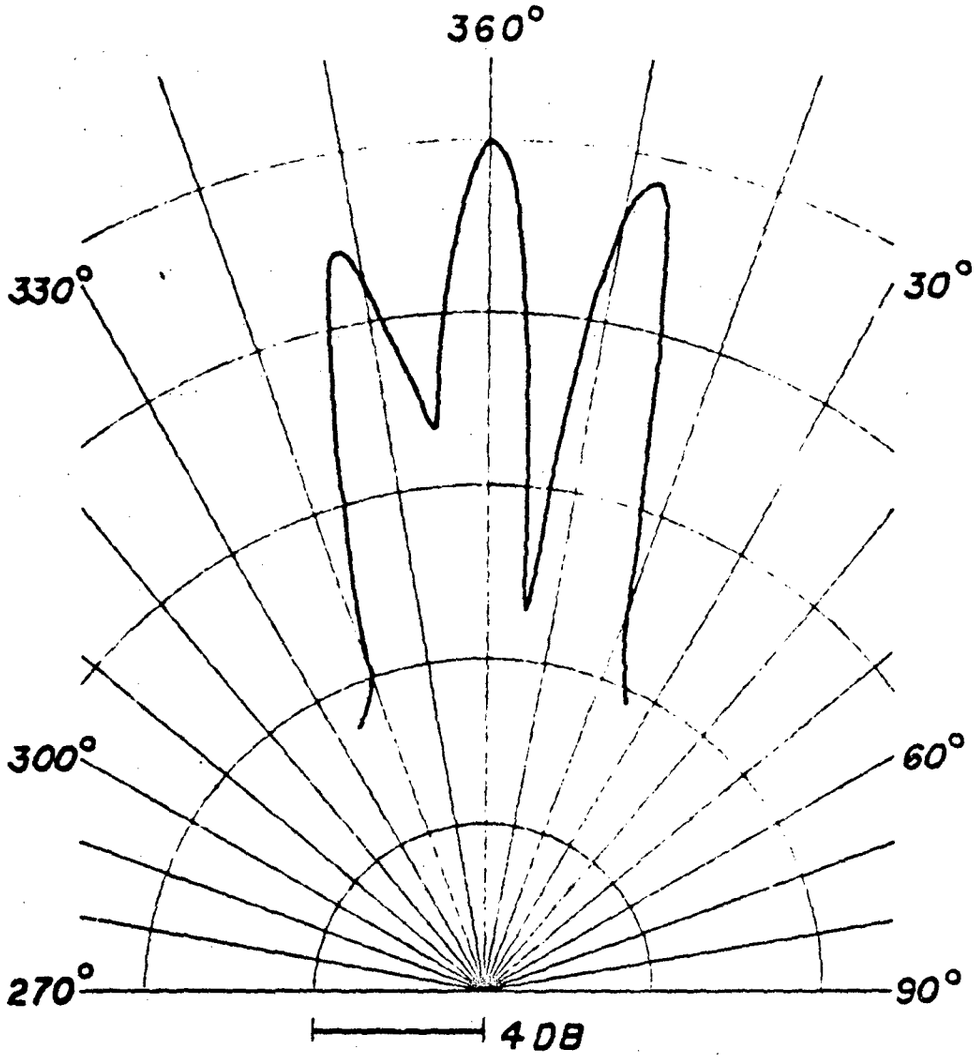

Fig. 3-5
Beam pattern of second prototype transducer at 79 kHz. (Mirrors attached)

uniform amplitude shading. The pattern appeared to be determined more by the shape of the mirror than the shape of the transducer elements.

The shock excitation transmit system was completed by this time and tested using this prototype. The response of the projector to shock excitation was encouraging as it produced a fairly clean pulse at approximately 79 kHz and 120 microseconds in length.

The examination of this second prototype provided some significant guidelines for consideration in designing the follow-on prototypes. First, the use of the CYANOLATE adhesive seemed to eliminate the added compliance seen in the first prototype and raised the resonant frequency toward the goal of 100 kHz. Second, the shape of the corner reflector would be crucial in forming an aperture that would approximate a circular piston.

4. Third Prototype

Utilizing the guidelines suggested by the examination of the second prototype, a third prototype was constructed. The design of this third prototype had three significant modifications from its predecessor; the brass loading plates were eliminated from the radiating surfaces, brass shim stock (0.001 inch) was substituted for the "EXMET" and the corner reflector was to be trimmed in such a manner as to present a nearly circular aperture. Unfortunately, this prototype suffered a catastrophic flooding

failure during admittance measurements and no reliable data were collected.

5. Fourth Prototype

Due to time constraints, the decision was made to press ahead with the full scale prototype and order a projector from ITC, concurrently.

The full scale prototype, constructed using the lessons learned from the second prototype, consisted of seven pairs of elements in a plexiglass sandwich. Details of the structure are shown in Figs. 3-6 through 3-10. The entire array was coated with several layers of liquid neoprene to ensure that a flooding casualty was not repeated. The corner reflector was cut to approximate a circular aperture when viewed from the direction of transmission. The initial material chosen was 0.375 inch mild steel. It was thought that a rigid reflection from a quarter wave thick surface would increase the power emitted from the aperture as compared to a pressure release reflection. However, shear waves were apparently generated in the steel and caused unacceptable pulse distortion. To remedy this situation, a composite of plexiglass and cell-tite neoprene was fixed to the steel reflecting surfaces to provide a pressure release reflection. The capacitance of this prototype, as measured using an HP-4261A LCR meter, is approximately 92 nanofarads, including 15 feet of coaxial cable. The electromechanical characteristics were

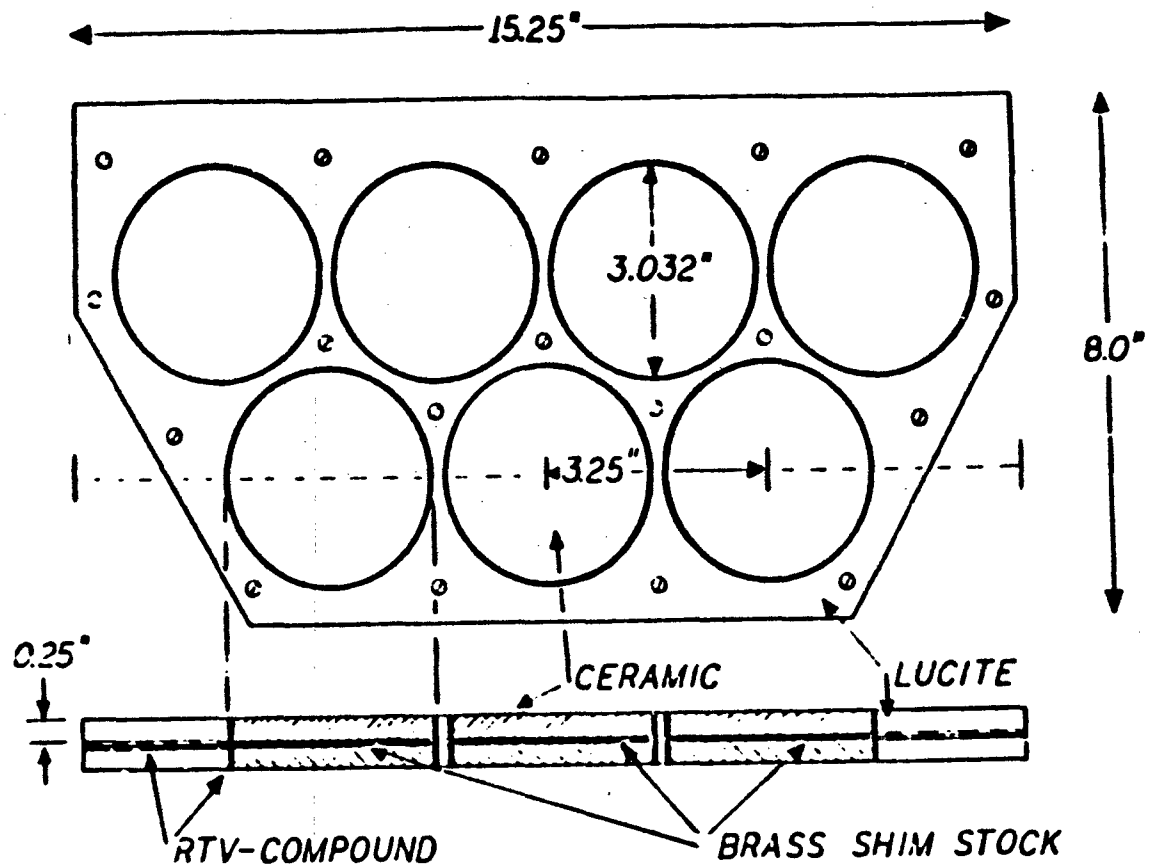

Fig. 3-6
Fourth prototype transducer array composition diagram.

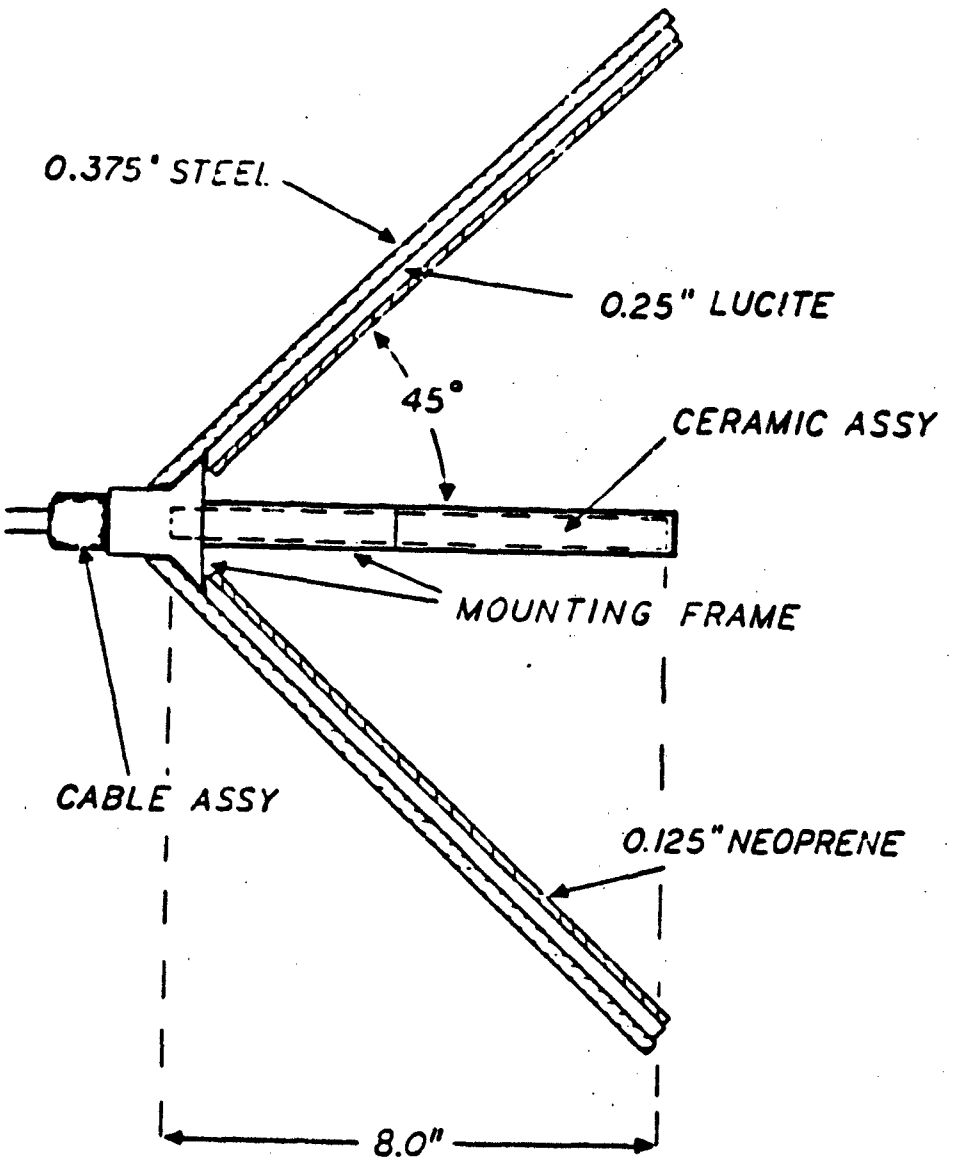

Fig. 3-7
Fourth prototype transducer construction diagram. (Top view)

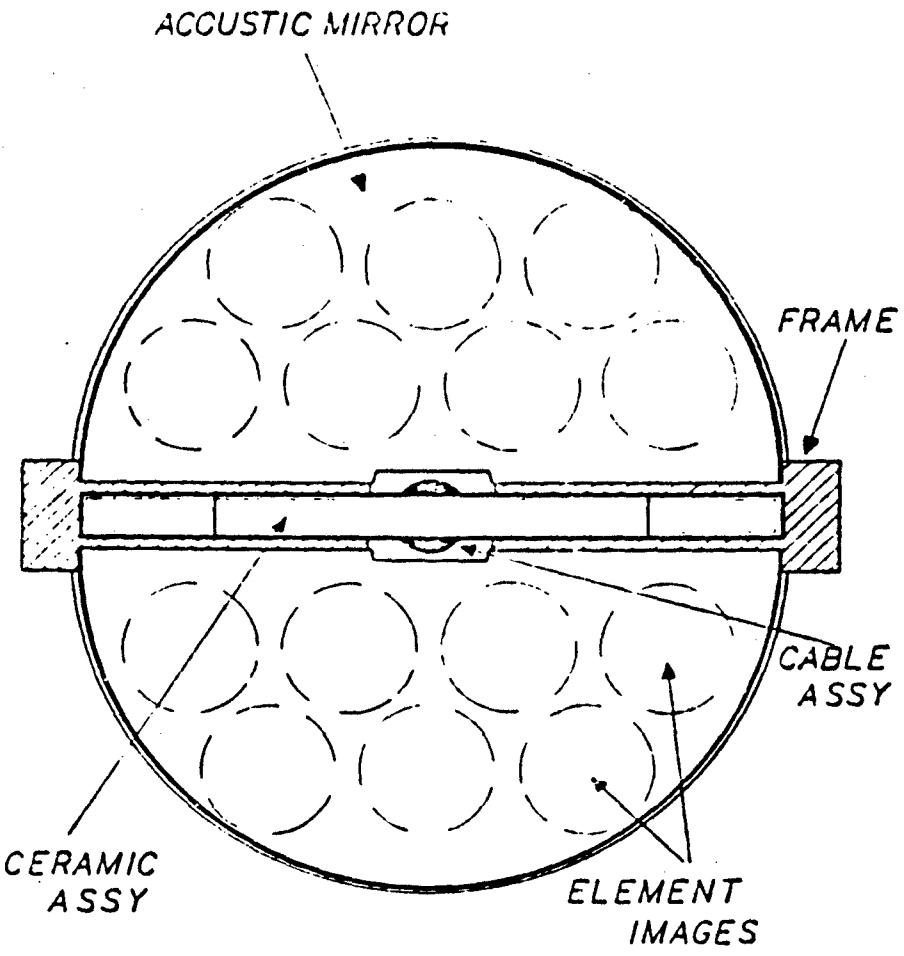

Fig. 3-8
Fourth prototype transducer construction diagram. (Front view)

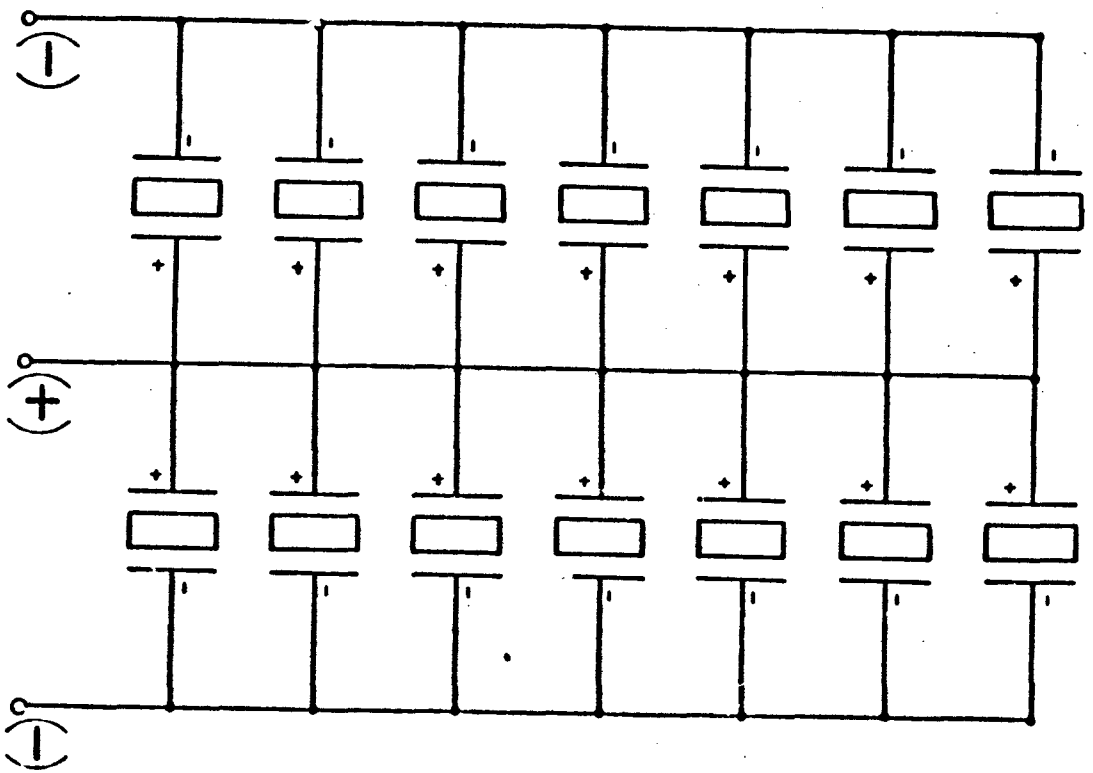

Fig. 3-9
Schematic diagram of electrical circuit in fourth prototype transducer.

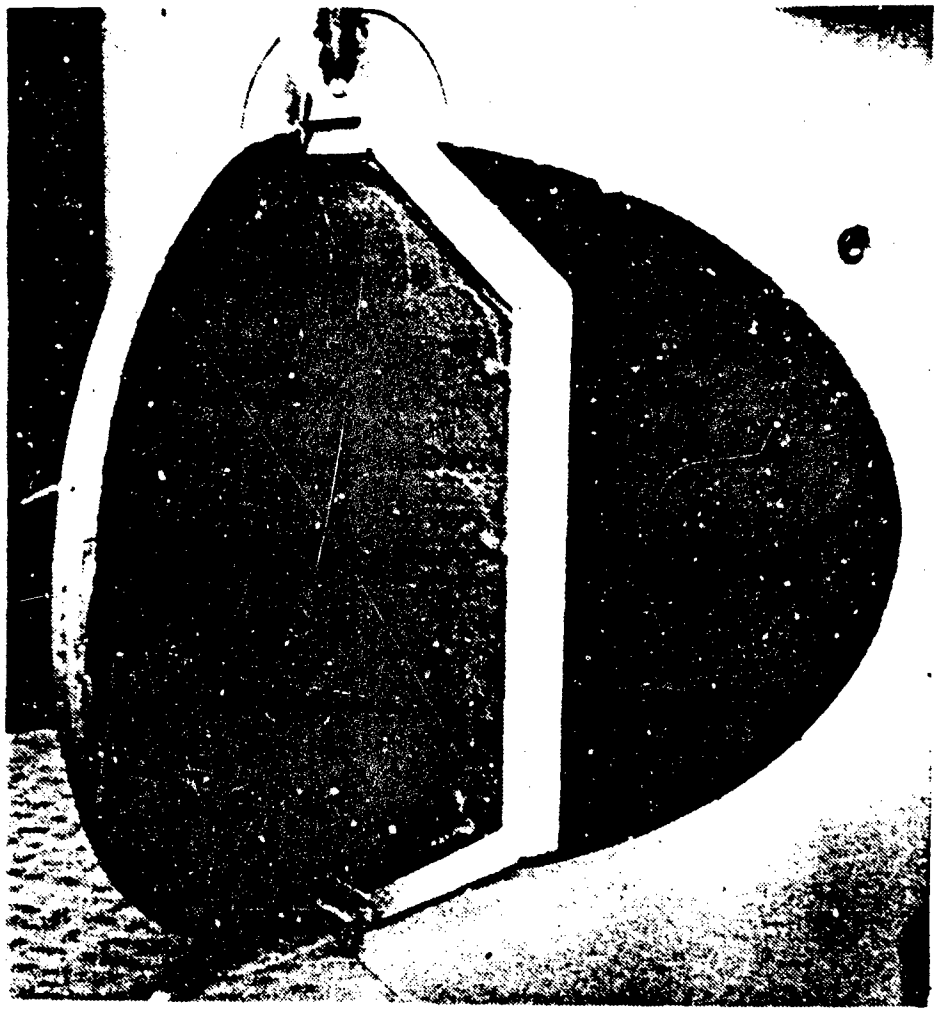

Fig. 3-10
Experimental corner reflector type projector constructed for thesis research. Consists of seven pairs of 3" ceramic elements in a planar array.

measured using a system developed by LCDR L.J. Skowronek, USN [Ref. 16] and are detailed in Figs. 3-11 through 3-13.

The prototype was suspended in an anechoic tank and preliminary data were taken to check out the overall system performance and response to shock excitation. The shock excited pulse, as seen at 3 meters from the source with an 800 VDC drive, was on the order of 210 dB re 1 micropascal but was decidedly not monochromatic. Fig. 3-14 shows this pulse as seen on the pulse transformer secondary. The pulse is approximately 100 microseconds in length but contains frequency components of approximately 200 kHz, 88 kHz and 33 kHz. A spectrum analysis of this pulse (as observed in water) using a Schlumberger analyzer with a translator is shown in Fig. 3-15. The wide spectrum produced by the lower primary frequencies of this pulse nearly overlaps the frequency range of the desired secondary spectrum, predicted to be approximately 5 kHz to 10 kHz based on overall pulse length. This was due to the apparent pulse length of the 200 kHz high power component, approximately 30 microseconds, generating a broad secondary spectrum centered around 30 kHz and enhanced by the 33 kHz component of the primary. In addition, the shape of the secondary pulse was not predictable enough to allow for signal processing. The rapid "turn-on, turn-off" of the three primary components produced a relatively broad spectrum of secondaries that was not widely separated from the primaries [Ref. 6]. It

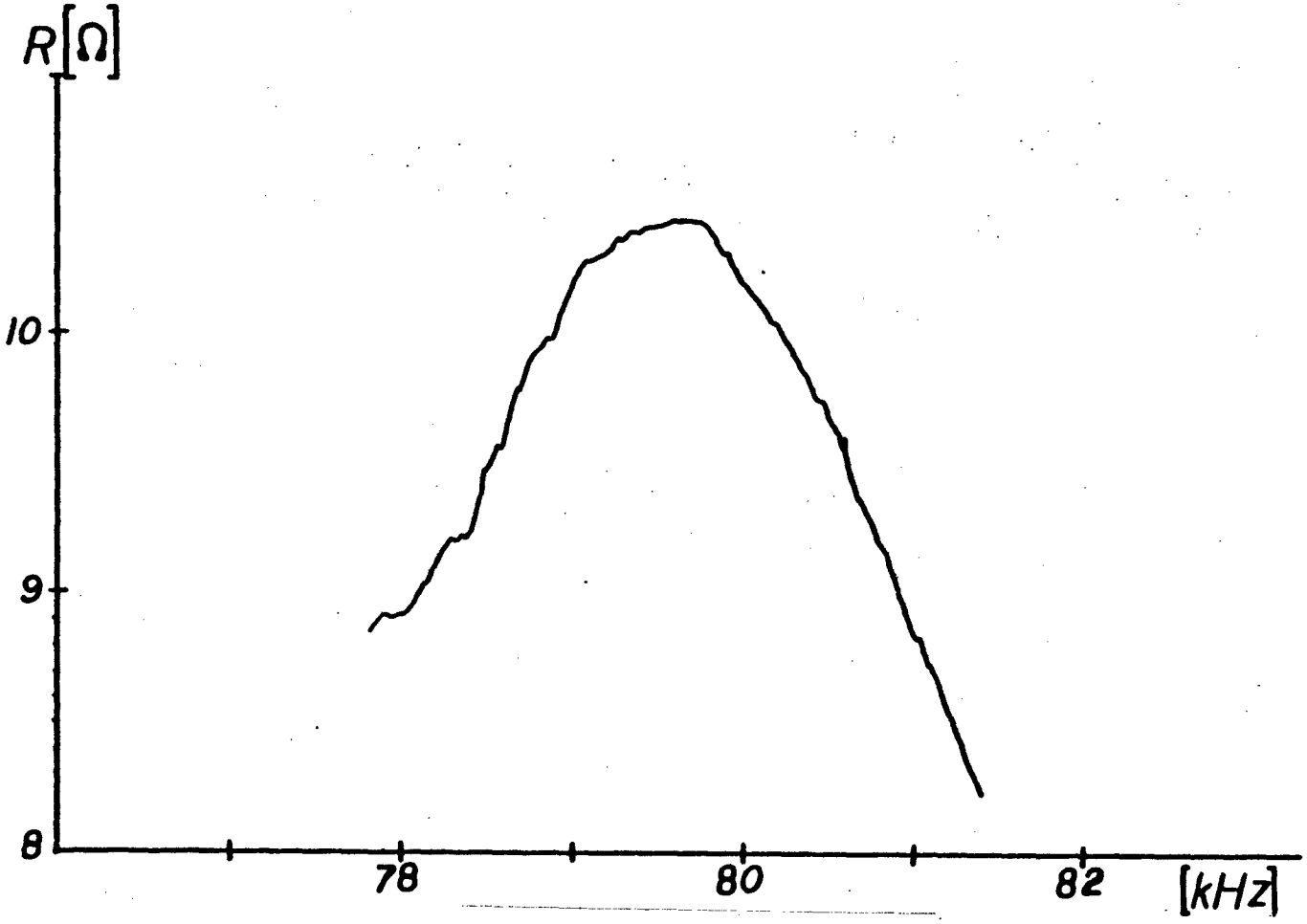

Fig. 3-11
Resistance as function of frequency for fourth prototype transducer.

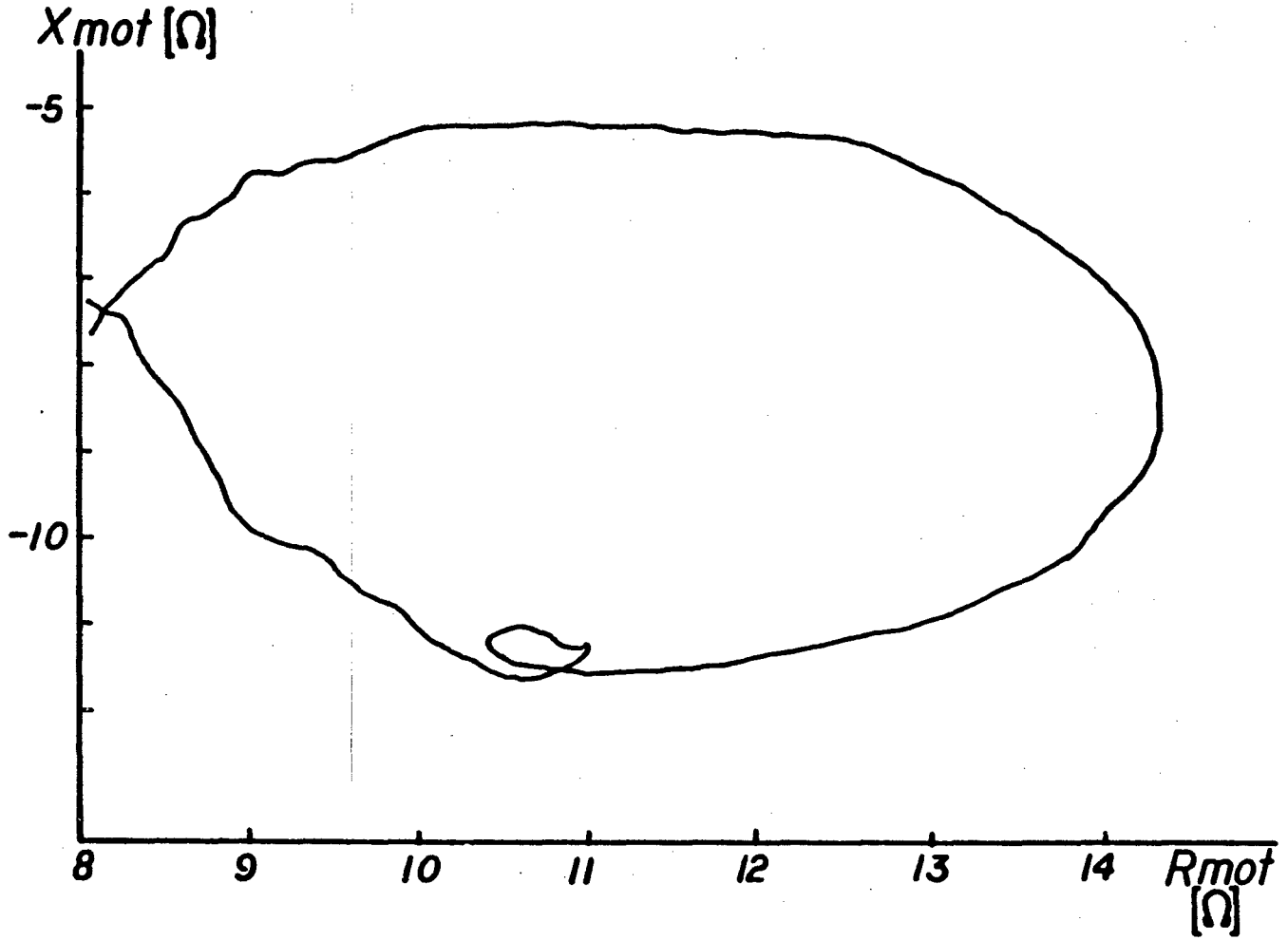

Fig. 3-12
Motional impedance circle for air-loaded fourth prototype transducer.

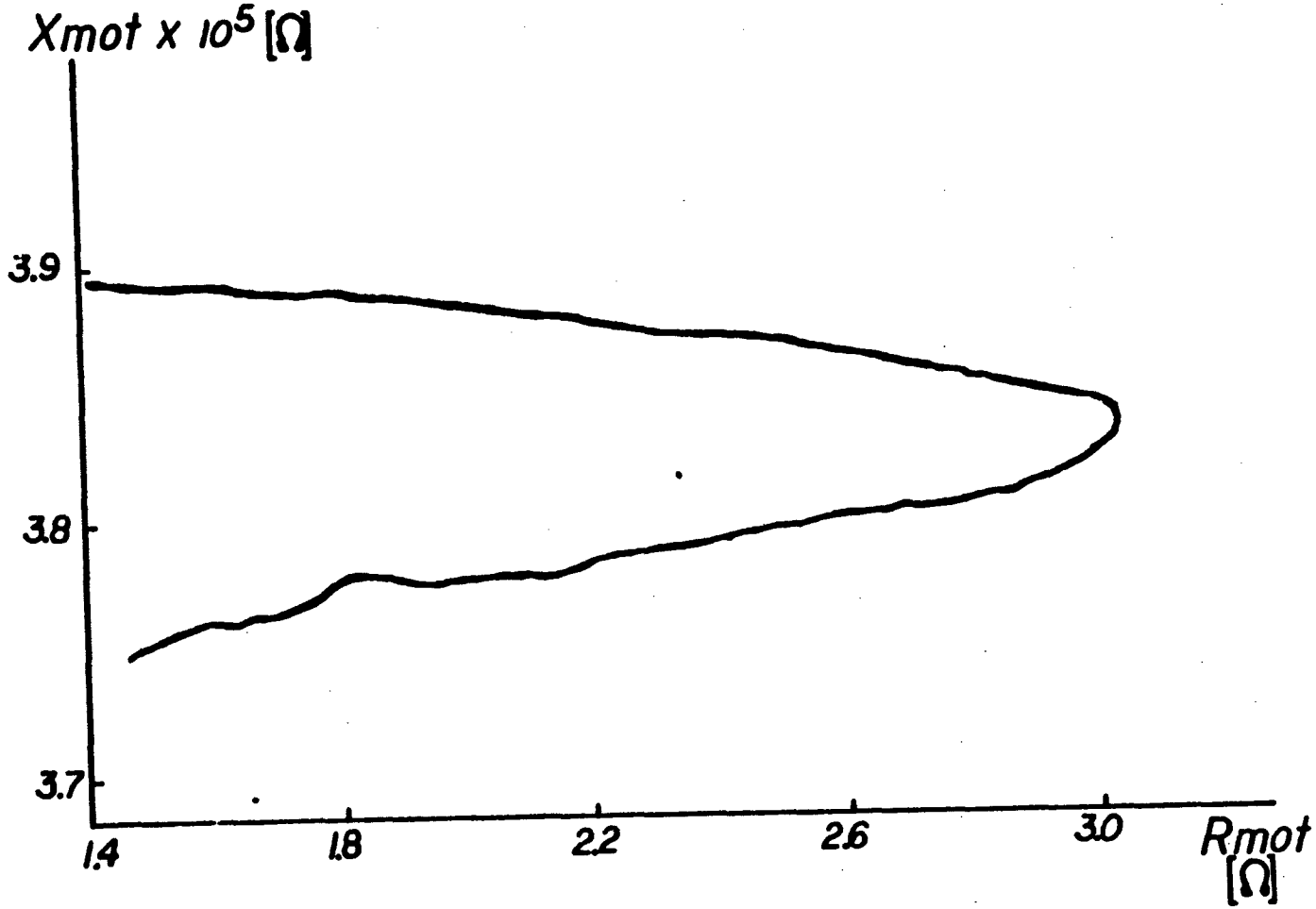

Fig. 3-13
Motional impedance circle for water-loaded fourth prototype transducer.

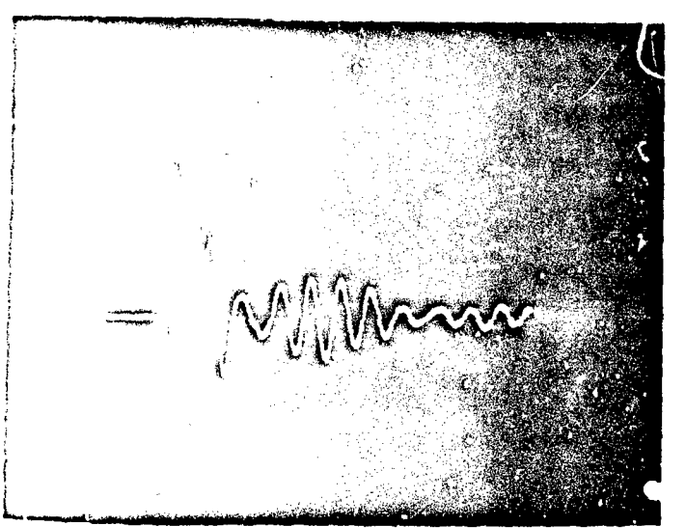

Fig. 3-14
Mode conversion in fourth prototype transducer as viewed on pulse transformer secondary.
Vertical; 200 volts/cm. Horizontal; 0.02 ms/cm.

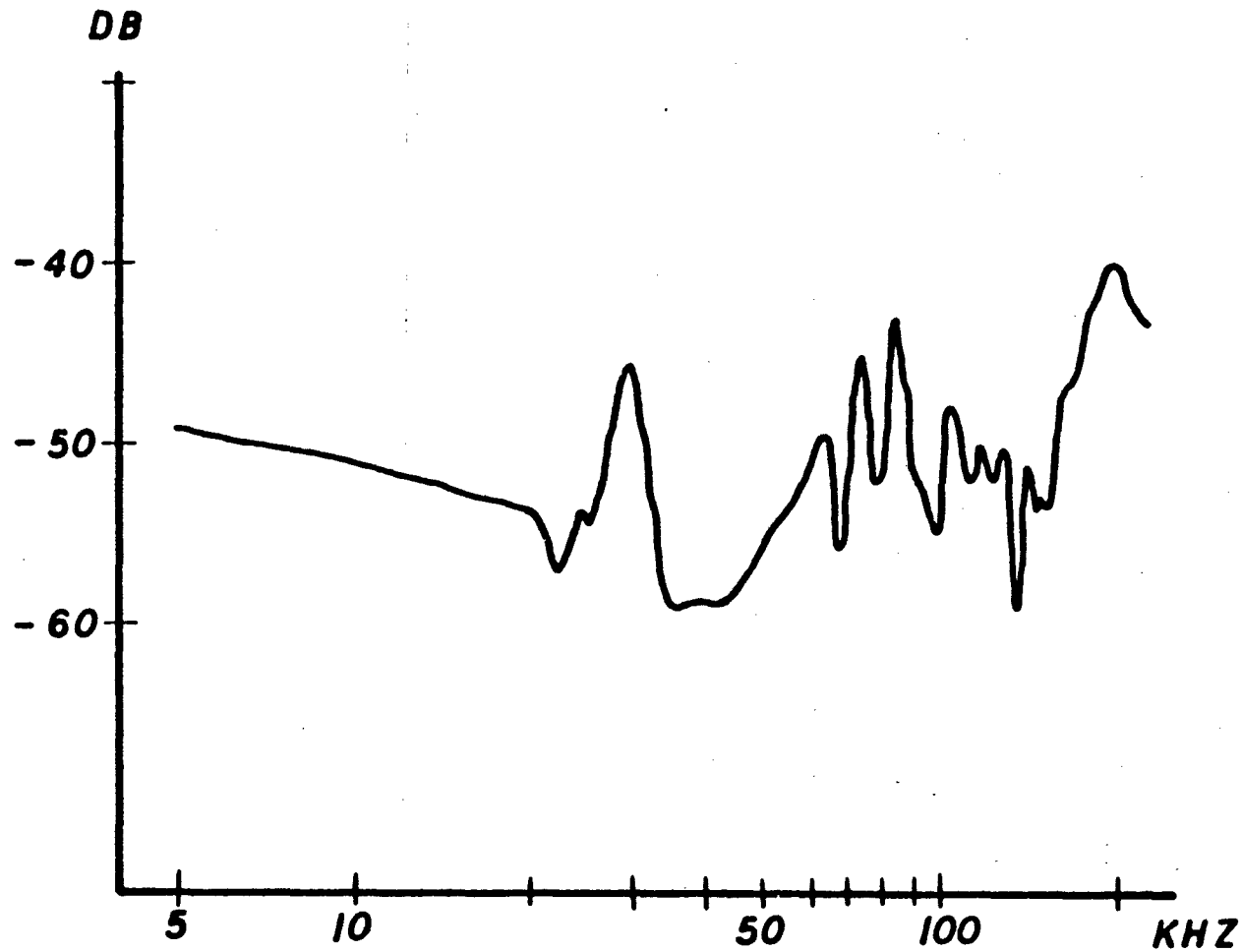

Fig. 3-15
Plot of frequency spectrum of primary pulse for fourth prototype transducer.

was determined that the element pairs were undergoing uncontrolled mode conversion in dissipating the energy applied by the shock excitation pulse.

Rather than scrapping the fourth prototype completely, it was decided to test it with a tone burst to determine its response to a clean pulsed input. Maximum response was at 76 kHz, Fig. 3-16. The excitation was a 76 kHz, 200 microsecond tone burst. As seen in Figs. 3-17 and 3-18, the prototype approached steady state in approximately 15 cycles and decayed to the 1/e point in approximately 10 cycles. This gives a fair estimate for the Q as on the order of 15 [Ref. 17], which is moderately low. Horizontal beam patterns were taken at 3 meters and are shown in Fig. 3-19.

The continuing time constraints, lack of pulse definition and receipt of the ITC projector precluded a continuation of the analysis of this prototype projector.

6. ITC Projector

The projector constructed by ITC is a line-in-cone arrangement of 14 "Channel 5400" [Ref. 15] cyclinders radially polarized. Details of the structure are shown in Figs. 3-20 through 3-22 [Ref. 18]. The measured capacitance was 38 nanofarads.

The design specifications given to ITC were that the projector have a low Q, high power rating, natural frequency of 100 kHz and be capable of depths on the order

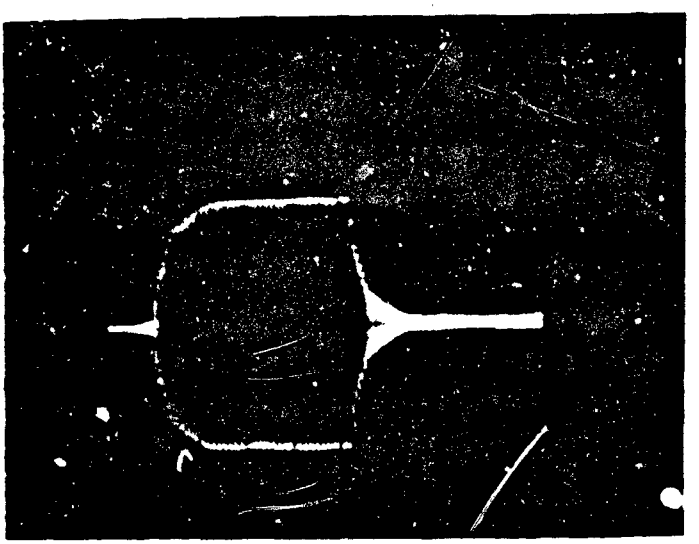

Fig. 3-16
Fourth prototype transducer tone burst response for 64 cycle tone burst at 76 kHz. Vertical; 0.05 volts/cm. Horizontal; 0.2 ms/cm.

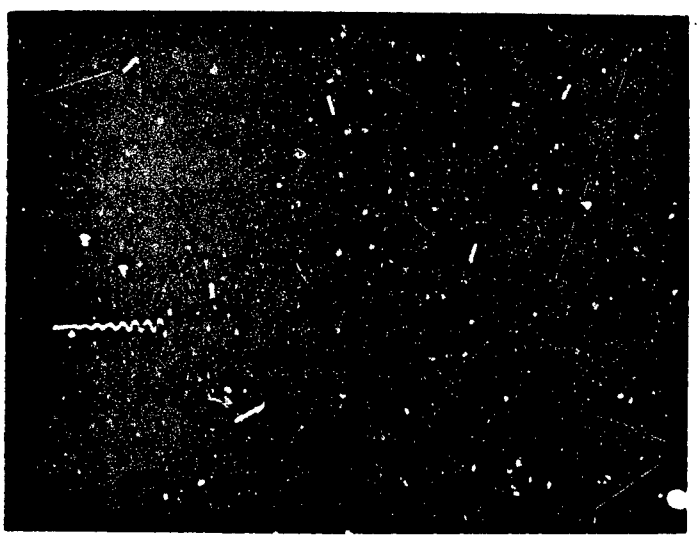

Fig. 3-17
Fourth prototype transducer tone burst rise time for 64 cycle burst at 76 kHz. Vertical; 0.05 volts/cm. Horizontal; 0.05 ms/cm.

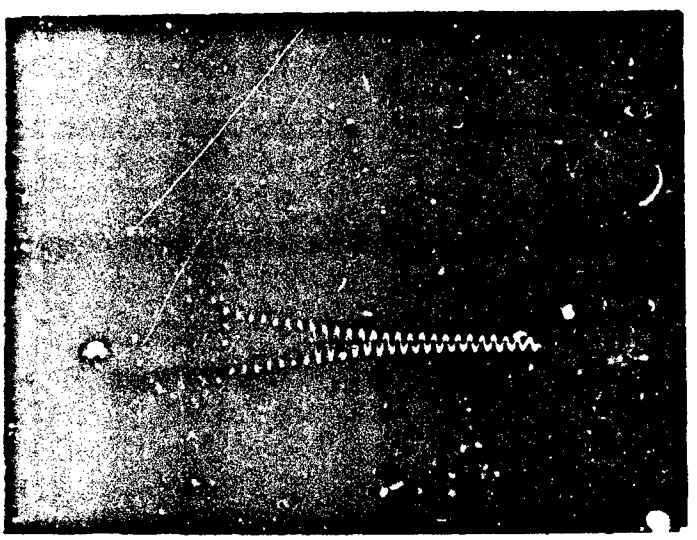

Fig. 3-18
Fourth prototype transducer tone burst fall time for 64 cycle burst at 76 kHz. Vertical; 0.05 volts/cm. Horizontal; 0.05 ms/cm.

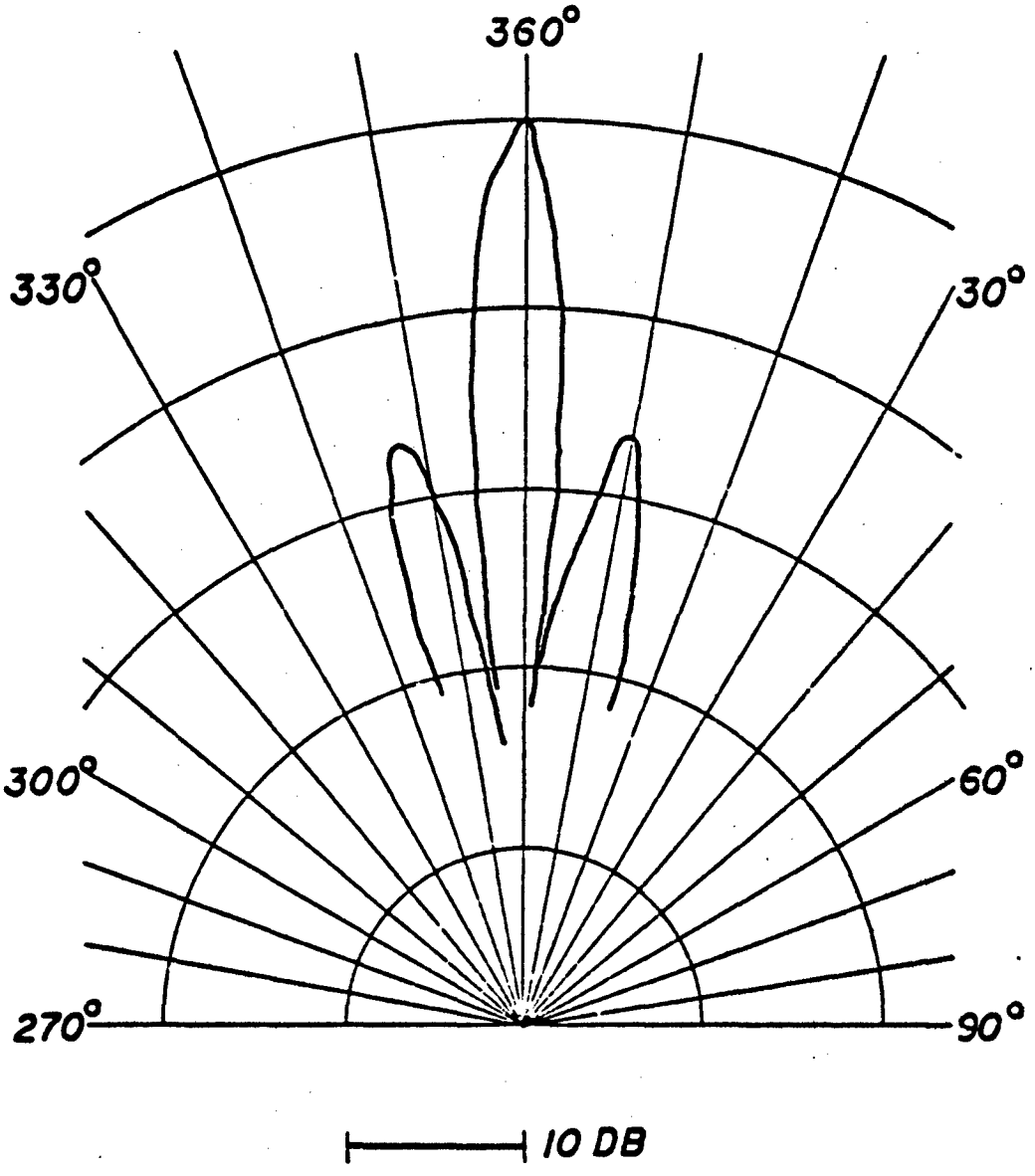

Fig. 3-19
Fourth prototype beam pattern at a range of 3 m at 78.8 kHz.

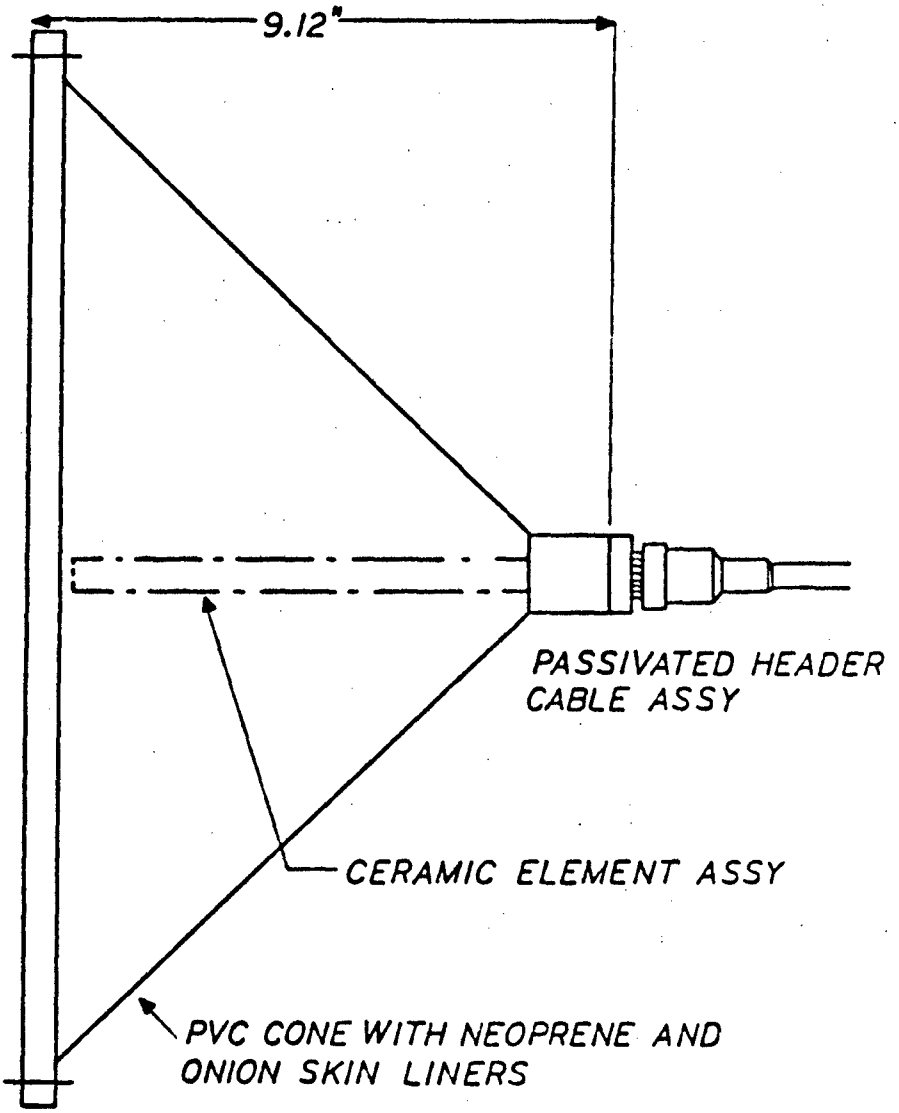

Fig. 3-20
Line-in-cone transducer construction diagram. (Side view)

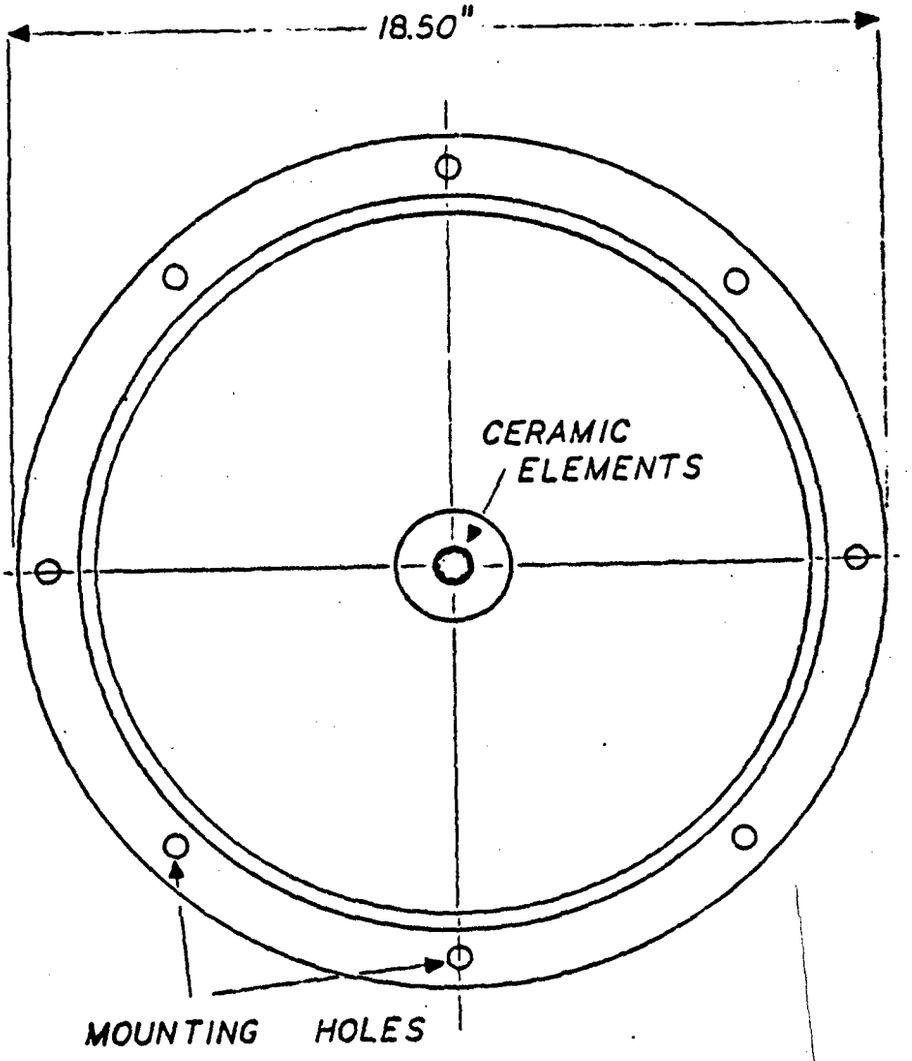

Fig. 3-21
Line-in-cone transducer construction diagram. (Front view)

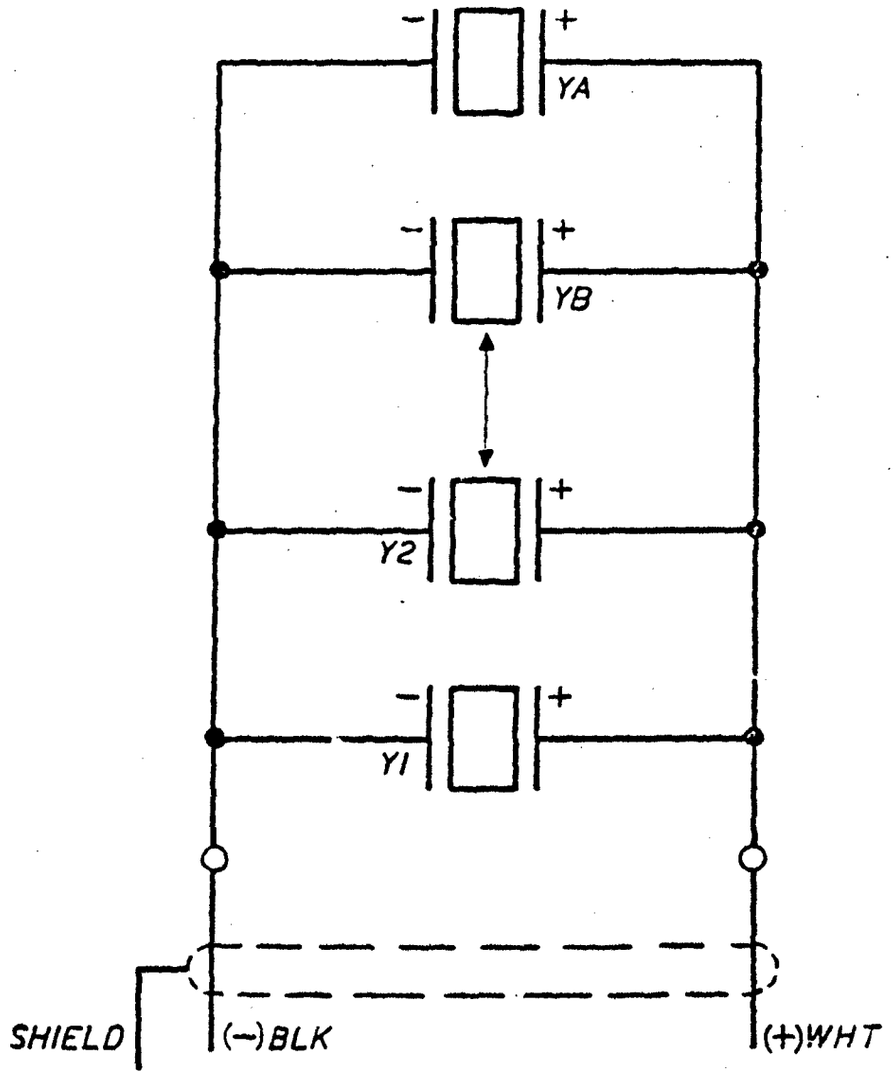

Fig. 3-22
Schematic diagram of electrical circuit in
14 element line array of ITC transducer.

of 400 meters. The line of cylinders is centered in a 45 degree cone covered with a pressure release material and sealed with neoprene rubber and potting compound. The line of cylinders is encased in potting compound with an acoustic impedance equivalent to sea-water. The electro-mechanical characteristics of the ITC projector are given in Figs. 3-23 through 3-25 and were determined by the same method as those of the fourth prototype [Ref. 16]. A specific near-field beam pattern at 100 kHz as provided by ITC is shown in Fig. 3-26.

The ITC projector was suspended in the anechoic tank and shock excited with a 200 VDC drive delivering a 240 volt spike to the projector. This produced a primary pulse that was nearly monochromatic at 91 kHz. The pulse shape displayed increased definition and was predictable in range and distance off axis. Photographs and details of this pulse are discussed in the following chapter. The subsequent operating drive voltage was 400 VDC which presented a 480 volt spike to the projector.

Due to the system design criterion of operating in close proximity to the bottom within the collimated near-field beam produced by this projector, a beam pattern in the classical sense is of marginal value. Therefore, a cross-section profile of the radiated pressure field was deemed to be more useful. These cross-sections were taken at various ranges between 2 and 6 meters. Vertical

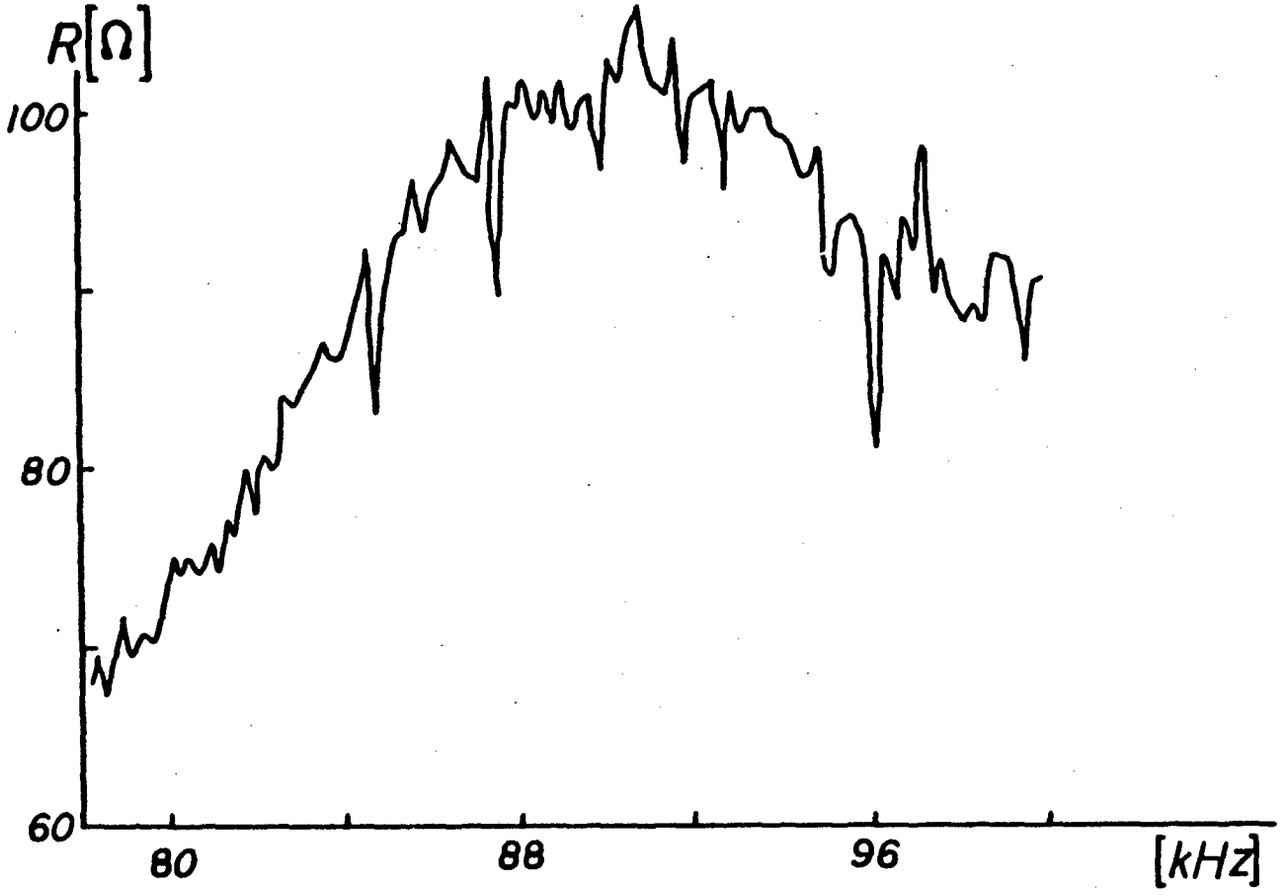

Fig. 3-23
Resistance as function of frequency for line-in-cone transducer. (In air)

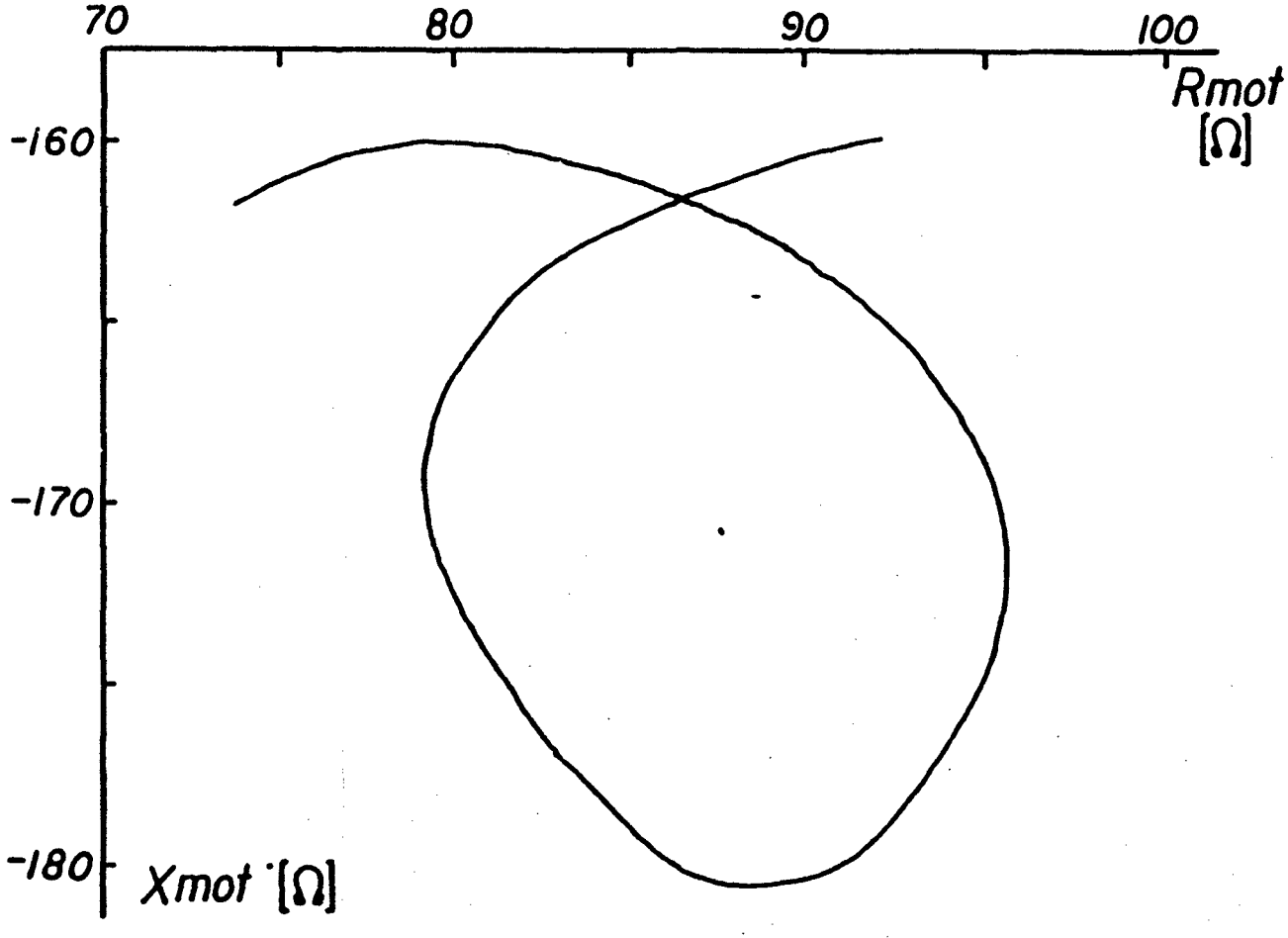

Fig. 3-24
Motional impedance circle for air-loaded line-in-cone transducer.

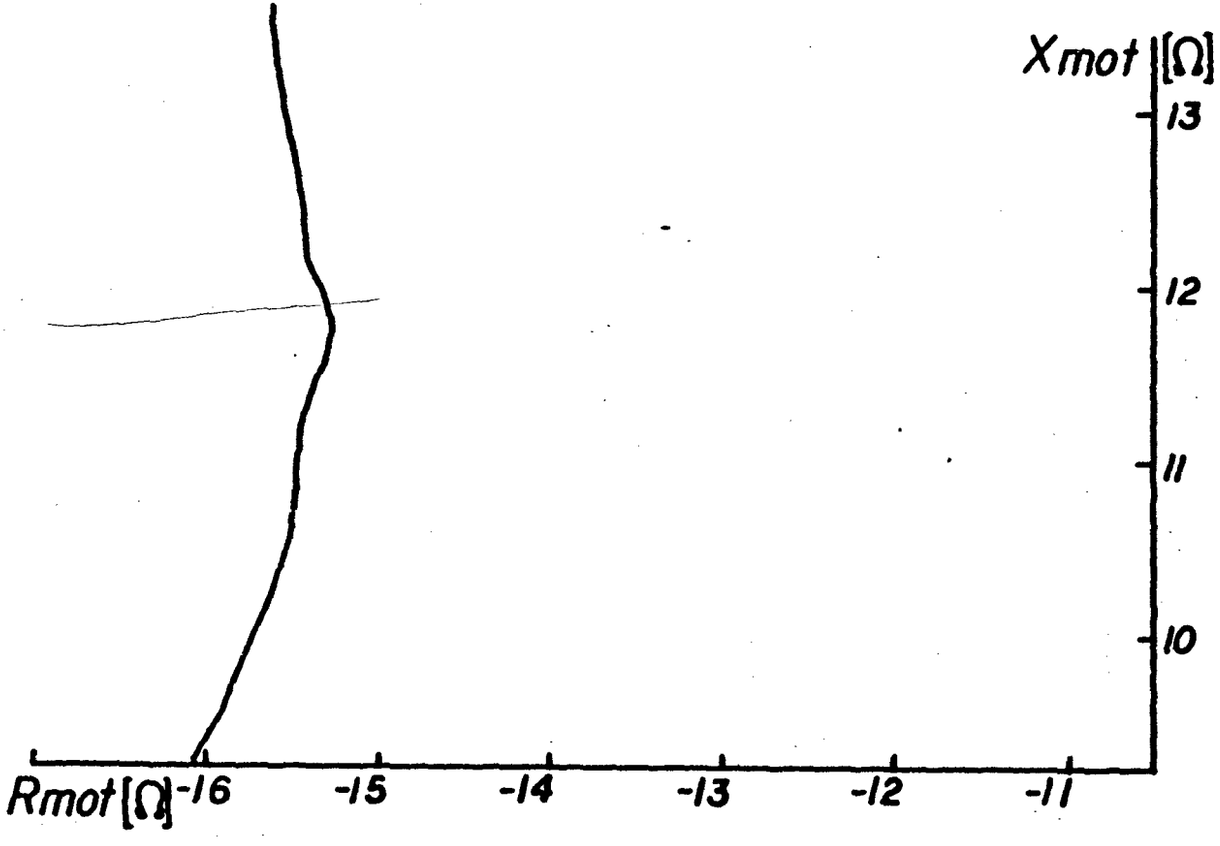

Fig. 3-25
Motional impedance circle for water-loaded line-in-cone transducer.

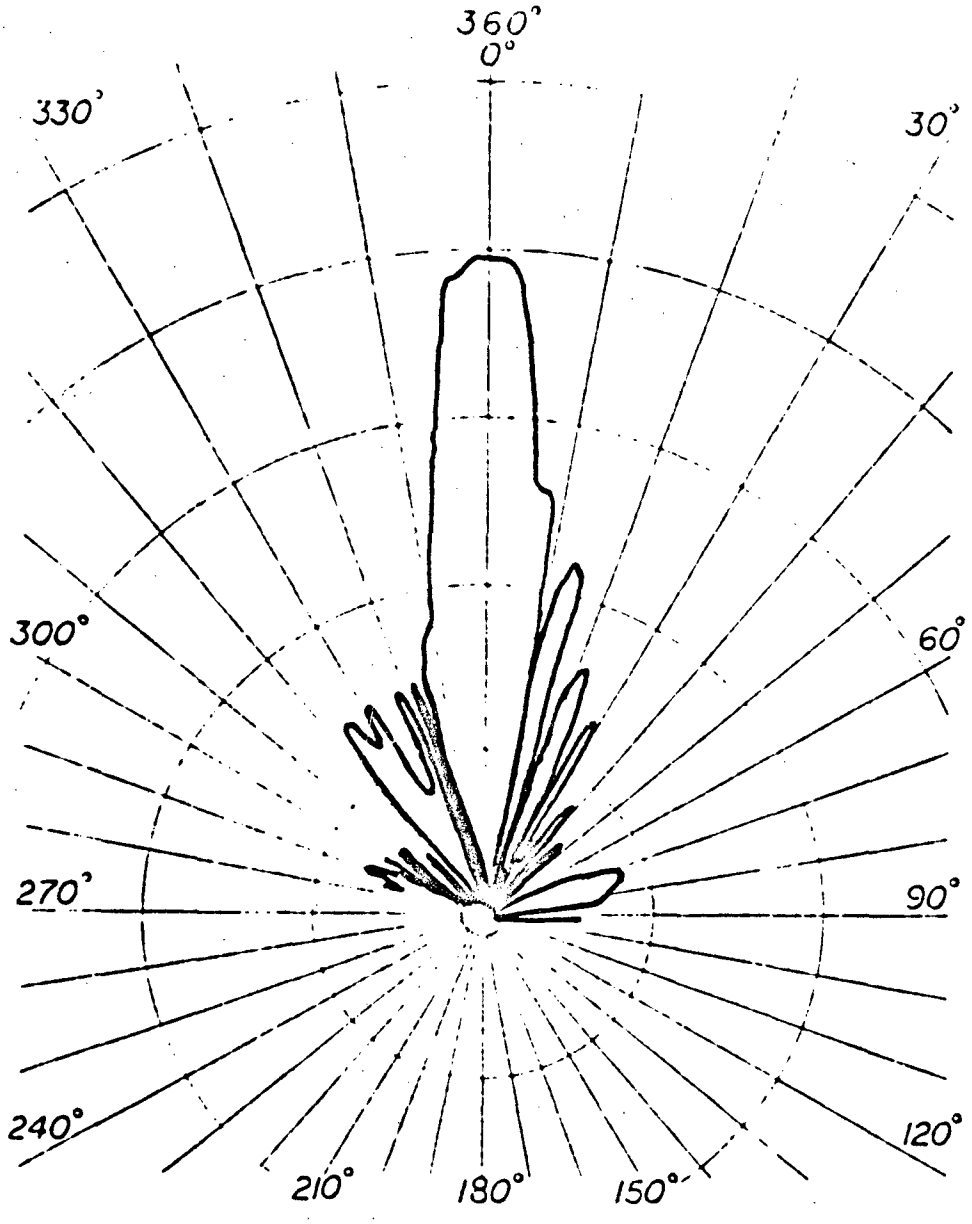

Fig. 3-26
Line-in-cone transducer beam pattern at a range of 2 m at 100 kHz (supplied by manufacturer). This pattern is misleading because it is measured in the cylindrical near-field portion of the field, rather than in the conical far-field.

cross-sections were taken only at 2, 3 and 4 meters to ensure symmetry with the horizontal cross-sections. Details of these profiles are given in the following chapter and exhibit some interesting characteristics not predicted by current theory [Ref. 6].

B. TRANSMITTER PULSE CIRCUIT DEVELOPMENT

The basic transmitter pulse circuit design was developed from a combined transmit/receive circuit employed in a side scanning sonar towfish developed by Klein Associates of Salem, New Hampshire [Ref. 19]. The Klein transmit pulse circuit contains a resistance charging network coupled to a 750 VDC power supply and fired by a silicon controlled rectifier (SCR) and a 15 volt trigger pulse. At triggering, the charging network discharges through a 2.5:1 (at 100 kHz) step up pulse transformer whose secondary is coupled to the towfish transducer.

Since this circuit met the basic design requirements for this thesis, a prototype was assembled from components. One deviation from the Klein circuit was the use of two Klein pulse transformers. The transformer primaries were connected in series and the secondaries in parallel for this experiment. This configuration was chosen because it was expected that the experimental transducer capacitance would be significantly higher than that of the Klein

transducer and the reduced secondary inductance would allow a higher resonant frequency. See Fig. 3-27 for details.

The circuit did not initially function as constructed in that the SCR would not trigger. It was determined that capacitor C-1, originally 2.2 microfarads, was defective. Capacitor C-1 was replaced with a 10 microfarad capacitor and the pulse circuit began to function.

A later problem encountered in the pulse circuit involved the overheating and opening of R-4 (10 kilo-ohm, 10 watts) at applied voltages above 400 VDC. The first replacement was a 5 kilo-ohm, 25 watt resistor. The lower resistance was chosen to reduce charge time and allow an increased pulse repetition rate. This resistor also overheated during operation and was replaced with the 5K ohm, 38 Watt resistor shown in Fig. 3-27. No further problems with charging resistor overheating were encountered.

During later experimentation at high applied voltages the SCR failed, probably due to excessive peak inverse voltage. This 800 volt SCR was replaced with the 1200 volt SCR shown in the schematic with no further failures.

The pulse circuit functioned well in conjunction with the second prototype transducer. The capacitance of the fourth prototype transducer, however, was so great that a different pulse transformer with greatly reduced secondary inductance was required. Several pulse transformer configurations were constructed, with the final version being

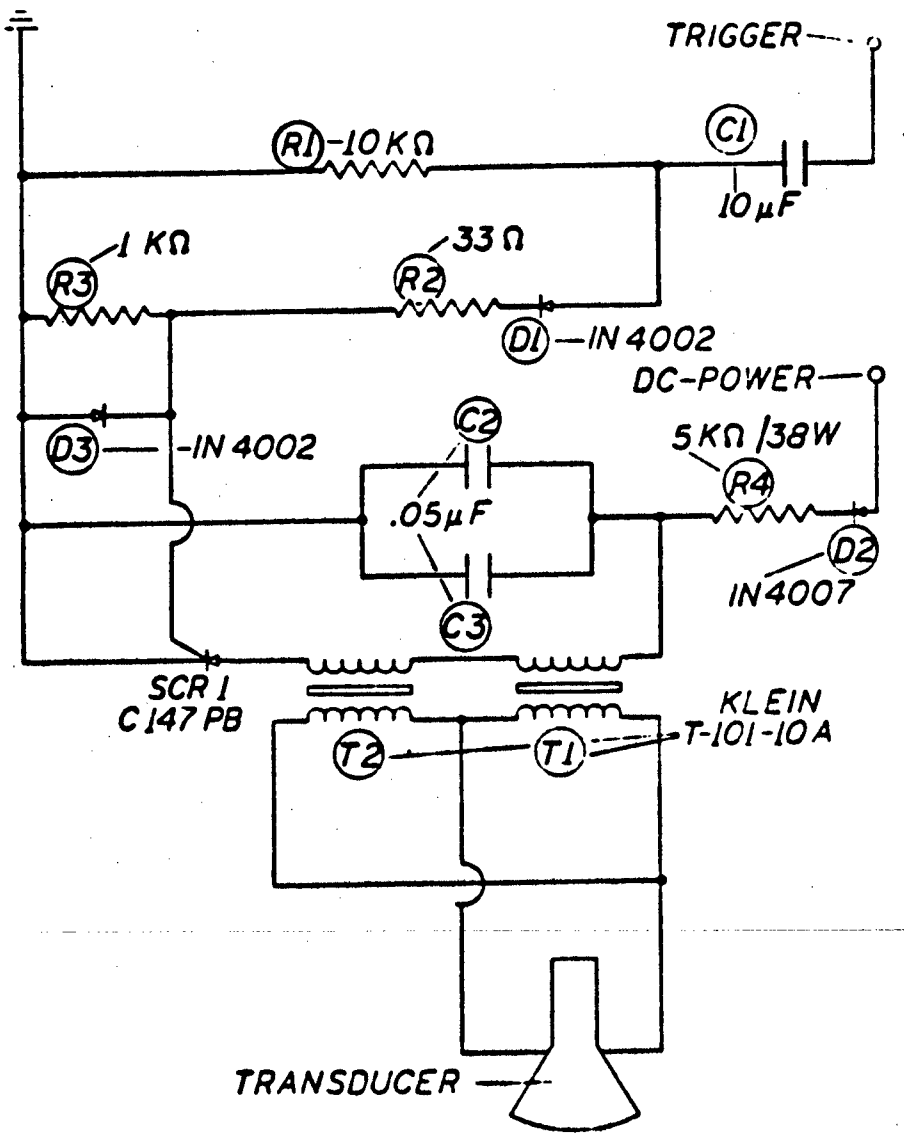

Fig. 3-27
Transmitter pulse circuit schematic diagram.

composed of an 8 centimeter diameter molybdenum toroidal core 2.5 centimeters thick with a 7 turn bifilar wound primary and a 14 turn bifilar wound secondary for 2:1 step up. All windings were of 14 gauge transformer wire. Even while employing this transformer, pulse clarity and efficiency were not as good as desired. Several loss inductors were inserted without success because the loss inductors matched the transmission line to the pulse circuit, instead of to the transducer. In addition, losses across the inductors drastically reduced pulse power. This configuration, however, functioned satisfactorily and was utilized until the transducer purchased from the International Transducer Corporation arrived. For this transducer the Klein transformers were reinstalled in the configuration previously described. The pulse circuit remained in this configuration for the remainder of the experiment with excellent results.

The high voltage potential to the transmitter pulse circuit was supplied by either one or two Hewlett Packard model 712A 0-500 VDC power supplies connected in series. The number of power supplies used depended on the source under test. The SCR trigger pulses were supplied by a Wavetek model 116 oscillator. During experimentation, DC potentials varied between 20 volts and 1000 volts while trigger pulse amplitude varied between 15 and 30 volts and pulse repetition frequency ranged between 15 and 40 HZ. The parameters used depended on the particular source

employed in the experiment. Fig. 3-28 shows a transmitter block diagram.

A different transmitter power configuration was employed during the tone burst analysis of each transducer. Two Wavetek model 116 oscillators were used to provide tone and pulse repetition. The output tone was then amplified using either an Instruments Incorporated model LCD3-2 Kilowatt amplifier or a Krohn-Hite model DCA-50, 50 Watt amplifier with a model MT-56 matching transformer. The load impedance setting on the matching transformer was set at 32 ohms.

C. LOW PASS FILTER CIRCUIT DEVELOPMENT

The low pass filter was employed to suppress primary frequency components from the received echo. The design is based on a filter used in previous experimentation in non-linear acoustics by the Naval Underwater Systems Center in New London, Connecticut [Ref. 20]. The filter is a passive network composed of three RC filters in cascade. All three stages have the same time constant. This filter was chosen for its passivity and because an LC filter would have caused ringing problems in the receiver system due to the short time duration of the desired signal return. The filter has a cutoff frequency of 5 kHz with a 60 dB/octave rolloff. A schematic of the filter is shown in Fig. 3-29.

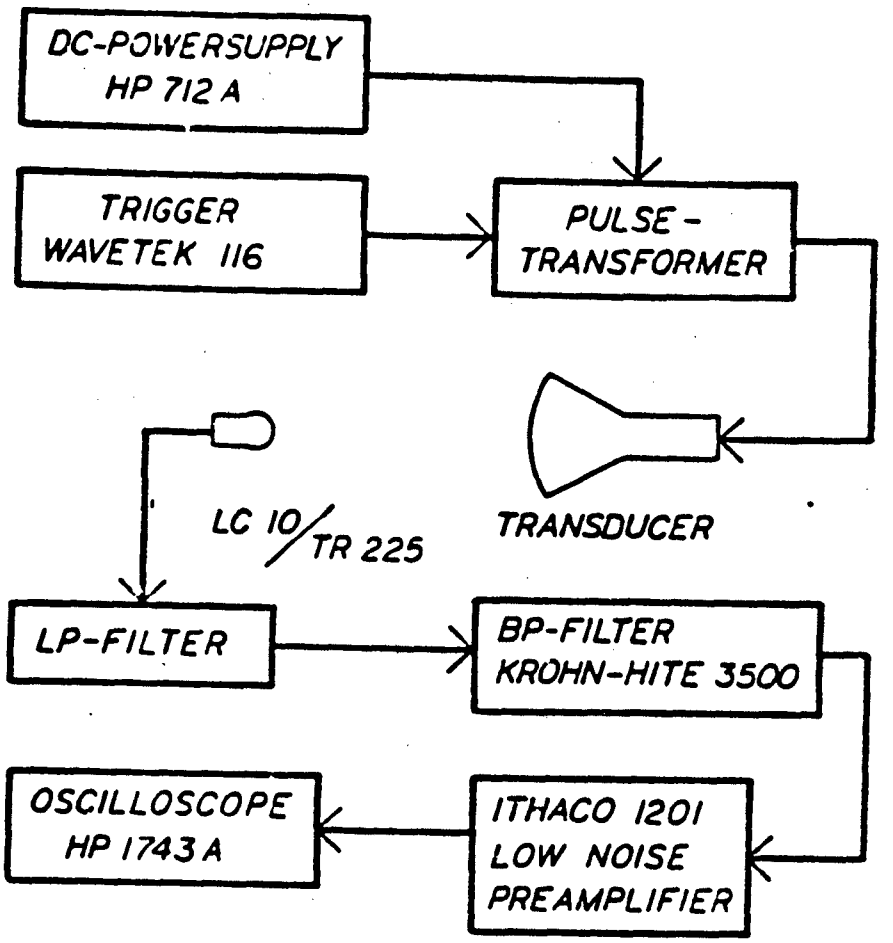

Fig. 3-28
Transmitter and receiver block diagram.

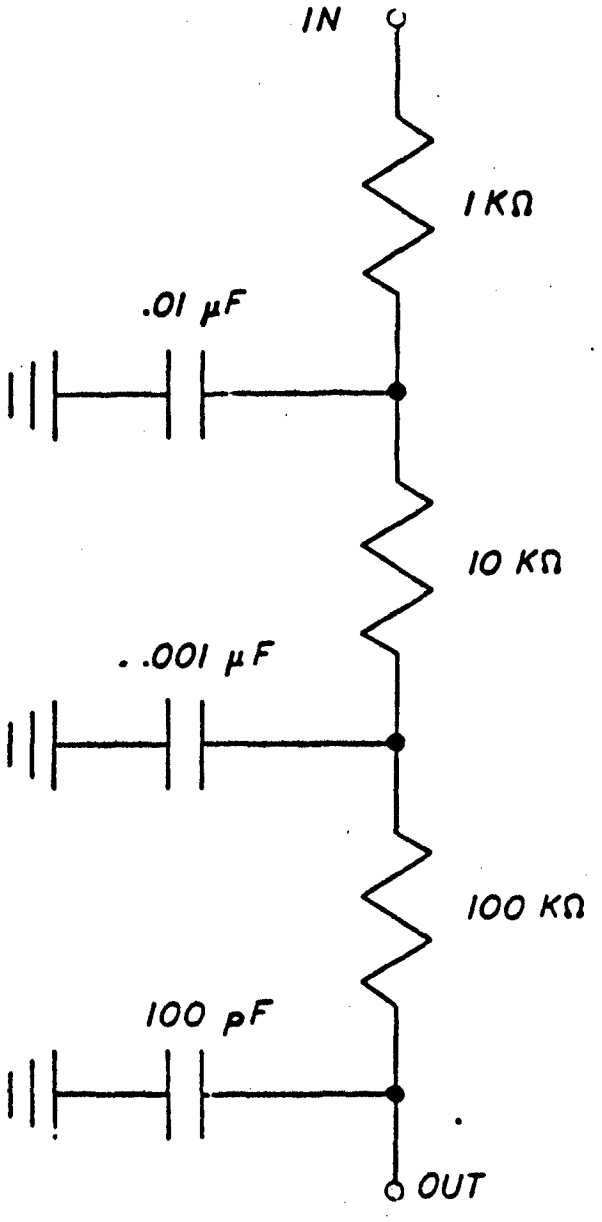

Fig. 3-29
Receiver circuit low pass filter schematic diagram.

D. RECEIVER CIRCUIT DEVELOPMENT

The same basic receiver configuration was utilized throughout the experiment. A block diagram of the system was shown in Fig. 3-28.

Experimentation during development was conducted in the Naval Postgraduate School anechoic tank and later in the swimming pool (these facilities will be described later). A Celesco LC 10 hydrophone was utilized as the acoustic sensor. Hydrophone specifications are presented in table 3-1 and Fig. 3-30 [Ref. 21]. Bistatic geometry was used throughout these experiments. The hydrophone output was split, with one output connected directly to the oscilloscope for primary frequency pulse observation. The second output was coupled to the low pass filter input for processing.

The low pass filter output was then connected to a Krohn-Hite model 3500 electronic band pass filter initially set at 20 Hz to 20 kHz. The band pass filter output was passed through an Ithaco model 1201 low noise preamplifier set at DC to 30 kHz bandpass with a gain of 500. The preamplifier output was coupled to the oscilloscope for observation of pulse self-demodulation.

The Krohn-Hite filter was placed before the preamplifier in the receiver circuit to avoid non-linear electronic effects, since the Krohn-Hite filter is overdriven by input voltages in excess of 0.5 volts. Most of these tests were

Table 3-1

CELESCO LC-10 HYDROPHONE PARAMETERS [Ref. 21]

Capacitance with 25 FT of cable	7500pf
Useful frequency range	0.1 to 120,000 Hz
DC resistance (minimum)	1000 Megohms
Maximum pressure	2000 psi
Horizontal directivity @ 100 kHz	+/- 0.1 dB
Vertical directivity @ 25 kHz	+/- 2.0 dB
Operating temperature range	-60 to 100 C
Thermal sensitivity	0.3 dB/C
Weight with 25 FT of cable	10 oz
Sensing element	Lead Zirconate Titanate

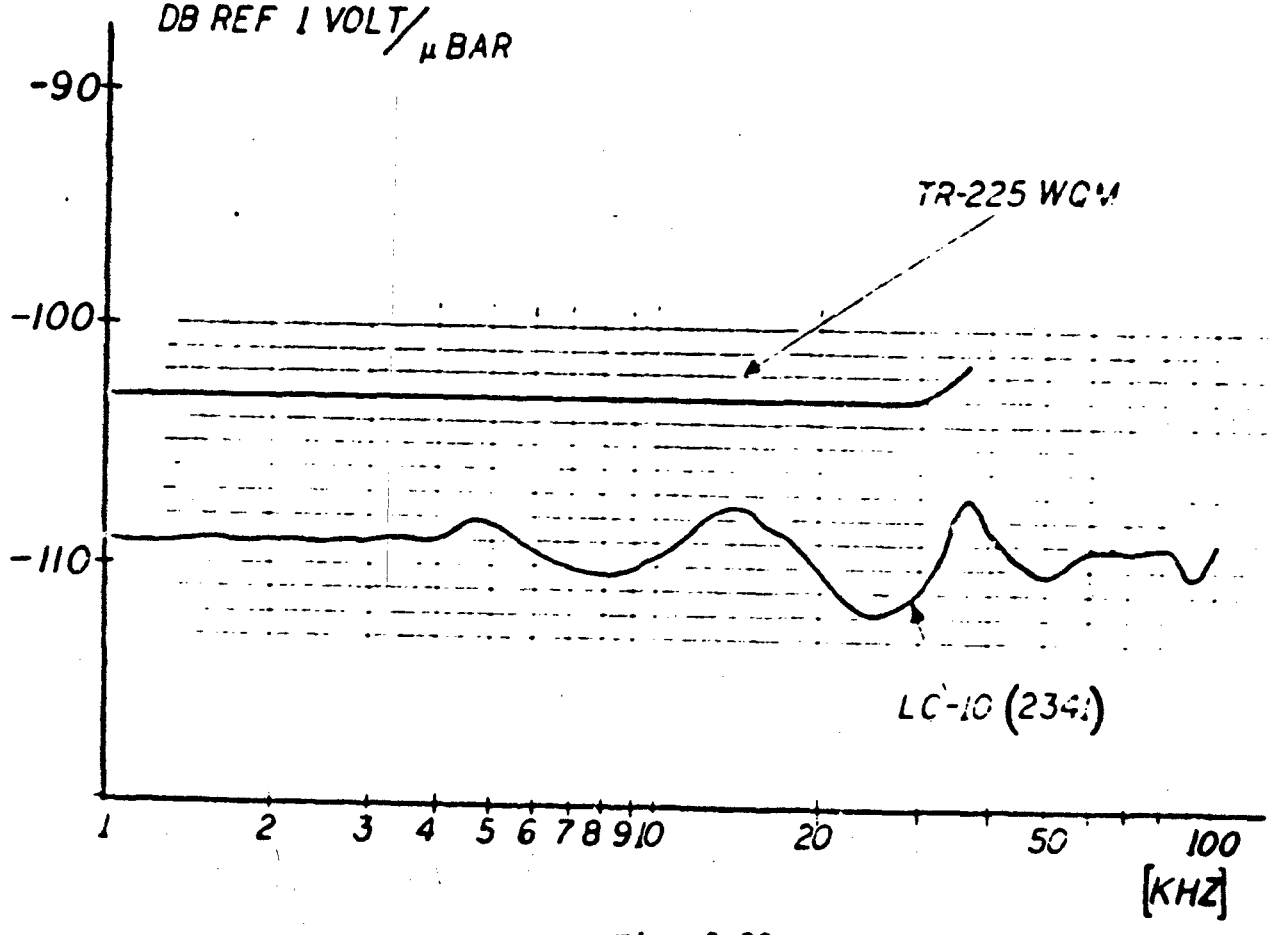

Fig. 3-30
Receiver system hydrophone sensitivities as a function of frequency.

at ranges of 15 meters or less and the preamplifier output would have been significantly greater than this limit. It was also felt that the noise levels in the test environment or the band pass filter would not be significant enough to dictate interchanging the position of the band pass filter and the preamplifier in the receiver system. This assumption did prove to be correct.

Later experiments were conducted in Liberty Bay at the Acoustic Test Facility, Naval Undersea Warfare Engineering Station, Keyport, Washington, (this facility will be described later). The longer ranges involved, 30 to 40 meters, dictated the use of a more sensitive and/or more directive acoustic sensor. A Scientific Atlanta, Inc. model TR225/WQM sonar test transducer was utilized (see Fig. 3-30) with a receiving voltage sensitivity of -203 dB re 1 micropascal. This element has a 5 dB to 6 dB advantage over the LC-10. Directivity gain was also improved via the use of an existing mount for the TR225 consisting of a cell-tite neoprene lined aluminum cone of 40.7 centimeter diameter. Cone height was approximately 11.3 centimeters. Based on a circular piston with a radius of 20.35 centimeters, and a mean secondary frequency of 9 kHz, the directivity index was estimated to be approximately 18 dB [Ref. 22].

An additional desirable trait of this sensor is that its sensitivity falls off rapidly for frequencies above 30 kHz.

This provides an additional filtering effect to suppress the primary frequency.

In addition to the employment of a different hydrophone for this test, the receiver circuitry was further optimized by the interchange of the low noise preamplifier and the band pass filter as mentioned earlier. Also, the preamplifier bandwidth was reduced to DC to 10 kHz and the band pass filter bandwidth was reduced to 20 Hz to 10 kHz. The receiver system performed well in both configurations. In the Liberty Bay test, however, the full directivity gain of the TR225 could not always be completely utilized because the bistatic geometry in use dictated that the receiver cone be physically displaced about 0.5 meters off the projector axis. Thus, the receiver system suffered somewhat from parallax. Fig. 3-31 shows the experimental configuration used in the Liberty Bay test.

All of the receiver circuitry was examined for linear behavior by injecting a tone burst of stepped amplitude into the receiver system and checking the output at each stage of the receiver with an oscilloscope. Linear response to amplitude changes and comparison of observed waveshape and frequency spectrum to theoretical predictions were made. Transient response amplitude was observed to be approximately 2% of the applied voltage. Both hydrophones were tested in a similar manner. No non-linear behavior was

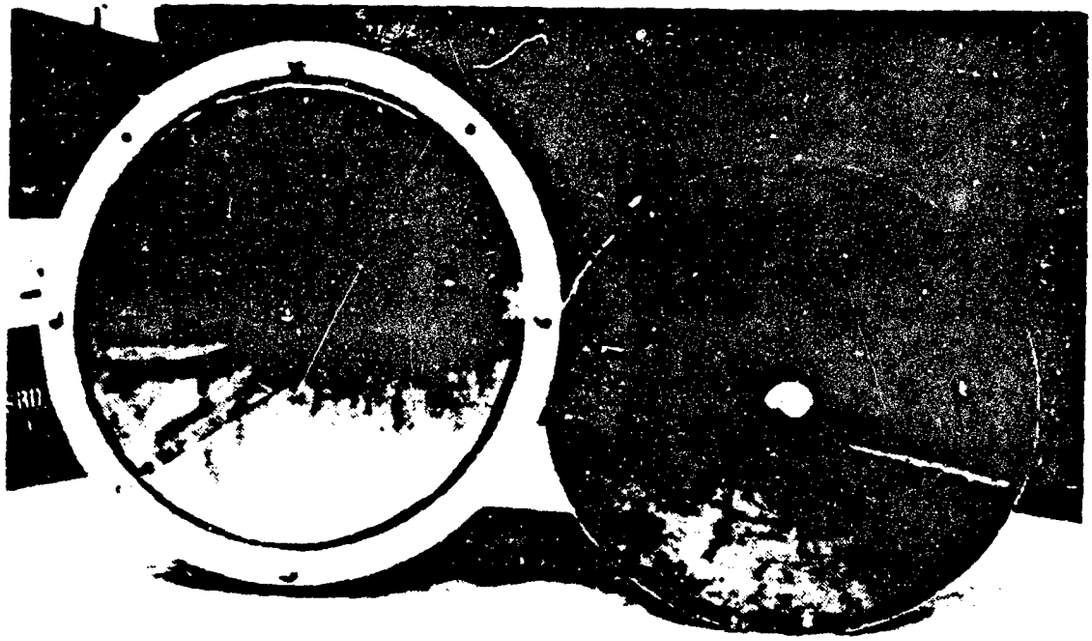

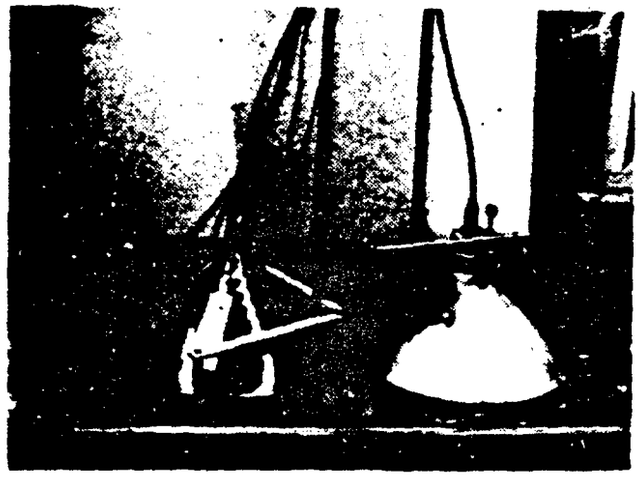

Fig. 3-31
Experimental projector (left) and receiver (right) configuration used for experiments at the Acoustic Test Facility, Keyport, Wa.

observed in the receiver system of the sensors. See Fig. 3-32 for receiver system tone burst response.

E. ANECHOIC TANK DESCRIPTION AND EXPERIMENTATION

Initial experimentation for all of the projectors occurred in one of two anechoic tanks located on the Naval Postgraduate School campus. The tanks are 7.3 meters long, 1.9 meters wide and are filled with fresh water to a depth of approximately 2 meters. Fluid temperature in these tanks remains fairly constant at 22 degrees centigrade. The walls and floor of the tanks are lined with an aluminum loaded butyl rubber anechoic material whose configuration consists of very closely spaced outward pointing cones 3.5 centimeters high and 2 centimeters in diameter at the base. A graph of reflection loss in dB versus frequency for normal incidence is included as Fig. 3-33.

The tanks were utilized for short range measurements involving near field and far field determinations for all of the projectors. Source level measurements were also made for the primary frequency pulse and the secondary pulse using the described receiver system. Some beam pattern data for the primary and secondary at several ranges were collected for the second and fourth prototypes. For the ITC projector, horizontal and vertical cross-sections for both signals of interest were collected instead because of the high level of collimation observed for this source. These

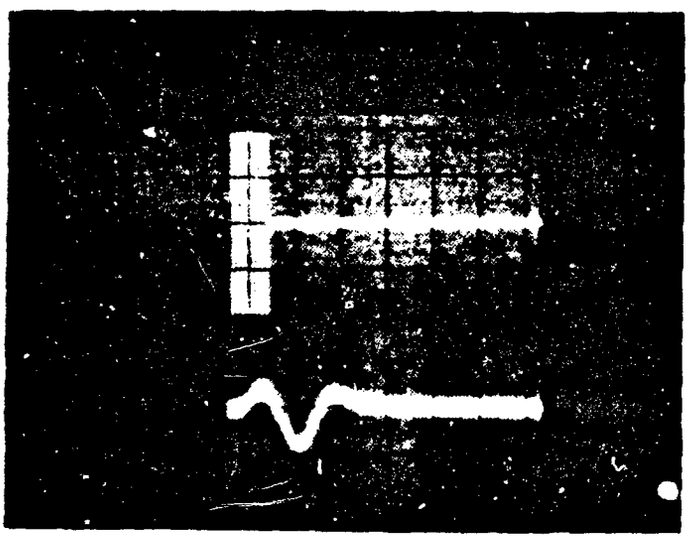

Fig. 3-32
Tone burst response of receiver circuit (without hydrophone) for 8 cycle tone burst at 91 kHz. Preamplifier gain = 1. Scales: Vertical (upper) 0.5 volts/cm, (lower) 0.02 volts/cm; Horizontal 0.1 ms/cm.

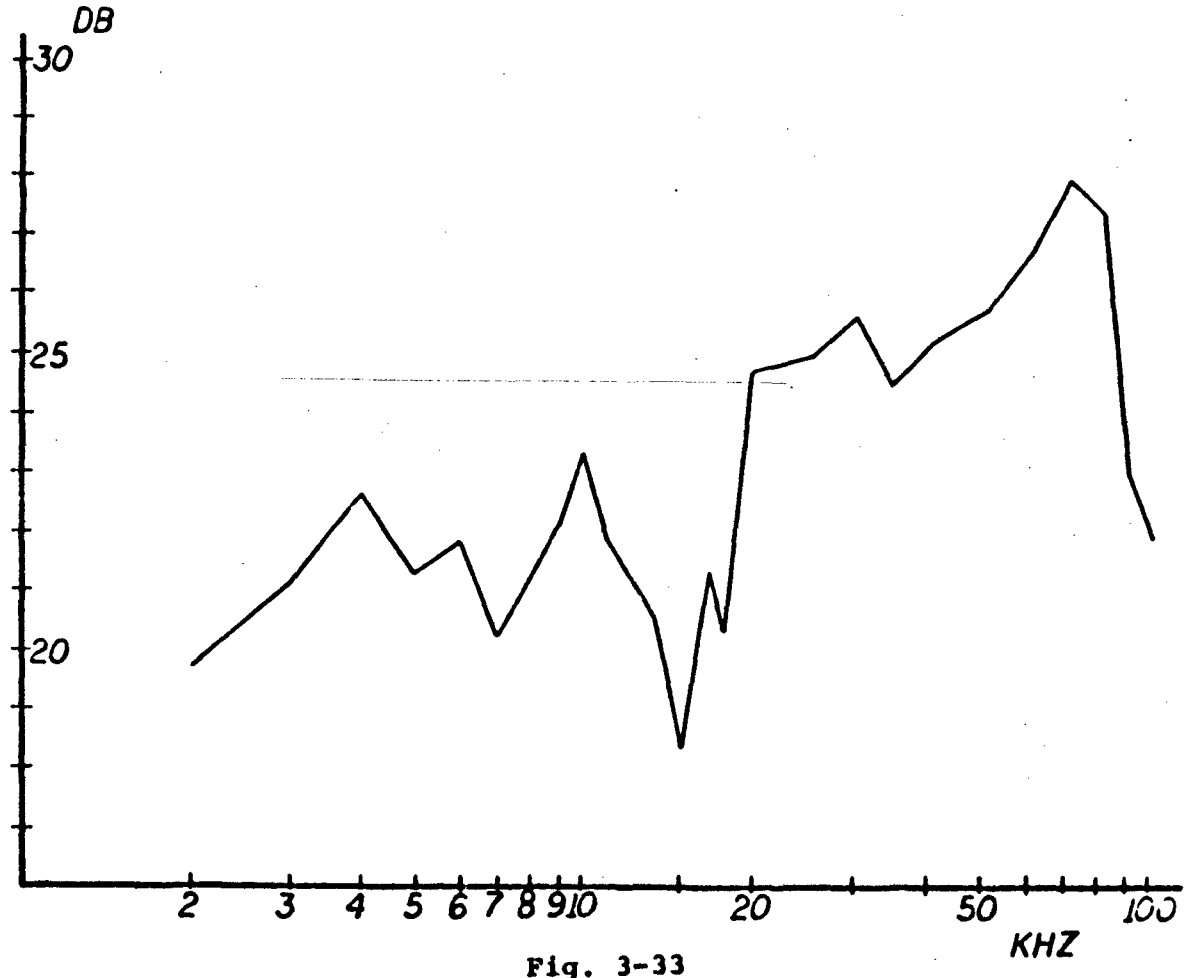

Fig. 3-33
Graph of anechoic tank reflection loss in dB versus frequency.
(Normal incidence)

data were also taken at several ranges of interest. Some reflection and penetration tests using a 2 millimeter thick steel plate were performed using the ITC projector. Background, primary and secondary frequency data was also collected for the ITC and fourth prototype projectors. The measurements in all cases were conducted by placing the projector at the center of one end of the tank and controlling receiver position in precise centimeter intervals, both horizontally and vertically, through the use of a mobile calibrated track that spanned the tank width. Source reflection problems from the wall behind the projector were not a problem because of the reflective apparatus on the projector and the anechoic material on the tank walls. Spot measurements of the sound fields behind the projectors demonstrated this assumption to be correct.

F. SWIMMING POOL DESCRIPTION AND EXPERIMENTATION

An attempt was made to utilize the Naval Postgraduate School swimming pool for acoustic measurements of the ITC and fourth prototype projectors at ranges greater than 6.5 meters. The pool is a concrete enclosure approximately 18 meters wide and 35 meters long with water depth varying from 3 meters at the deep end to 1 meter at the shallow end. During experimentation, the water composition was essentially fresh with an average temperature of 29 degrees centigrade.

Both sources were suspended from the diving board to a depth of approximately 1.3 meters. For the fourth prototype projector, beam cross-sections were taken at ranges out to 15 meters. For the ITC projector, one cross-pool data set was taken at a range of approximately 17.5 meters. All data were taken in the deep end of the pool. In both cases the data were extremely difficult to accurately collect due to high levels of radio frequency and 60 Hz line noise in the pool. Several 60 Hz notch filters were inserted in the receiver system, but little improvement was noted. Again, the sound fields behind the projectors were probed and found to be negligible. Because of the noise and range limitations imposed by the pool, the decision was made to attempt more extensive, longer range experiments at another location. The Acoustic Test Facility at the Naval Undersea Warfare Engineering Station, Keyport, Washington was chosen.

G. ACOUSTIC TEST FACILITY DESCRIPTION AND EXPERIMENTATION

The Acoustic Test Facility, Naval Undersea Warfare Engineering Station, Keyport, Washington is a barge of approximately 0.6 meters draft located in Liberty Bay, an arm of the Pacific Ocean. Thus, the facility is located in an essentially ocean environment. During the three days of experimentation, water depth varied between 8 meters and 15 meters, depending on the tide. Sediment conditions below the barge, as provided by divers, were 30 to 50 centimeters

of moderately firm silt with a wet density of approximately 1627 kilograms per cubic meter [Ref. 13]. The sound speed in the region at an average temperature of 10 degrees centigrade is approximately 1491 m/s. The ITC projector was the only one used during these tests.

Three major experiments were conducted. In the first, no targets were employed and attempts to determine sediment depth data from the time difference between the primary and secondary pulse returns were conducted with some success. For the second test, a 20 centimeter diameter sphere made of 14 gauge steel and filled with a fluid mixture of freon and ethanol was utilized. Sphere weight in air was 8.86 kilograms. The sphere had sufficient mass per unit area in water to at least partially penetrate the sediment, and by tracking the primary and secondary returns as the sphere was lowered into the bottom, estimates of the sediment depth could be obtained and compared to the previous data. For the third experiment, an inert and nearly neutrally bouyant MK-46 torpedo body was the target. The torpedo is approximately 2.6 meters long and 46 centimeters in diameter. Since the torpedo was nearly neutrally bouyant, it did not penetrate the sediment. The torpedo did, however, provide the opportunity to observe primary and secondary returns from a hard object other than the bottom. Data were collected for torpedo orientations which were both lateral and longitudinal with respect to the source.

One 60 Hz notch filter was employed in the receiver system during these tests. No radio frequency or line frequency noise interference was noted.

IV. EXPERIMENTAL RESULTS AND ANALYSIS

A. EQUIVALENT CIRCUIT

An equivalent circuit model for the ITC line-in-cone transducer is shown in Fig. 4-1 [Ref. 23]. The component designations are defined as follows:

Rd -- dielectric loss resistance

Co -- blocked capacitance

Rl -- mechanical loss resistance

Rr -- radiation resistance

C -- mechanical capacitance

L -- mechanical inductance

For the purpose of this thesis, Rd is assumed to be an open circuit, as dielectric losses are assumed negligible in comparison with other circuit losses. The other component values were determined from data obtained during an investigation via a computerized transducer analysis system [Ref. 16]. The transducer was operated in air and the analysis system provided values for the resonance frequency, blocked capacitance, mechanical loss resistance, mechanical quality factor (Q), static coupling coefficient and dynamic electromechanical coupling coefficient.

The blocked capacitance and mechanical loss resistance values were applied directly. The electromechanical coupling coefficient and blocked capacitance values were

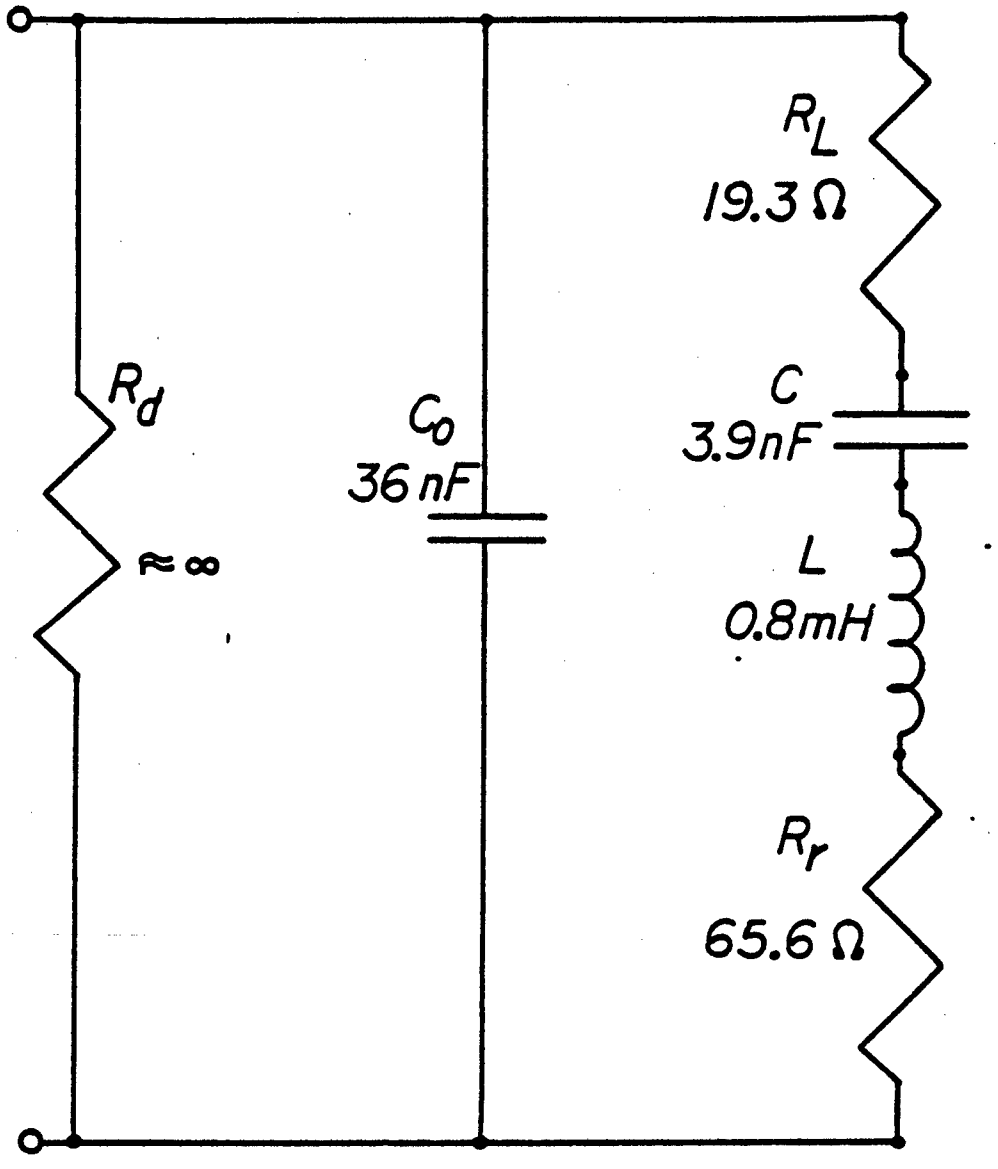

Fig. 4-1
Equivalent electrical circuit for line-in-cone transducer.

used to find C as per equation 14.46a of Ref. 22. Equation 5.38 of Ref. 23 was then used to find L. The value for Rr was determined by measuring the "circle" diameters of Figs. 3-24 and 3-25 and utilizing several of the equations presented in chapter 5 of Ref. 23. Of note is the fact that Fig. 3-25 does not display a clear-cut circle. A circle diameter of 0.9 ohms was assumed, based on a revolution of the small arc between 11.5 and 12.1 ohms on the motional reactance scale. It is acknowledged that this is not the best approach, but it is accurate enough for this thesis.

The computer calculated value for the blocked capacitance compared very favorably with the value measured using an HP 4261A LCR meter noted in Chapter III of this thesis. Further, the computer calculated resonance frequency and quality factor compared favorably with observed data at 89.3 kHz and 5.9, respectively.

With regards to coupling coefficients, the computer analysis produced a static k of 0.73 and an electromechanical coupling coefficient of approximately 0.1 for the air-loaded case. The static k compares favorably with the general specifications listed in Ref. 24, especially for this transducer in which the individual ceramic elements are isolated from each other. The electromechanical coupling coefficient is also reasonable for a low Q transducer operated away from resonance.

B. TRANSDUCER EFFICIENCY

There are two different approaches which will be used to calculate the efficiency of the ITC line-in-cone transducer. The first is a graphic method employing the data of Figs. 3-23 through 3-25. The second approach utilizes an output power/input power ratio.

For the first method, equation 4.21 of Ref. 25 will be employed:

$$E_{ff} = \frac{(D_V - D_L)}{D_V} \frac{D_L}{R_{ee}} \qquad (4\text{-}1)$$

Dv is the motional impedance circle diameter from Fig. 3-24, DL is the motional impedance circle diameter from Fig. 3-25 and Ree is the resistance value at resonance from Fig. 3-23. From these figures: Dv = 19.25 ohms, DL = 0.9 ohms and Ree = 26 ohms. Therefore, by this approach, Efficiency = 0.033 or 3.3%.

The second approach is detailed in equation (2.101) of Ref. 17. Basically, efficiency for this method is defined as:

$$E_{ff} = \frac{P_{out}}{P_{in}} = \frac{4\pi P_r^2 Z}{D\rho c V^2 \cos\theta} \qquad (4\text{-}2)$$

where: Pr = peak axial acoustic pressure at 1 meter

D = directivity of the source

ρc = characteristic impedance of the medium

V = peak voltage input to the transducer

$\cos\theta$ = power factor due to input impedance

From oscilloscope and impedance meters, it was determined that during normal operation, (configuration described in Chapter III), V = 480 volts, Z = 14.8 ohms and = 39 degrees. The characteristic impedance for the anechoic tank is approximately 1.478×10^6 Pa.s/m.

The directivity is stated to be 3467 (this figure will be derived later in this chapter) and the peak axial pressure at one meter was measured to be 3.09×10^5 Pa. Inserting these figures into equation 4-2 results in an efficiency for this approach of 0.019 or 1.9%.

Comparison of the results of both methods demonstrates that the agreement between the two approaches is not excellent. The general implication is, however, that the transducer is operating at a very low efficiency, probably around 1 to 3 percent.

C. ON-AXIS BEHAVIOR

The on-axis data of the primary and secondary peak voltage amplitudes were taken in the tank in the basement of Spanagel Hall using the same source and receiver configuration as described in Chapter III. The LC-10 hydrophone was mounted to a metal rod that was clamped vertically to horizontal metal rails. The rails as well as the rod were scaled and the position of the hydrophone could be adjusted in horizontal and vertical position with an accuracy within 0.5 centimeters. The ITC transducer was mounted to a metal rod and submerged to a depth of one meter pointing along the length of the tank. The input voltage was set to 400 VDC from the power supply with a pulse repetition rate of 25 Hz. The primary peak voltage amplitude was monitored directly on the oscilloscope and the secondary pulse was processed through the receiver system previously described. The setting on the Krohn-Hite bandpass filter was 20 Hz to 10 kHz. The Ithaco low noise amplifier was AC coupled and set to DC to 10 kHz with a gain of 500. This experimental setup was used in all the experiments conducted and any

deviations from these settings will be mentioned when describing the respective experiment.

The on-axis data were taken in 5 centimeter intervals from 0.6 meters to 2.5 meters distance from the source and from there on in 50 centimeter increments to a distance of 6 meters. For both pulses the peak voltage amplitude was recorded at each position and the data are plotted in Fig. 4-2 for the primary and Fig. 4-3 for the secondary. Both graphs show the 1/R behavior of the on-axis peak voltage after the last maximum. Although the maximum of the secondary pulse is more distinct, one basically can assume that both maxima coincide. Further analysis of these data will be presented later in this chapter.

D. BEAM CROSS-SECTIONS

Instead of taking beam patterns of the primary and secondary pulses, cross-sections of the peak voltage amplitude were established at various ranges. This method was believed to demonstrate more clearly the degree of collimation of the primary beam. The data were taken at 2, 3 and 4 meters distance from the source in horizontal and vertical directions. These cross-sections showed near-perfect symmetry of the beam. Therefore, only horizontal cross-sections were taken beyond 4 meters. All data are tabulated in Tables 4-1 to 4-10 at the end of this chapter. Composite graphs of primary and secondary beam cross-sections are

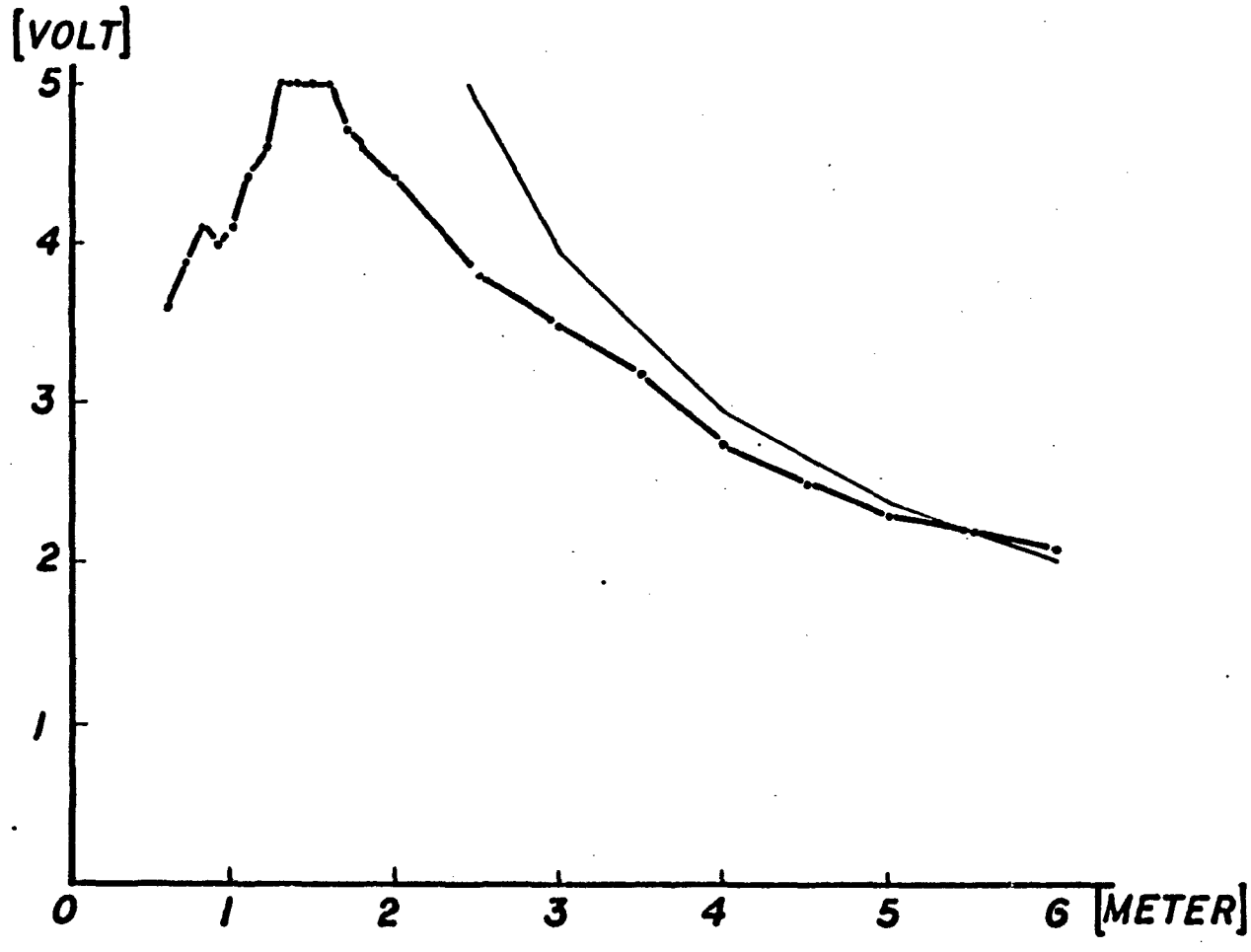

Fig. 4-2
On-axis primary peak voltage amplitude

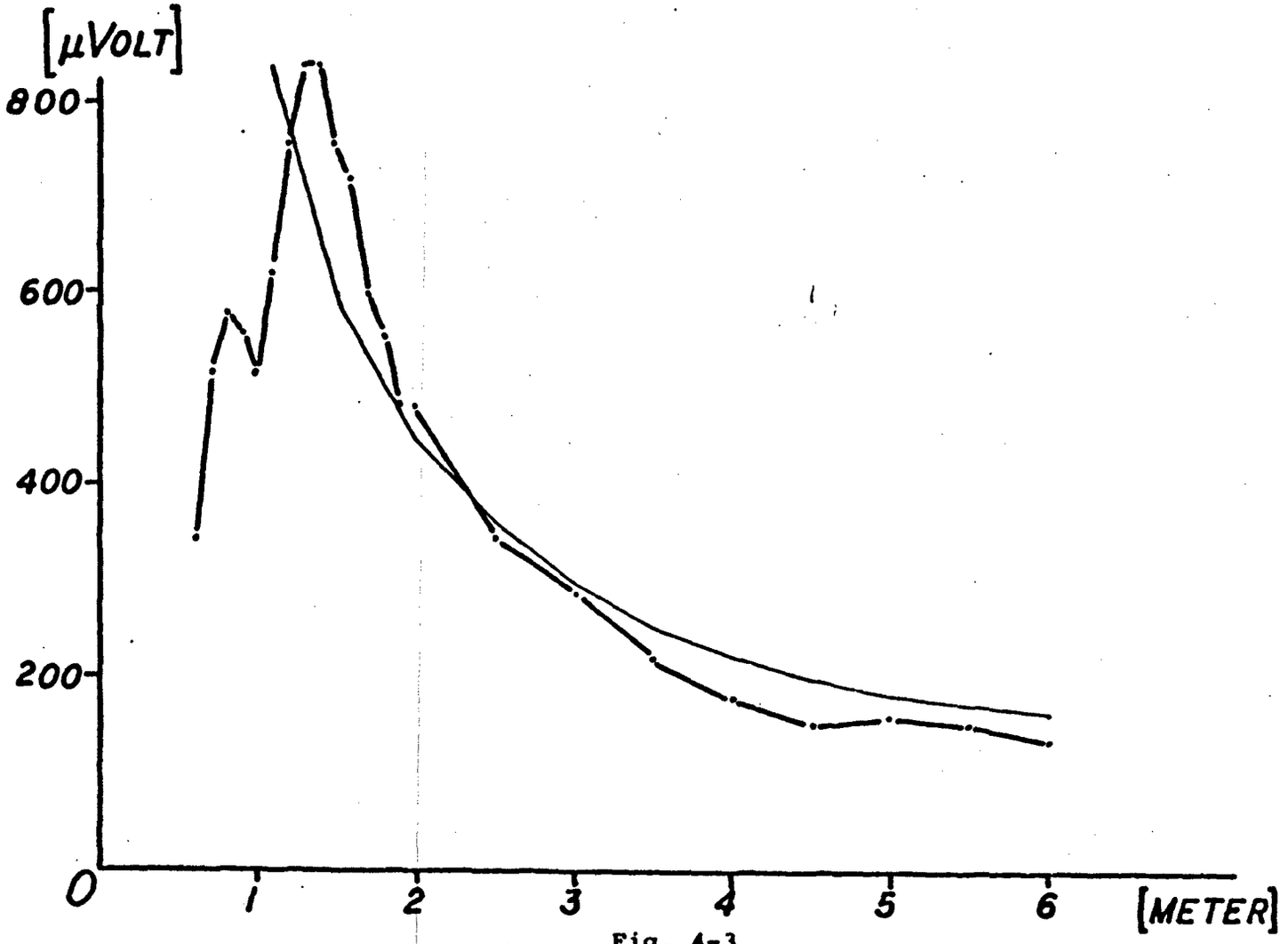

Fig. 4-3
On-axis secondary peak voltage amplitude

shown in Figs. 4-4 and 4-5, respectively. The primary beam proved to be not perfectly collimated and evaluation of the data revealed an average -3dB beam width of 3.4 degrees. The secondary peak voltage amplitude cross-sections show a rather peculiar behavior. Instead of decreasing in amplitude at both sides of the beam axis, the peak voltage amplitude increases until it reaches a maximum value off-axis and then falls off faster than the peak voltage amplitude of the primary pulse. A similar behavior was observed by Moffet, Westervelt, and Beyer [Ref. 10, 11] when they rotated the transducer in their experiment and kept the hydrophone in a fixed position. They also offered a possible explanation for this phenomenon by suggesting that a spatial as well as temporal differentiation of the primary pulse is taking place. Berktay's original analytical development [Ref. 6] does not include this spatial differentiation primarily because he assumed a perfectly collimated beam. However, in the case of a sound source with finite directivity, the spread of the propagation vectors in the primary beam seems to make this effect plausible. Further substantiation of this theory is expected from a computer study on difference frequency propagation from a real source that was conducted but not yet published by D. Blackstock at the Applied Research Laboratory in Austin, Texas.

The composite graphs of the secondary beam cross-sections show that the off-axis maxima of the secondary

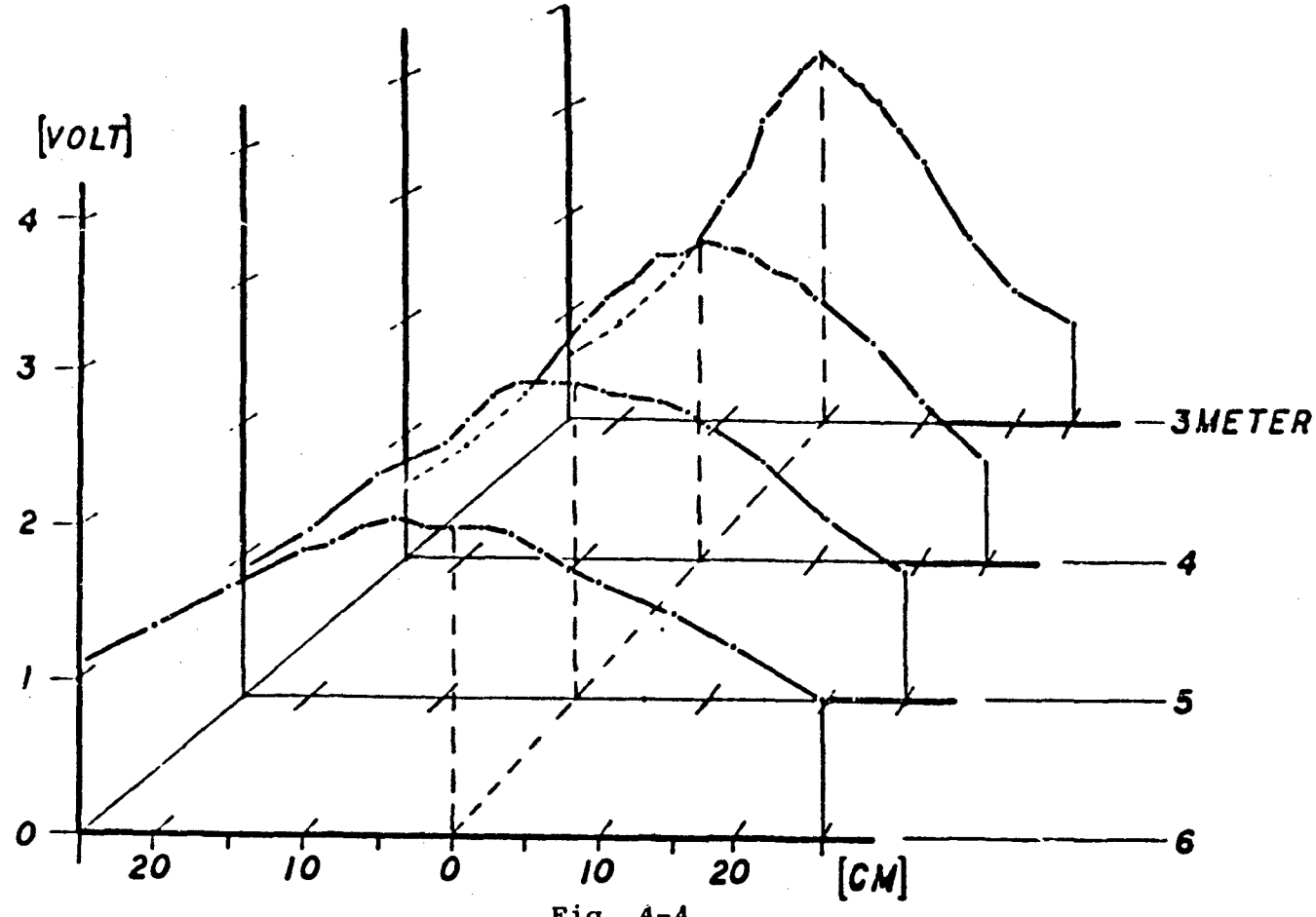

Fig. 4-4
Plot of line-in-cone transducer beam cross section as a function of range from source for primary pulse.

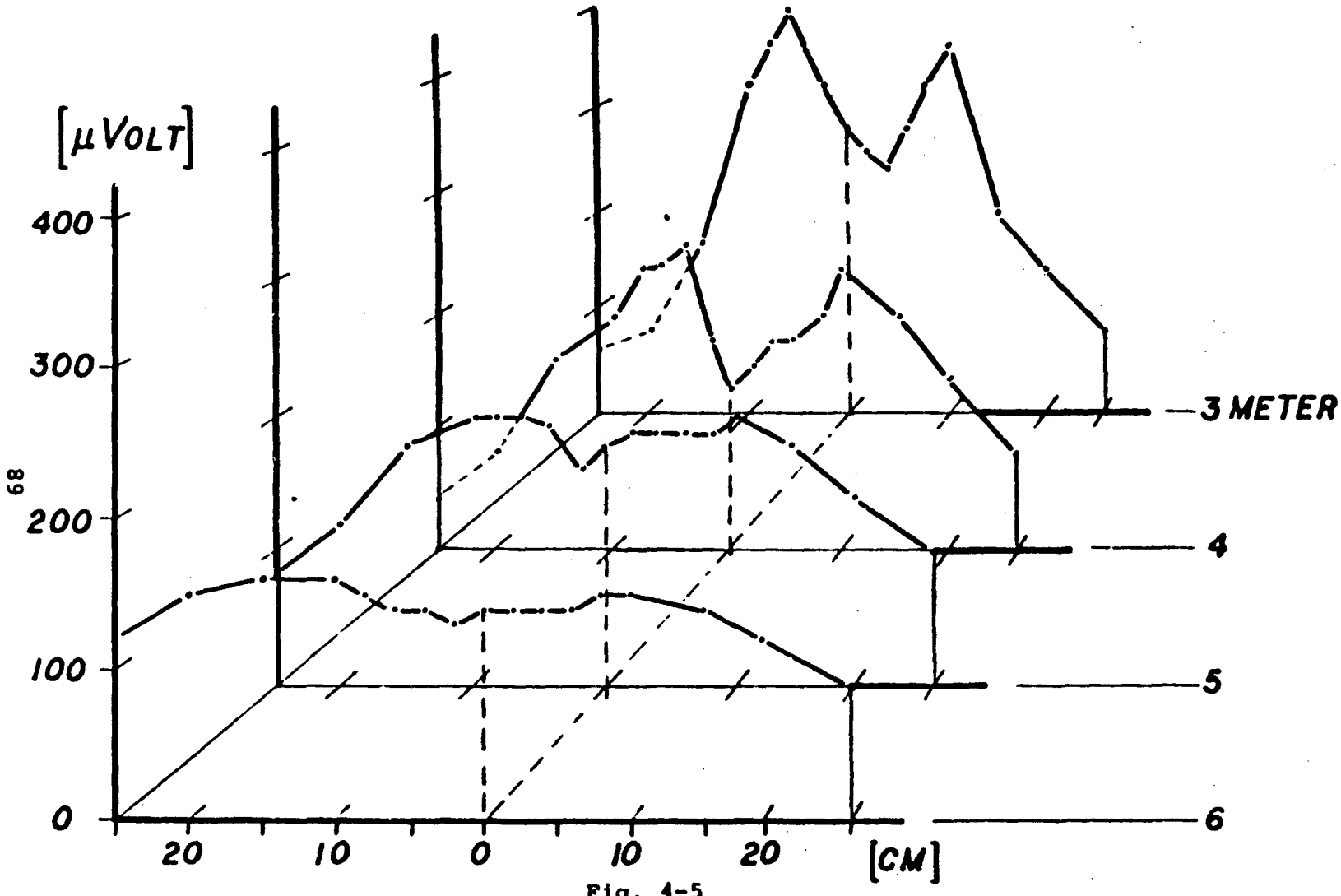

Fig. 4-5
Plot of line-in-cone transducer beam cross section as a function of range from source for processed secondary envelope without gain of 500.

peak amplitude decreases with increasing range and it is expected that they will completely disappear beyond a certain range. Despite the unorthodox beam shape, the -3 dB beam width of the secondary pulse was calculated at different ranges and a decrease of this beam width from 4.7 degrees at 3 meters to 4.3 degrees at 6 meters was noted. Unfortunately, the size of the tank limited the experimental distance, but projecting this trend of the -3 dB beam width to greater ranges shows that at approximately 15 meters distance from the source the secondary beam width will be on the order of the primary beam width with a single maximum on the projector axis.

E. MODELLING OF THE SOURCE

Based on the on-axis data and the beam cross-sections, an attempt was made to model the rather complex line-in-cone transducer as a circular plane piston and calculate effective source parameters from the experimental data. For this purpose it was decided to include the primary pulse data taken at 17.5 meters in the swimming pool. A beam pattern of the primary is shown in Fig. 4-6.

1. Effective Aperture

The effective radius of the ITC transducer was determined using equation 8.34 of Ref. 22 in conjunction with the last on-axis maximum of the primary pulse and using a primary frequency of 90.9 kHz as determined from

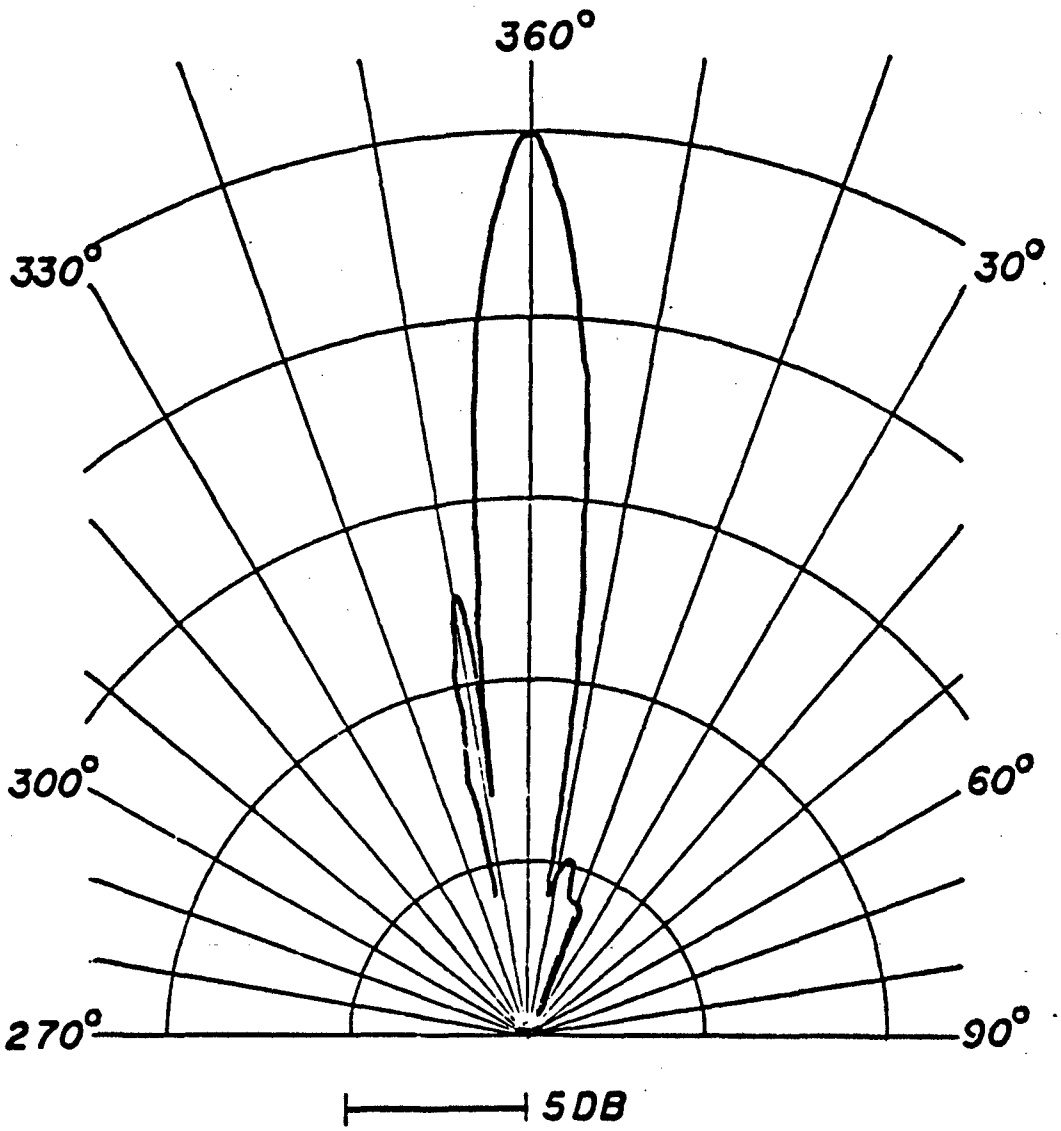

Fig. 4-6
Line-in-cone beam pattern at a range of 17.5 meters at 90.9 kHz.

oscilloscope photographs. The calculated values for the effective radius of the transducer range from 0.149 meters to 0.157 meters depending on the distance used for the on-axis maximum of the primary pulse. Evaluation of the -3 dB beam width of the primary pulse at different distances and using equation 8.36 of Ref. 22 resulted in an average effective radius of 0.145 meters. For further analysis in this paper, the plane piston model is used in describing the propagation of the primary pulse by assuming a 0.15 meter effective radius of the piston. The accuracy of this calculation is within 5 millimeters. To calculate an effective aperture of the source for the secondary pulse is futile since Berktay's theoretical development [Ref. 6] does not use an actual physical source but rather a source region of indeterminate length but with a finite cross-section. To calculate an effective cross-section for this source region further analysis will be made later in this thesis and the result will be presented and discussed later in this chapter.

2. Source Level

Based on the on-axis data of the primary pulse and using equation 8.37 of Ref. 18, the peak source level of the primary pulse was calculated. The sensitivity level of the receiver hydrophone was taken from Fig. 3-30. The source level of the primary was determined to be 229.8 dB re 1 micropascal which corresponds to a peak pressure of

3.09×10^5 Pa at 1 meter. The accuracy of this calculation is within 0.5 dB or 0.17×10^5 Pa. This source level was used in modeling the on-axis behavior of the secondary pulse.

3. Directivity

Based on the calculated effective radius of the transducer and calculating the magnitude of the propagation vectors, assuming a primary frequency of 90.9 kHz and a sound speed of 1481 m/s, the directivity of the transducer was found by using equation 8.51 of Ref. 22. A value of 35.4 dB for the directivity index was calculated and again the accuracy is within 0.5 dB.

F. ACOUSTIC POWER

Using the beam cross-section data, from Table 4-1 the acoustic power in the primary and processed secondary beam (without the gain of 500) was calculated by using the QTFG subroutine on the IBM 370/3033 AP of the Naval Postgraduate School. This program used the trapezoidal rule to perform integration on monotonically tabulated data. The integral used to determine the acoustic power was:

$$W = \frac{2\pi}{M^2 \rho c} \int_0^a V^2(r)\, r\, dr \qquad (4\text{-}3)$$

where:

W = acoustic power in Watts

M = hydrophone sensitivity in volts/Pascal

V(r) = peak voltage amplitude at distance r in meters from the axis

a = maximum distance from axis (0.25 meters)

$\rho c = 1.48 \times 10^{6}$ Pa.s/m [Ref. 22]

The acoustic power calculated at different ranges was as follows:

Distance from Source (M)	Primary Acoustic Power (Watts)	Secondary Acoustic Power (Watts)
3.0	861	14.45×10^{-6}
4.0	756	7.73×10^{-6}
5.0	756	7.01×10^{-6}
6.0	704	5.55×10^{-6}

The results show that the power in the secondary beam decreases faster than 1/R, an observation that must be viewed in context with the decrease in the off-axis maxima of the peak voltage amplitude with increasing distance from the source as described previously. In contrast to this rapid fall off, the primary power decreases slower with increasing range. The reduction is only 18% between 3.0 and 6.0 meters and may be regarded as a measure of the degree of collimation in the primary beam.

G. EFFECTS OF THE MEDIUM

In order to ensure that essed secondary pulse was actually due to the self-demodulation of the primary pulse, experiments were conducted to investigate the non-linear growth of the secondary pulse amplitude with respect to the primary peak pressure amplitude at 1.0 meter, and to observe the independent propagation through an interface. In addition, computer simulations were performed to analyze the pulse shape of the secondary as a function of the envelope of the primary pulse and the processing in the receiver system.

1. Non-linear Growth

The growth of the primary and secondary pulses with respect to input voltage was investigated at 3, 4, 5 and 6 meters distance from the source. The input voltage from the DC power supply was increased from 0 to 400 VDC in 40 volt steps. The receiver settings were the same as described in Section C of this chapter. The recorded data at the various ranges are plotted in Figs. 4-7 through 4-10. The data show a perfectly linear behavior of the primary peak voltage amplitude with respect to the input voltage. The secondary peak voltage amplitude grows non-linearly and evaluation of the data shows an average value for the exponent of 1.6. That implies that the secondary peak voltage is dependent on the primary peak voltage raised to the power of 1.6 since the primary peak voltage amplitude behaved linearly with the

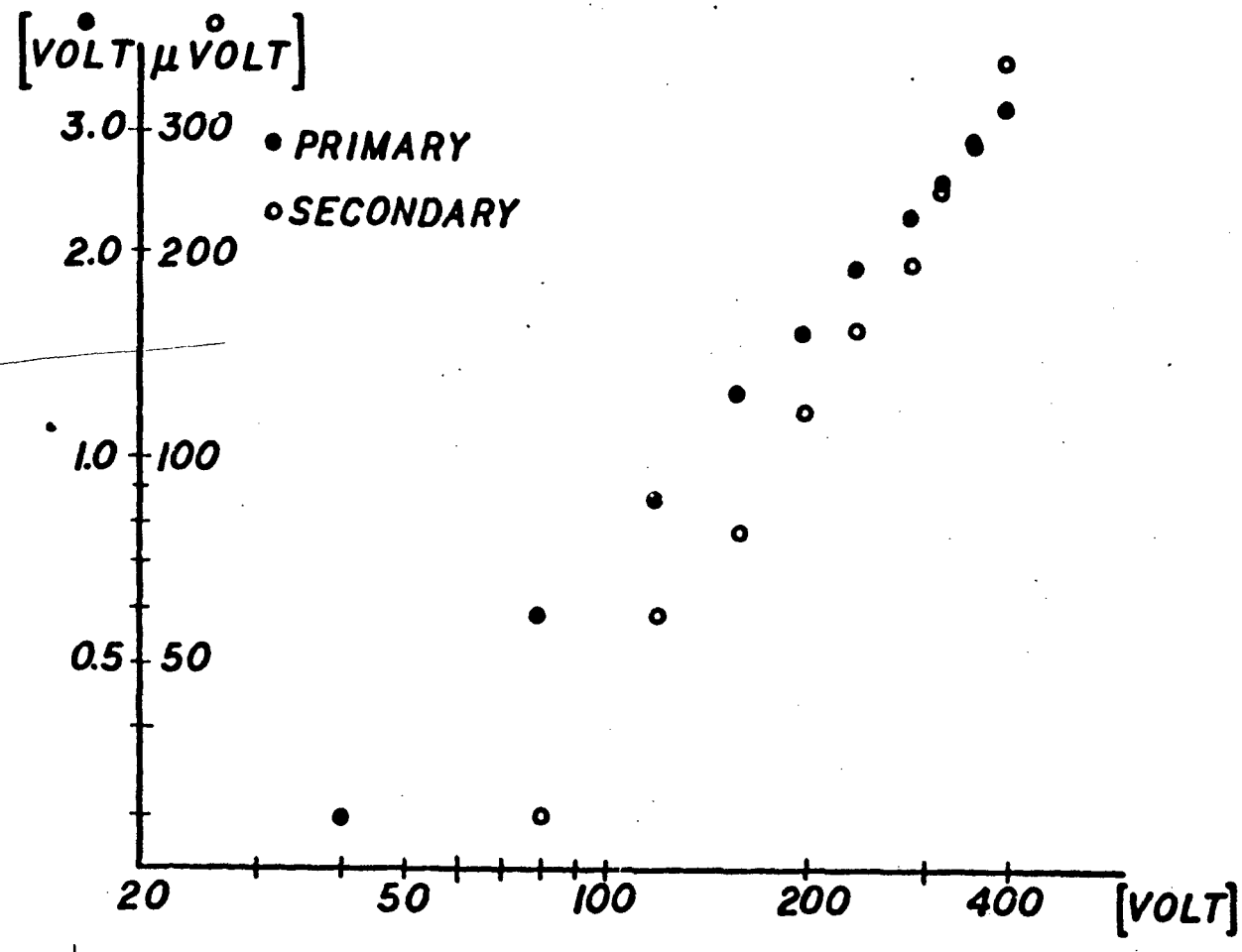

Fig. 4-7
Primary and secondary peak voltage amplitude as a function of drive voltage at a range of 3 m.

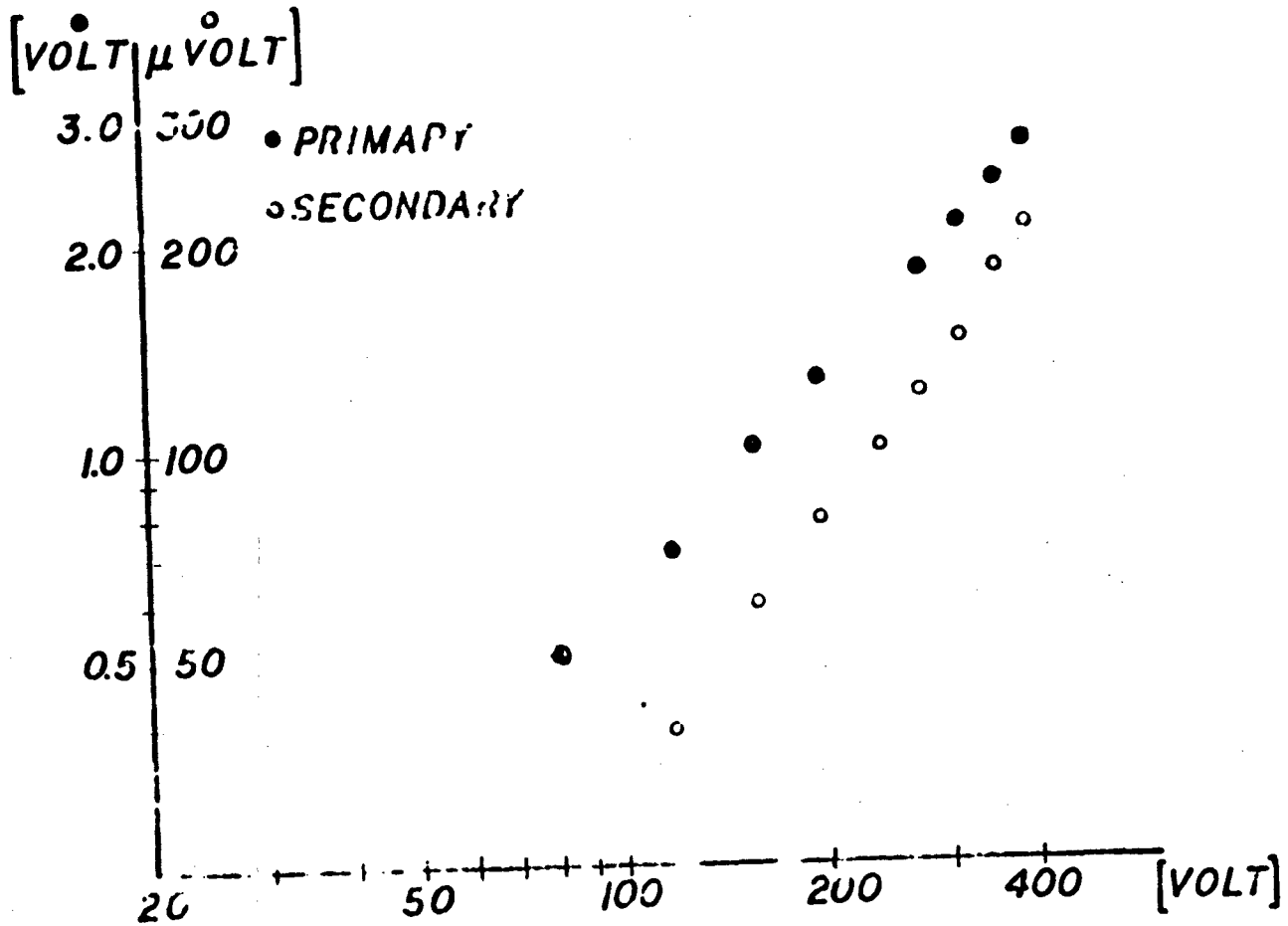

Fig. 4-8
Primary and secondary peak voltage amplitude as a function of drive voltage at a range of 4 m.

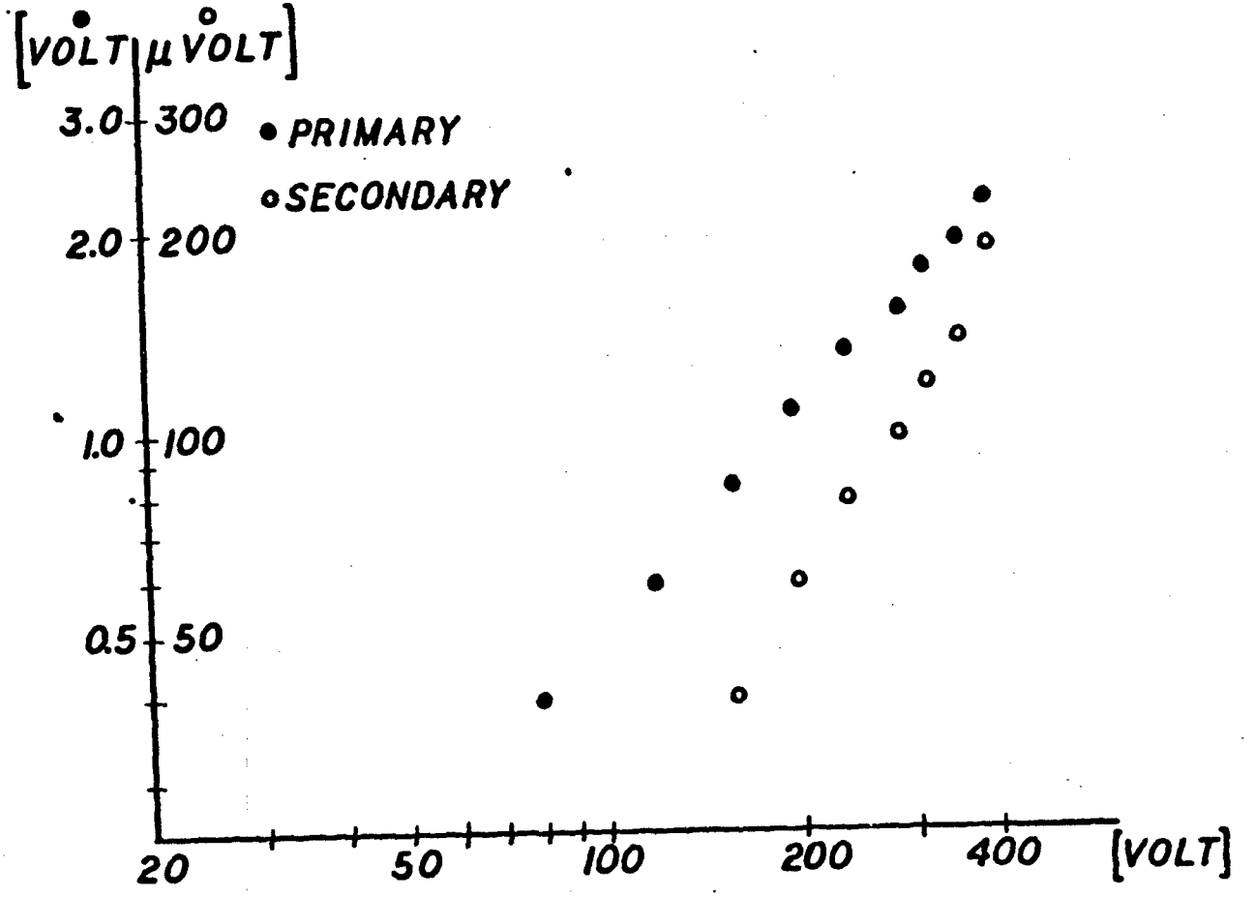

Fig. 4-9
Primary and secondary peak voltage amplitude as a function of drive voltage at a range of 5 m.

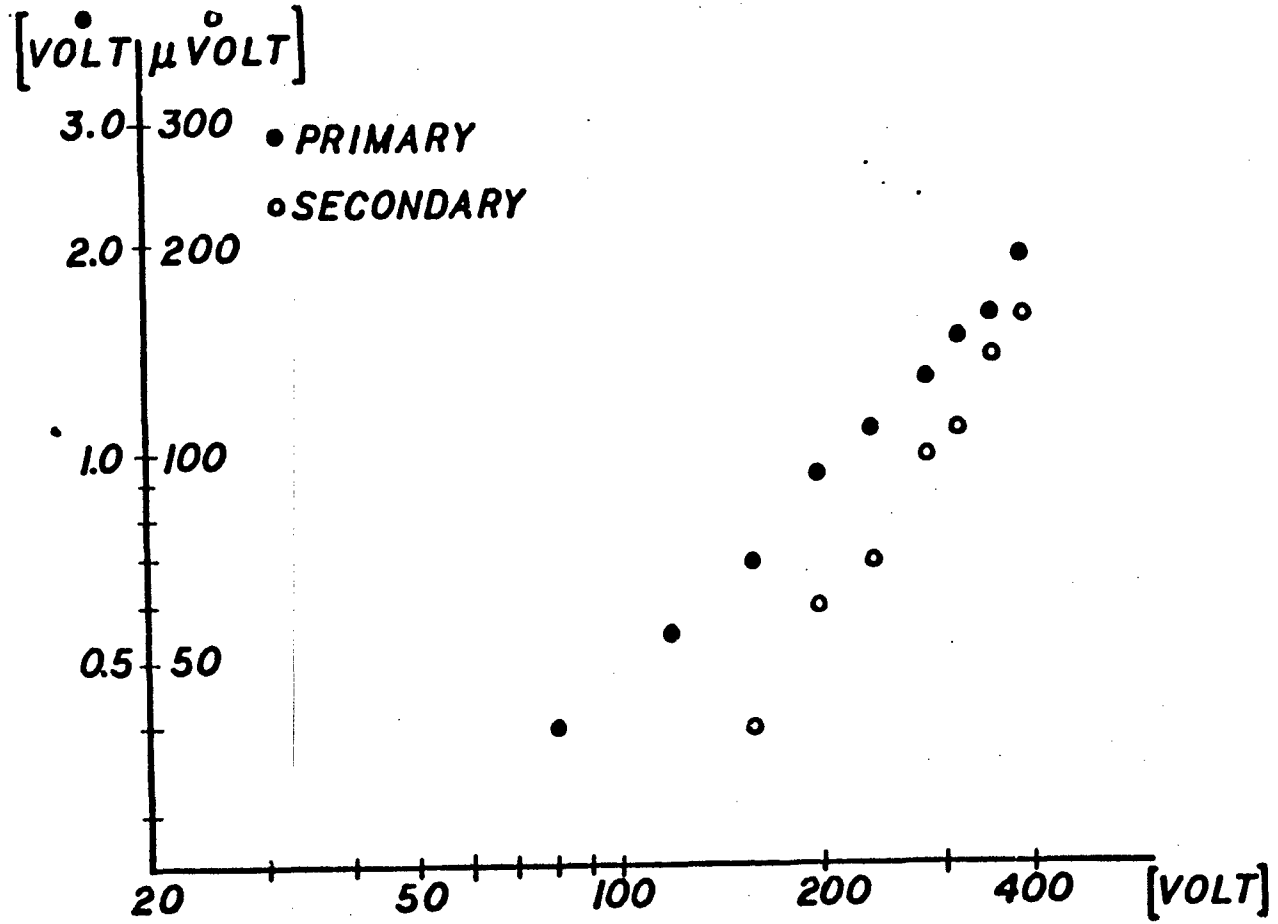

Fig. 4-10
Primary and secondary peak voltage amplitude as a function of drive voltage at a range of 6 m.

input voltage. The ideal exponent is 2.0 as found by Berktay [Ref. 6], but due to the not perfectly collimated primary beam, one expects spreading losses and, therefore, the exponent must be less than 2.0. Again, this experimental value of 1.6 was used as an effective parameter value for further analysis.

2. Interface

The independent propagation of the two pulses through an interface was investigated by placing a steel plate of 2 mm thickness in the beam and taking beam cross-sections of the primary and secondary peak voltage amplitudes then comparing those to cross-sections taken without the steel plate. The receiver hydrophone was placed 3.0 meters from the source and the receiver system settings were as previously described. The primary and secondary voltages were recorded and photographs of the oscilloscope presentations were taken. The steel plate was then placed between the source and receiver at a point 0.7 meters from the hydrophone. The same cross-sections were taken again and the photographs were repeated. Without the plate, received peak primary and peak secondary voltage amplitudes were 3.4 volts and 0.12 volts, respectively. With the steel plate, the amplitudes were 1.8 volts and 0.11 volts, respectively. Thus, the steel plate caused a 47% reduction in the received primary peak voltage on axis, while the secondary peak voltage amplitude experienced only a very

minute reduction. The photographs are shown in Fig. 4-11. Another interesting result of this experiment is that the off-axis maxima had disappeared, but the on-axis secondary peak voltage amplitude had not changed by any significant amount.

3. Computer Simulation

Berktay's theoretical development [Ref. 6] shows that the secondary pulse is proportional to the second time derivative of the square of the envelope of the primary pulse. To ensure that the observed secondary pulse that was processed through the receiver system shows this proportionality, a computer simulation of the receiver system was generated. For this purpose, the envelope of the primary pulse was developed from oscilloscope photographs, normalized to unit amplitude and digitized in 80 data points at 1 microsecond intervals. A smoothed graph of this envelope is shown in Fig. 4-12. Based on these eighty data points a five point numerical differentiation of the envelope was performed twice by using the DET5 subroutine on the IBM 370/3033 AP of the Naval Postgraduate School. A graph of the resultant pulse is shown in Fig. 4-13. As expected, the leading edge of the primary envelope created high frequency second derivatives since it is only 1.5 to 2 cycles of the primary frequency long. These frequency components are on the order of the primary frequency. The longer trailing edge of the primary envelope extends over 6 to 8

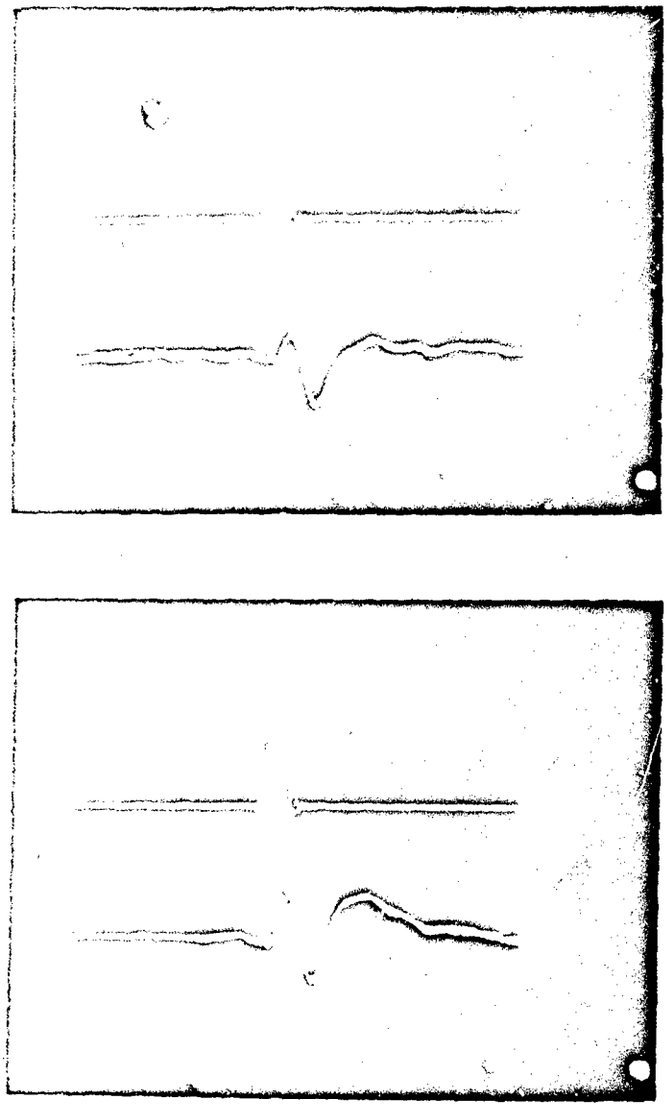

Fig. 4-11
Received primary pulse and processed secondary envelope at 3 meters with steel plate (top) and without plate (bottom). Vertical; (upper) 2 volts/cm, (lower) 0.1 volts/cm. Horizontal; 0.1 ms/cm.

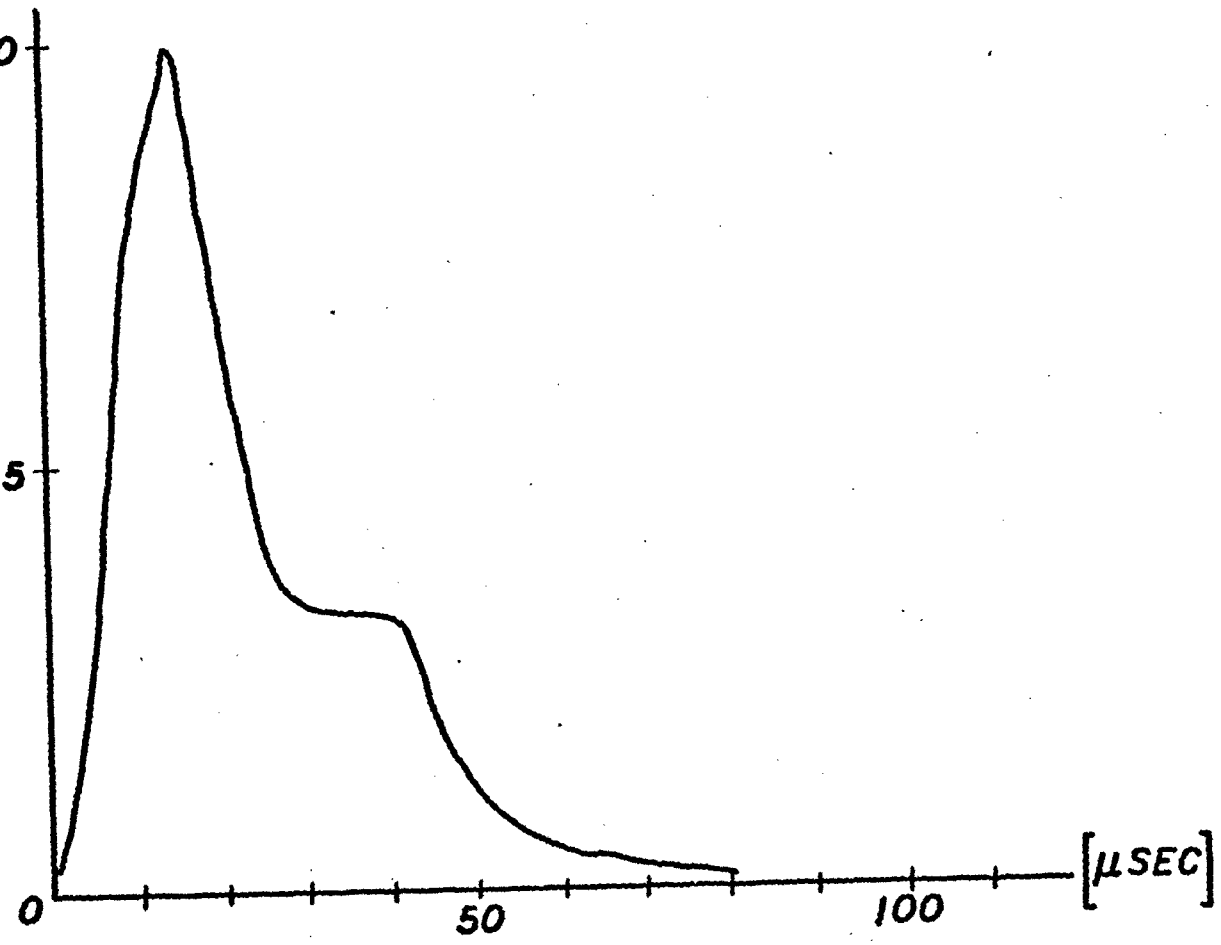

Fig. 4-12
Normalized envelope of the primary pulse.

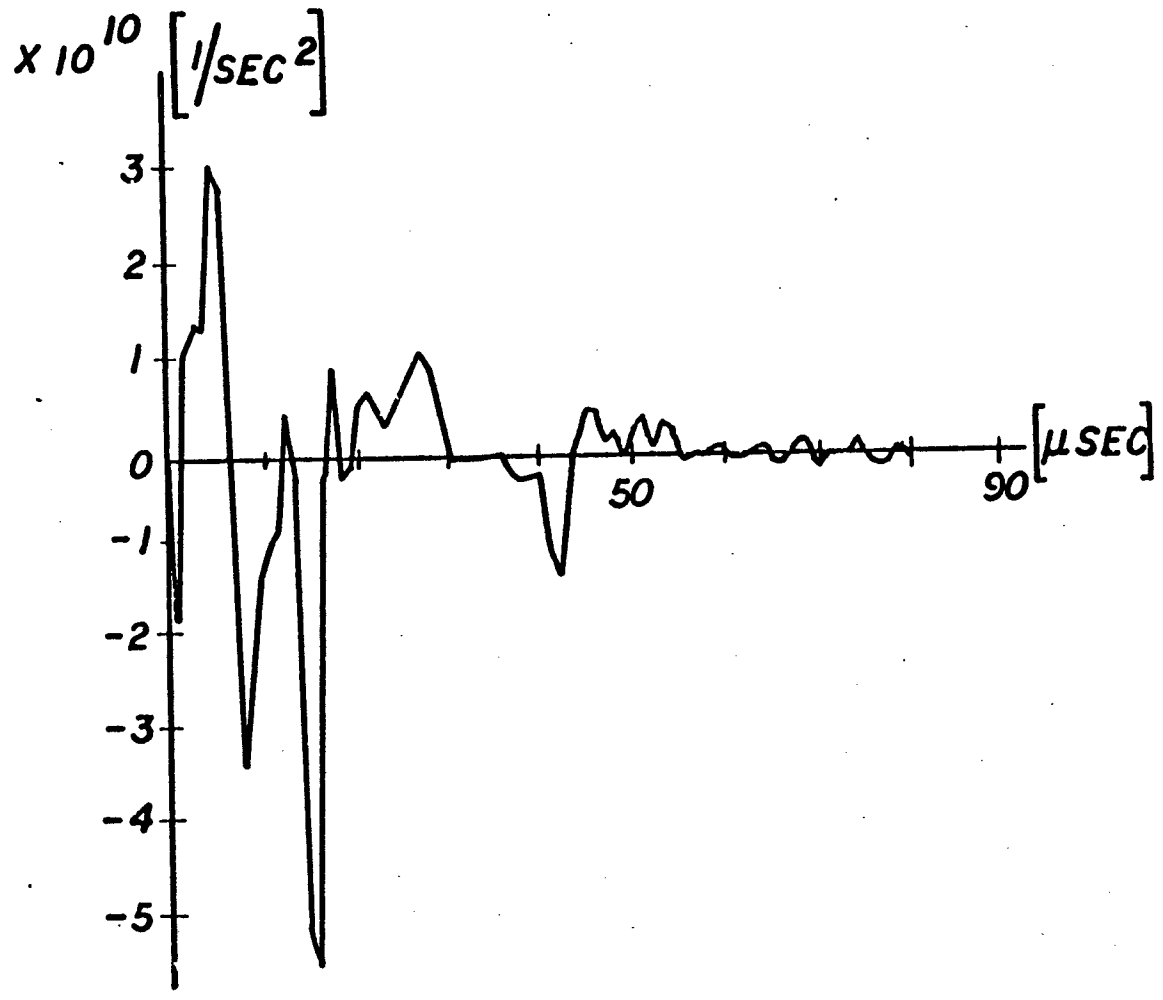

Fig. 4-13
Second time derivative of the square of the envelope of the primary pulse as shown in Fig. 4-12.

cycles of the primary frequency and produced second derivatives that are lower in amplitude and frequency as compared to the derivatives produced by the leading edge. These lower frequency components are on the order of 15 to 20 kHz and have an amplitude of $1.0 \times 10^{10}/sec^2$ to $1.5 \times 10^{10}/sec^2$. The following computer simulation of the low pass filter shows that these components form the major part of the observed processed secondary pulse. Before describing the simulation of the low pass filter it appears to be necessary to state once more the reason for using the filter on the receiving side: to simulate the attenuation of the medium over long distances by suppressing the high frequency components of the primary pulse. The calculated second derivative of the square of the primary pulse envelope was further processed by performing a numerical convolution with the impulse response of the low pass filter. To this end, the nodal equations of the circuit shown in Fig. 3-31 were developed and the impulse response of the low pass filter was computed using the IODE subroutine on the IBM 370/3033 AP. This subroutine solves systems of first order differential equations and allows the simulation of a delta function input. The impulse response computed by this program is shown in Fig. 4-14. The convolution of this impulse response with the second derivative was performed by an algorithm based on a numerical convolution technique [Ref. 26] which was modified for use on the IBM 370/3033 AP.

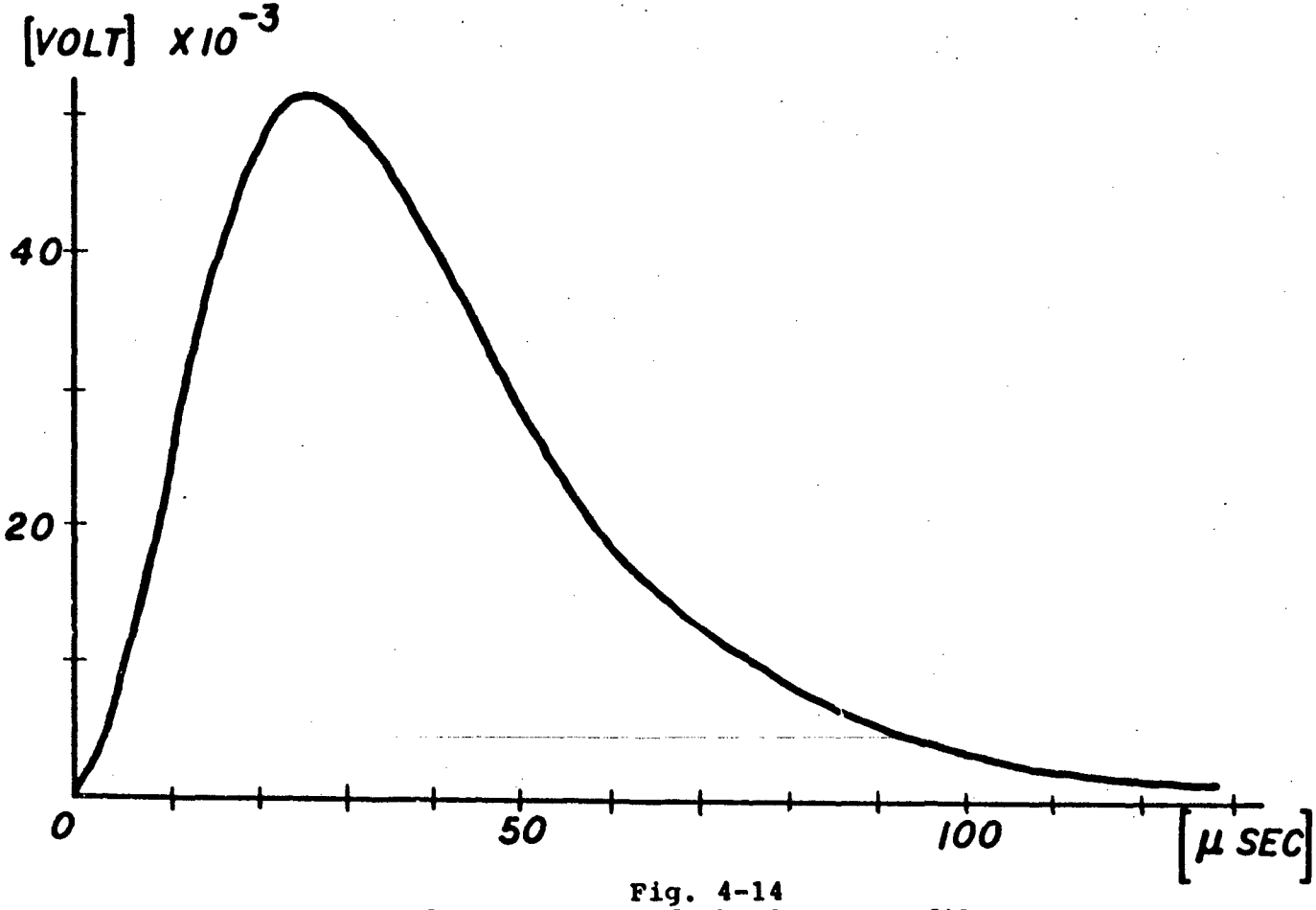

Fig. 4-14
Impulse response of the low pass filter.

The result of this convolution is shown in Fig. 4-15. As can be seen in this figure, the high frequency components are completely removed, the electronic time delay caused by the low pass filter is on the order of 40 to 50 microseconds and the shape of the pulse is already close to the secondary pulse shape observed. A one to one comparison is not appropriate since our computer simulation did not include the minute primary carrier frequency phase components that were also processed through the actual receiver system. It is also not possible to address one distinct secondary frequency as can be clearly seen from Fig. 4-15, although the main frequency component is on the order of 15 kHz. The maximum value of the second time derivative of the square of the primary envelope was determined to be approximately $2.5 \times 10^9/sec^2$ including compensation for the low pass filter. To account for the effects of the Krohn-Hite bandpass filter and the Ithaco bandpass amplifier no further computer simulation was performed. The incoherent attenuation and summing of the frequency and phase components by these filters makes any detailed simulation very complicated. Therefore, for further analysis a main frequency component of 15 kHz in the secondary pulse was assumed and the attenuation of both filters at this frequency and the gain of 500 were combined into one amplification factor. The Krohn-Hite bandpass filter has an attenuation of 15 dB at 15 kHz when set to a bandpass of 20 Hz to 10 kHz

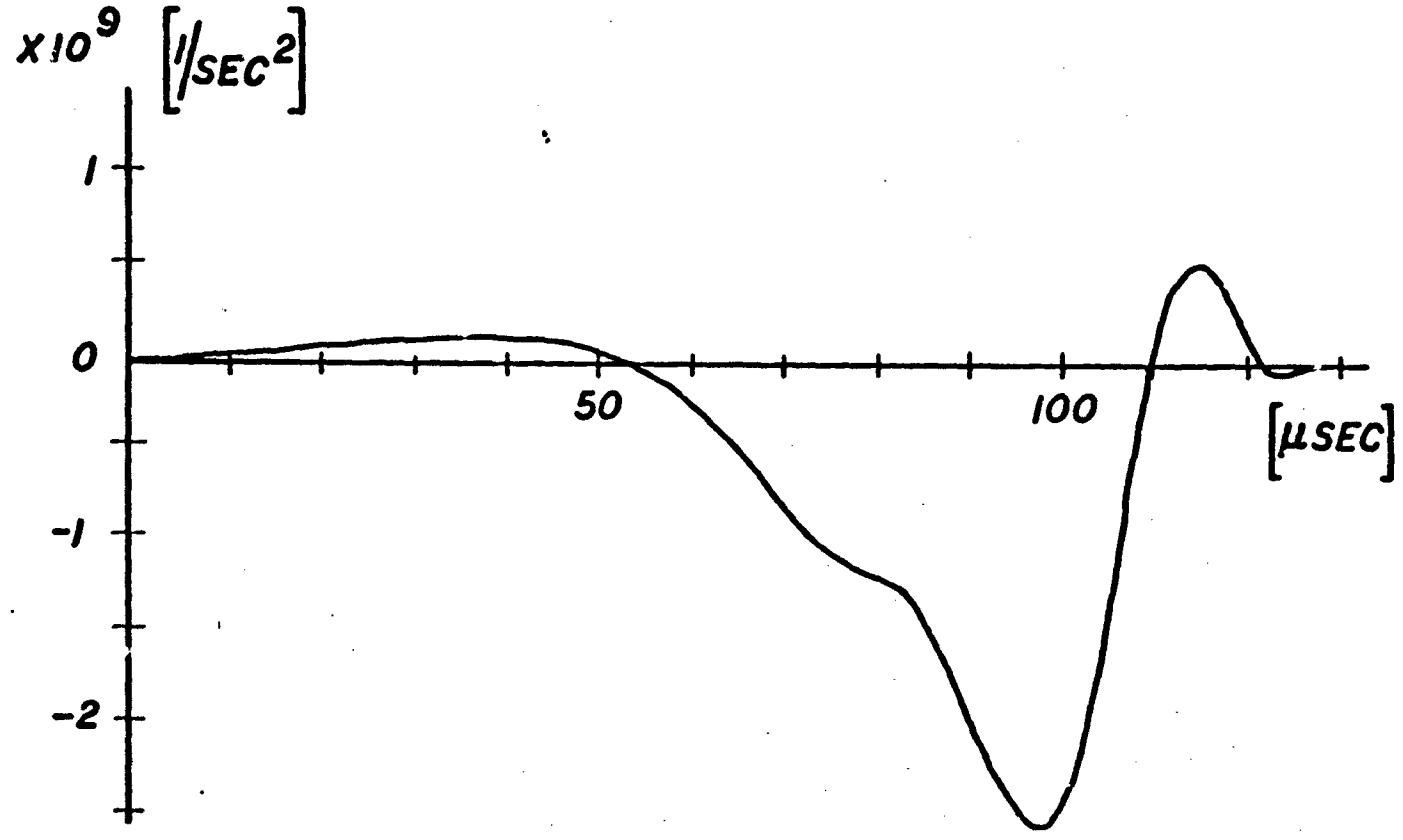

Fig. 4-15
The secondary pulse after convolution of the pulse shown in Fig. 4-13 with the impulse response shown in Fig. 4-14.

[Ref. 27]. The Ithaco bandpass amplifier has an attenuation of 6 dB at 15 kHz when set to DC to 10 kHz [Ref. 28]. Including the gain of 500, the total gain of the two filters was determined to be 33 dB with an estimated accuracy of 1.0 dB. Another effect of the two filters was that the main observed frequency component was shifted from 15 kHz to approximately 5 kHz by the selected band pass. In addition, the two filtering processes and the amplification causes further electronic time delay on the order of 100 microseconds.

4. Spectrum Analysis

Presence of the self-demodulation effect and its relative amplitude are indicated in Fig. 4-16. These photos were taken in the anechoic tank with the LC-10 hydrophone located 3 meters from the ITC transducer. The receiver circuit was configured as described in Chapter III. The displayed bandwidth is DC to 25.6 kHz.

The top photograph shows the spectrum of the background noise present (transmitter turned off). The level of the displayed spectrum ranges from -65 dB re 1 volt at DC to -80 dB re 1 volt at 20 kHz. The slight "hump" apparent in the photograph terminates at 11.25 kHz.

For the lower photograph, the transducer was in operation. The spuctral level ranges from -60 dB re 1 volt at DC to -75 dB re 1 volt at 20 kHz. Over the frequency

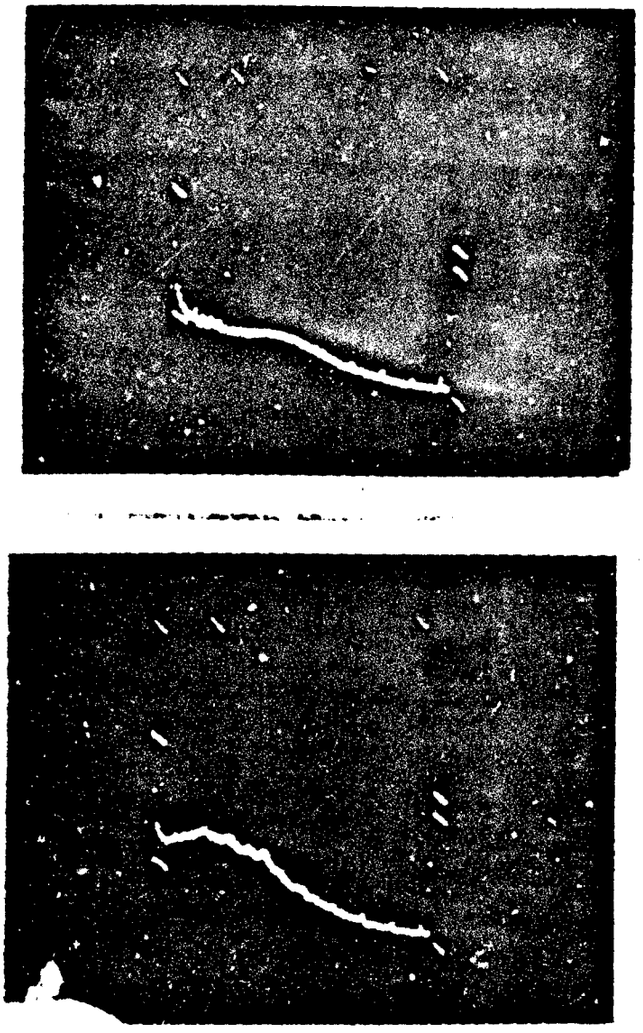

Fig. 4-16
Frequency spectrum of background noise (top) and ITC transducer (bottom) as seen at receiver circuit output. Displayed bandwidth 0-25.6 kHz. Difference between spectrums on vertical scale is approximately 10 dB.

range DC to 11.25 kHz, the difference between the spectrums is greater than 5 dB and less than or equal to 10 dB.

This indicates that the transducer does produce detectable low frequency spectral components which are believed to result from pulse self-demodulation, as the only other low frequency component known to be present was the 25 Hz pulse repetition rate. Further, considering the gain of 500 (54 dB) applied to the received signal by the Ithaco band pass amplifier, the true received voltage level at 3.75 kHz is approximately -114 dB re 1 volt. This equates to a received RMS voltage of 2 microvolts, which is consistent with theoretical voltage amplitudes for the pulse self-demodulation effect.

H. EFFECTIVE ON-AXIS EQUATION

The preceding presentation of the experimental data and their analysis now permits a comparison with Berktay's theory and a modification of it as applied to this system. Berktay bases his theory on several assumptions that are summarized as follows:

(a) the normalized envelope function of the primary pulse varies slowly with respect to the primary frequency; i.e., the frequency components of the envelope function are well separated from the carrier frequency.

(b) the attenuation constant for all frequencies can be taken to be the attenuation constant of the carrier

frequency because the envelope function covers only a relatively small frequency band.

(c) the primary wave is considered to be a plane wave and the primary beam is collimated. For cylindrically or spherically spreading waves, his expression for the on-axis pressure of the secondary pulse is valid provided the -3 dB beam width does not exceed the value given by equation I.13 of Ref. 6. For a narrow primary beam, the results should be similar.

(d) the attenuation of the secondary pulse is negligible.

(e) the cross-sectional area of the primary column is small compared to the wavelength of the frequencies of interest; i.e., the main frequency component of the secondary pulse.

Under these conditions, the peak pressure of the secondary pulse along the axis of the beam is given by equation IV.9 of Ref. 6:

$$P(r,f) = \left(1 + \frac{B}{2A}\right) \frac{P_1^2 S}{8\pi \rho c^4 \alpha r} \frac{d^2}{dt^2}\left[f^2\left(t - \frac{r}{c}\right)\right] \qquad (4\text{-}4)$$

where:

P(r,t) = the on-axis peak pressure amplitude of the secondary pulse in Pascals

B/A = parameter of non-linearity; which for this case was taken to be 5.2 [Ref. 29]

P = the initial peak pressure amplitude of the primary pulse at 1 meter in Pascals

S = the cross-sectional area of the primary beam column

ρ = the density of the water (998 KG/m^3) [Ref. 22]

c = speed of sound (1481 m/s)

α = absorption coefficient of the carrier frequency (196.6 x 10^{-6} x 10^{-6} Np/m) [Ref. 18]

r = range in meters from the source

Comparing the primary pulse envelope and the primary beamwidth produced by the ITC transducer with Berktay's assumptions reveals two violations:

(a) the leading edge of the primary pulse produced frequency components that were not well separated from the carrier frequency, but these were filtered out in the receiver system.

(b) the -3 dB beamwidth of the primary pulse exceeded the limit given by equation I.13 of Ref. 6, but was sufficiently narrow to expect similar results.

The last effective parameter that had to be determined in order to modify Berktay's equation was the effective cross-sectional area of the primary column. Solving equation 4-4 for S by using the values found in the experimental data and computer simulation, the average effective

cross-sectional area of the primary column was determined to be approximately 1.4×10^{-3} square meters. This corresponds to a circle of 2.1 centimeter radius. The calculation was made using the following values and assumptions:

(a) the on-axis secondary peak pressure amplitude decreases inversely with distance from the source.

(b) the peak pressure amplitude of the primary column is 3.09×10^{5} Pa at 1 meter, the source level of the primary beam.

(c) the extent of the source region is the immediate near-field of the transducer, which was found to be approximately 1.5 meters.

(d) the sensitivity of the hydrophone for the secondary pulse was taken to be that at 15 kHz.

(e) the effective exponent for the primary peak pressure amplitude is 1.6 vice 2.0.

(f) the value of the second time derivative of the square of the envelope, including compensation for the low pass filter was $2.5 \times 10^{9}/\text{sec}^{2}$.

(g) the total gain in the receiver system was 33 dB.

(h) all other parameter values were as previously noted.

The diameter of the effective cross-section is indeed less than a wavelength of the main frequency component of the secondary pulse as postulated by Berktay. This effective cross-sectional area, together with the other effective parameters determined in the analysis, allows one to modify

Berktay's on-axis equation to obtain good approximate values of the on-axis peak pressure amplitude of the secondary pulse for ranges beyond those available in the experimental set-up. The beamwidth of the secondary pulse can be expected to be on the order of the primary for ranges beyond 15 meters. Based on this evaluation, a virtual source level for the secondary pulse at 1 meter from the source (excluding the receiver gain) was calculated to be 320 Pascals, which is on the order of 10^{-3} smaller than the primary source level. This result is approximately one order of magnitude higher than the estimation given in Chapter II. Table 4-11 shows a comparison of the values calculated using equation 4-4 as modified by the effective parameters and "driven" through the receiver system with the peak voltage levels of the secondary as seen on the oscilloscope.

I. ACOUSTIC TEST FACILITY RESULTS AND ANALYSIS

Several interesting and confirming results were obtained during experimentation at the Acoustic Test Facility (ATF). The following discussion addresses the three experiments conducted with a view to demonstrate the practicality of using the pulse self-demodulation effect in a sub-bottom profiling sonar system.

1. Bottom Reflection

At the ATF, the system was set up as described in Chapter III. The first experiment consisted of simply

Table 4-11

CALCULATED AND OBSERVED SECONDARY VOLTAGE AT VARIOUS RANGES

Distance from Source (M)	Calculated Secondary Peak Voltage (V)	Observed Secondary Peak Voltage (V)
2.0	0.25	0.24
2.5	0.20	0.17 - 0.22
3.0	0.17	0.14 - 0.20
3.5	0.15	0.11 - 0.16
4.0	0.13	0.07 - 0.13
4.5	0.11	0.07 - 0.14
5.0	0.10	0.08 - 0.10
5.5	0.09	0.08 - 0.095
6.0	0.08	0.005 - 0.08

pointing the transmitter and receiver at the bottom directly below the test barge. Fig. 4-17 shows the received echo for this test. At first, the approximately 140 microsecond delay between the leading edges of both waveforms was thought to be due to the unknown sediment depth. Upon closer examination and comparison of Fig. 4-17 with Fig. 3-32, however, the time delay was deemed as probably attributable to the electronic time delay in the receiver circuitry. Unfortunately, the sediment depth and composition at this particular location is not known.

2. Focused Sphere Experiment

For the focused 8 inch diameter sphere experiment, the sphere was suspended via a nylon rope and net so that the sphere position with respect to the sediment could be coarsely controlled. The sphere is filled with a mixture of ethanol and freon and is approximately 14 N negatively bouyant in water. Sound speed in the sphere is approximately 800 m/s. In Fig. 4-18, the sphere position is approximately 0.75 meters above the sediment surface. The first, small primary reflection is the sphere.

The sphere was lowered to the sediment and appeared to penetrate the sediment, as denoted by a slight slackening of the support line and a visible "distortion" of the secondary waveform which appeared to propagate through the waveform as the sphere was lowered further. This "distortion" appeared as a small amplitude waveform very similar in

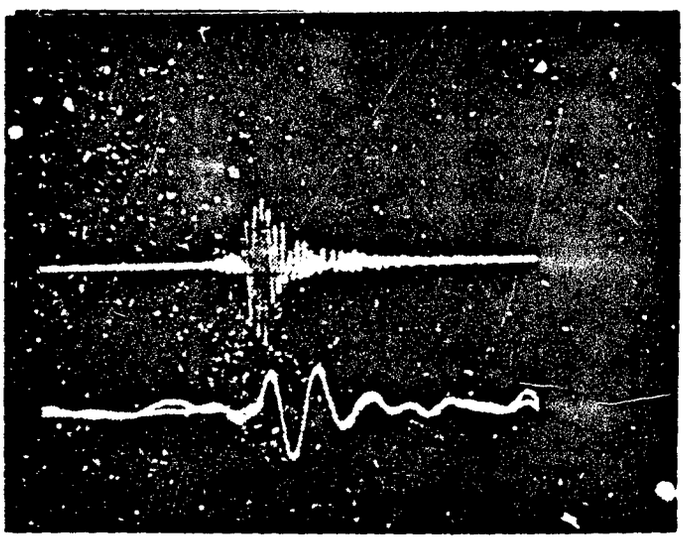

Fig. 4-17
Received primary pulse and processed secondary envelope at r=7 meters. Bottom reflection, Acoustic Test Facility, Keyport, Wa. Vertical; (upper) 0.05 volts/cm, (lower) 0.02 volts/cm. Horizontal; 0.1 ms/cm.

shape to the secondary waveform shown in Fig. 4-18 and superposed on it.

When the support line went completely slack, the time delay between the leading edge of the primary and the processed secondary return from the sphere was measured to be approximately 350 microseconds. Assuming the time delay is directly attributable to sediment penetration results in a sediment surface to sphere depth of (350 microseconds x 1491 m/s) approximately 0.52 meters. Given a 20.3 centimeter diameter sphere, this would imply a sediment depth of at least 0.75 meters.

On the other hand, if it is assumed that approximately 140 microseconds of the time delay is attributable to receiver circuit electronic delay as mentioned earlier, then the remaining 210 microseconds equates to a sediment depth of 0.31 meters. Adding in the sphere diameter results in a minimum sediment depth of approximately 0.54 meters. The actual sediment depth at the sphere's location (which was not directly below the source) was crudely measured by divers to be approximately 0.54 meters.

A closer examination of Fig. 4-17 yields a possible small amplitude secondary return whose time delay is about 440 microseconds. Subtracting electronic delay, this would equate to a sediment depth of 0.45 meters directly below the source. These small amplitude returns are not

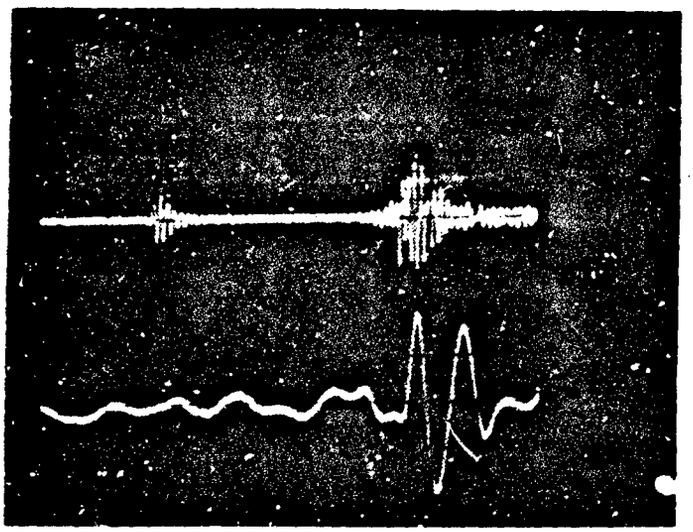

Fig. 4-18
Target sphere and sediment surface reflection, Liberty Bay tests. Sphere approximately 0.75 meters above sediment surface. Scales: Vertical (upper) 0.5 volts/cm, (lower) 0.01 volts/cm; Horizontal 0.1 ms/cm.

inconsistent considering the increased attenuation presented by the unconsolidated sediment even at lower frequencies.

These experiments lend credence to the assumptions that; (a) the electronic time delay is approximately 140 microseconds in duration, and more importantly, (b) pulse self-demodulation effects are present and are of sufficient amplitude to allow detection of objects buried in sediments, though considerably more receiver gain will probably be required for objects buried more deeply in the sediment.

3. MK 46 Torpedo Experiments

Two experiments were conducted at the ATF using an inert, nearly neutrally bouyant MK 46 torpedo. For the first experiment, the torpedo was oriented such that it was perpendicular to the direction of sound propagation from the source. For the second experiment, the torpedo was parallel to the direction of propagation. Fig. 4-19 (bottom) shows the received echoes for the perpendicular orientation and Fig. 4-20 shows the received echoes for the parallel orientation. A check by divers verified that the torpedo did not sink into the sediment in either experiment.

The most notable feature in both figures is the 180 degree phase shift apparent in the secondary signal returns, compared to the transmitted pulse and sphere returns. This phase shift, which is typical for a pressure release reflection, is consistent since the dummy torpedo does contain several finite air masses in the propulsion, control and

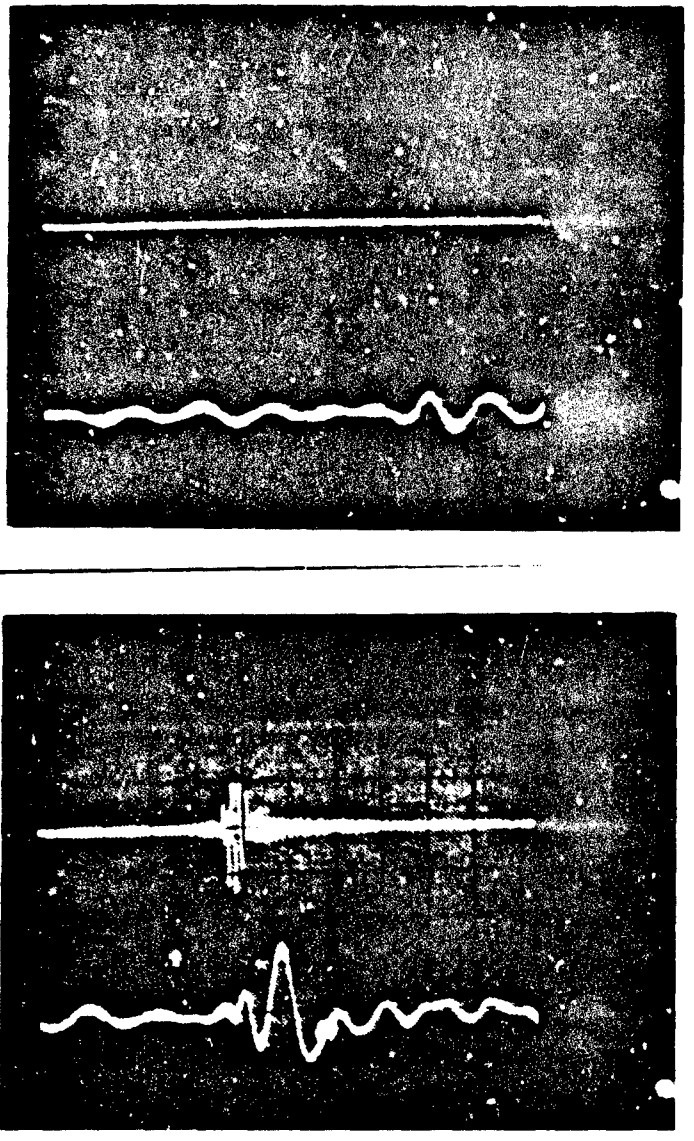

Fig. 4-19
Received primary pulse and processed secondary envelope at 7 meters for no torpedo (top) and torpedo lateral to source (bottom). Vertical; (upper) 0.2 volts/cm, (lower) 0.02 volts/cm. Horizontal; 0.1 ms/cm.

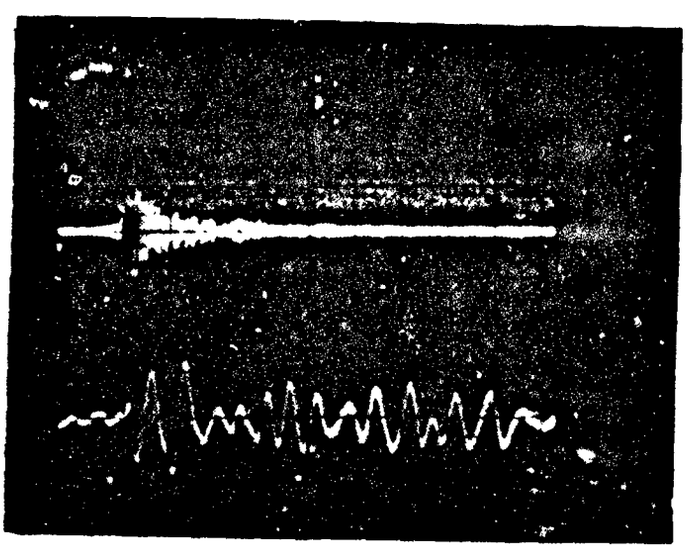

Fig. 4-20
Received primary pulse and processed secondary envelope at 14 meters with torpedo longitudinal to source. Vertical; (upper) 0.5 volts/cm, (lower) 0.1 volts/cm. Horizontal; 0.2 ms/cm.

voided fuel tank sections. This phase shift is not apparent in the primary signal returns. This indicates that a future sub-bottom high resolution sonar system utilizing this technique would not only be able to detect objects in the unconsolidated sediments, but would also be able to classify them to some extent.

Another notable feature of Fig. 4-19 is apparent when it is understood that both photographs display the same time period; i.e., no receiver controls were altered. In the top photograph, a secondary echo occurs approximately 360 microseconds later than the torpedo reflection shown in the bottom photograph. This equates to a propagation distance of approximately 0.54 meters. The diameter of a MK 46 torpedo is approximately 0.32 meters. The 0.22 meter discrepancy can be partially accounted for by the geometry of the experiment, which required the source to be tilted to approximately a 42 degree angle with respect to the local vertical in order to be aimed at the target.

Fig. 4-20 displays another interesting effect for the parallel target case. From the photograph, it can be seen that the duration of the secondary return is about 1.7 milliseconds, which equates to a propagation distance of (1.7 ms x 1491 m/s) approximately 2.53 meters. A MK 46 torpedo is 2.59 meters in length. The obvious implication is that a future sub-bottom imaging system may be capable of discerning target orientation in the sediment via echo

duration for the secondary return. No such pulse stretching was observed for the primary high frequency echo which is typical of specular reflections from extended objects.

Therefore, the ATF experiment demonstrated to a great extent the feasibility of utilizing the pulse self-demodulation effect in a sub-bottom high resolution sonar system. Further, the accuracy and target discrimination demonstrated by this system during the experiments make it highly suited for this particular application.

Table 4-1

HORIZONTAL BEAM CROSS SECTION DATA AT 2 METERS RANGE
(Preamplifier gain = 500)

Receiver Position Left or Right of Axis (cm)	Received Peak Voltage (Volts) Primary	Secondary
0	4.4	0.31
2 left	4.4	0.32
4 "	4.2	0.33
6 "	3.7	0.32
8 "	3.0	0.27
10 "	2.4	0.20
12 "	1.8	0.14
14 "	1.4	0.10
16 "	1.0	0.07
18 "	0.8	0.05
20 "	0.7	0.045
22 "	0.6	0.04
2 right	4.2	0.32
4 "	3.8	0.32
6 "	3.3	0.30
8 "	2.6	0.23
10 "	2.0	0.16
12 "	1.5	0.11
14 "	1.2	0.08
16 "	1.0	0.06
18 "	0.8	0.05
20 "	0.7	0.05
22 "	0.6	0.05

Table 4-2

VERTICAL BEAM CROSS SECTION DATA AT 2.0 METERS RANGE
(Preamplifier gain = 500)

Receiver Position Above or Below Axis (cm)	Received Peak Voltage (Volts) Primary	Secondary
0 above	4.4	0.31
2 "	4.0	0.33
4 "	3.4	0.29
6 "	2.6	0.24
8 "	2.2	0.20
10 "	1.8	0.14
12 "	1.3	0.08
14 "	1.0	0.06
16 "	0.95	0.05
18 "	0.9	0.05
20 "	0.8	0.05
22 "	0.6	0.04
2 below	4.5	0.32
4 "	4.4	0.34
6 "	4.2	0.36
8 "	3.8	0.32
10 "	3.0	0.22
12 "	2.3	0.14
14 "	2.0	0.12
16 "	1.7	0.10
18 "	1.5	0.07
20 "	1.2	0.06
22 "	1.1	0.05

Table 4-3

HORIZONTAL BEAM CROSS SECTION DATA AT 3 METERS RANGE
(Preamplifier gain = 500)

Receiver Position Left or Right of Axis (cm)	Received Peak Voltage (Volts) Primary	Secondary
0	3.5	0.12
2 left	3.4	0.14
4 "	3.2	0.17
6 "	3.0	0.18
8 "	2.6	0.18
10 "	2.2	0.17
15 "	1.4	0.10
20 "	0.8	0.06
25 "	0.4	0.04
2 right	3.5	0.11
4 "	3.4	0.12
6 "	3.1	0.14
8 "	2.8	0.16
10 "	2.6	0.17
15 "	1.7	0.13
20 "	1.0	0.07
25 "	0.4	0.04

Table 4-4

VERTICAL BEAM CROSS SECTION DATA AT 3 METERS RANGE
(Preamplifier gain = 500)

Receiver Position Above or Below Axis (cm)	Received Peak Voltage (Volts) Primary	Secondary
0	3.4	0.12
2 above	3.4	0.14
4 "	3.3	0.17
6 "	3.1	0.19
8 "	2.8	0.19
10 "	2.5	0.17
12 "	2.0	0.15
14 "	1.6	0.13
16 "	1.4	0.11
18 "	1.2	0.08
2 below	3.4	0.14
4 "	3.2	0.16
6 "	3.0	0.18
8 "	2.7	0.18
10 "	2.4	0.17
12 "	2.0	0.14
14 "	1.6	0.10
16 "	1.2	0.08
18 "	1.0	0.07

Table 4-5

HORIZONTAL BEAM CROSS SECTION DATA AT 3.5 METERS RANGE
(Preamplifier gain = 500)

Receiver Position Left or Right of Axis (cm)	Received Peak Voltage (Volts) Primary	Secondary
0	3.1	0.11
2 left	3.0	0.11
4 "	2.9	0.14
6 "	2.8	0.16
8 "	2.4	0.16
10 "	2.2	0.15
12 "	1.8	0.12
15 "	1.4	0.09
20 "	0.9	0.04
25 "	0.6	0.03
2 right	3.0	0.12
4 "	2.9	0.12
6 "	2.8	0.12
8 "	2.6	0.12
10 "	2.4	0.13
12 "	2.2	0.12
15 "	1.8	0.10
20 "	1.3	0.06
25 "	0.85	0.04

Table 4-6

HORIZONTAL BEAM CROSS SECTION DATA AT 4 METERS RANGE
(Preamplifier gain = 500)

Receiver Position Left or Right of Axis (cm)	Received Peak Voltage (Volts) Primary	Secondary
0	2.75	0.07
2 left	2.6	0.09
4 "	2.6	0.13
6 "	2.35	0.12
8 "	2.2	0.12
10 "	2.0	0.10
15 "	1.4	0.08
20 "	0.9	0.04
25 "	0.6	0.02
2 right	2.7	0.08
4 "	2.6	0.09
6 "	2.5	0.09
8 "	2.4	0.10
10 "	2.2	0.12
15 "	1.8	0.10
20 "	1.3	0.07
25 "	0.8	0.04

Table 4-7

HORIZONTAL BEAM CROSS SECTION DATA AT 4.5 METERS RANGE
(Preamplifier gain = 500)

Receiver Position Left or Right of Axis (cm)	Received Peak Voltage (Volts) Primary	Secondary
0	2.5	0.12
2 left	2.2	0.12
4 "	2.15	0.14
6 "	1.95	0.12
8 "	1.8	0.11
10 "	1.6	0.095
15 "	1.15	0.06
20 "	0.8	0.04
25 "	0.5	0.03
2 right	2.45	0.08
4 "	2.5	0.07
6 "	2.5	0.075
8 "	2.4	0.08
10 "	2.3	0.08
15 "	2.0	0.09
20 "	1.7	0.08
25 "	1.3	0.07

Table 4-8

HORIZONTAL BEAM CROSS SECTION DATA AT 5 METERS RANGE
(Preamplifier gain = 500)

Receiver Position Left or Right of Axis (cm)	Received Peak Voltage (Volts) Primary	Secondary
0	2.3	0.085
2 left	2.3	0.08
4 "	2.3	0.095
6 "	2.2	0.10
8 "	2.05	0.10
10 "	1.95	0.10
15 "	1.6	0.085
20 "	1.2	0.06
25 "	0.9	0.04
2 right	2.3	0.09
4 "	2.25	0.09
6 "	2.2	0.09
8 "	2.1	0.09
10 "	2.0	0.10
15 "	1.7	0.09
20 "	1.35	0.07
25 "	0.9	0.05

Table 4-9

HORIZONTAL BEAM CROSS SECTION DATA AT 5.5 METERS RANGE
(Preamplifier gain = 500)

Receiver Position Left or Right of Axis (cm)	Received Peak Voltage (Volts) Primary	Secondary
0	2.15	0.08
2 left	2.15	0.08
4 "	2.2	0.085
6 "	2.1	0.085
8 "	2.1	0.09
10 "	1.95	0.095
15 "	1.7	0.09
20 "	1.4	0.07
25 "	1.1	0.055
2 right	2.1	0.085
4 "	2.05	0.09
6 "	1.95	0.085
8 "	1.85	0.09
10 "	1.75	0.09
15 "	1.5	0.075
20 "	1.25	0.06
25 "	0.855	0.045

Table 4-10

HORIZONTAL BEAM CROSS SECTION DATA AT 6 METERS RANGE
(Preamplifier gain = 500)

Receiver Position Left or Right of Axis (cm)	Received Peak Voltage (Volts) Primary	Secondary
0	2.0	0.07
2 left	2.0	0.065
4 "	2.05	0.07
6 "	2.0	0.07
8 "	1.9	0.075
10 "	1.85	0.08
15 "	1.6	0.08
20 "	1.35	0.075
25 "	1.1	0.06
2 right	2.0	0.07
4 "	1.95	0.07
6 "	1.85	0.07
8 "	1.755	0.075
10 "	1.655	0.075
15 "	1.45	0.07
20 "	1.25	0.06
25 "	0.9	0.045

V. CONCLUSIONS AND RECOMMENDATIONS

The primary goal of this thesis was to design and construct a sub-bottom high resolution sonar utilizing the non-linear self-demodulation of a pulsed carrier to locate and resolve gross features of objects buried in unconsolidated marine sediments. This goal was apparently achieved although the system is not optimized and could not be tested under operational (deep water) conditions. The presentation shows that the self-demodulation effect can be employed in a real world environment and is in fact a very promising approach to solve the problem described in Chapter II of this thesis. It was also shown that the physics of the effect must be further analyzed to completely understand the propagation of the demodulated pulse from a real source. However, equation IV.9 of Ref. 6 can be modified by empirically developed parameter values in order to allow fairly accurate predictions of the secondary sound field as shown in Chapter IV.

Due to time constraints, the transmission through an interface into a soft sediment could not be investigated to the desired extent but the experiments conducted at the Acoustic Test Facility, Keyport, Washington, indicate that the self-demodulation effect is indeed a viable solution to this problem. This is evident in that in addition to

detection, a means of target classification is available. By monitoring the phase of the secondary return to determine whether a rigid or pressure release reflection is involved, and by measuring the length of the secondary return an excellent indicator of target size is obtained.

As stated earlier, the system cannot be regarded as optimized. This is due primarily to the fact that with the exception of the ITC projector, all components were either "home made" or off the shelf and not specifically designed for this system. Under these conditions, the system performed rather well.

The design of the corner reflector transducer needs to be revised in order to eliminate the mode conversion by dicing the ceramics. Such a modification would make this transducer very efficient when operated in the pulse excitation mode. The overall efficiency of the transmitting side of the system can also be increased by improving the matching between the pulse forming network and the transducer. The ideal transmitting system, which depends primarily on the transducer, should create a symmetric primary pulse of approximately 200 microseconds duration with rise and fall times on the order of 100 microseconds, maintain a constant carrier frequency and reach a source level in excess of 230 dB re 1 micropascal. This optimized primary pulse would create a secondary pulse with one strong main frequency component of approximately 7.5 kHz and would

therefore allow a simplification of the filtering process on the receiving side by using only one bandpass filter centered on the secondary main frequency component. If the overall dimensions of the transducer cannot be increased, a primary carrier frequency higher than 100 kHz should be considered in order to further collimate the primary beam and thereby decrease the spreading losses in the secondary beam. If by this means the effective exponent for the primary peak pressure amplitude could be raised from 1.6 to 1.9 a significant increase in the secondary peak pressure amplitude would be achieved, although a higher carrier frequency also increases the absorption coefficient which would in turn decrease the secondary peak pressure amplitude as seen from equation 4-4. There definitely exists an optimum carrier frequency for a given aperture which still must be determined. The answer to this problem can be found through further analytical and experimental studies on the propagation of the secondary pulse from a real source and further efforts in this field are highly recommended.

Hindsight indicates a further modification to the receiver circuitry. The pass bands of the receiver filters were chosen based on expected results. The computer simulations, however, indicated that the stronger secondary frequency components were in the neighborhood of 15 kHz. As a result, an unnecessary 18 dB of attenuation was probably applied to the signal of interest. Therefore,

future experiments with this particular system configuration should probably include modification of the filter pass band to something on the order of 5 kHz to 20 kHz.

One of the most interesting physical results of this thesis involves the observed "double hump" in the secondary beam cross sections. Further efforts should be directed not only at determining the cause of this effect, but also perhaps exploiting it for its possible signal processing advantages.

The effect is definitely not due to a measurement artifact, since it was observed with several different receiver hydrophones. Further, this "double hump" has been observed in at least two other experiments. A similar effect was observed in a non-linear Surface Acoustic Wave experiment presented at the IEEE Sonics and Ultrasonics Symposium in October 1982 [Ref. 30]. The effect also presented itself in a computer simulation of parametric conversion in the presence of dispersion conducted by Fenlon and Hamilton [Ref. 31]. Several plausible mechanisms for the "double hump" have been postulated. One mechanism suggested by D. Blackstock [Ref. 32] attributes it to a difference in the parametric array on and off axis response in that the axial response is a function of the second derivative of the square of the pulse envelope while the primary determinant for the off-axis response is the first derivative of the square of the envelope [Ref. 33]. Similarly, Morse

[Ref. 34] in discussing piston transients, showed that the axial response of the piston is a function of piston acceleration, while piston velocity becomes dominant away from the piston axis. At the Naval Postgraduate School, Dr. Steve Garrett proposes that the effect could be caused by a spread in the propagation vectors due to imperfect transducer beam collimation. Regardless of the mechanism, the apparent "double hump" is a significant physical phenomenon and definitely merits future attention.

LIST OF REFERENCES

1. Ingard, U., and Pridmore-Brown, D. C., J. Acoust. Soc. Am. (28), 367 (1956).

2. Westervelt, P. J., J. Acoust. Soc. Am. (29), 199 (1957), 934 (1957).

3. Westervelt, P. J., J. Acoust. Soc. Am. (35), 535 (1963).

4. Westervelt, P. J., J. Acoust. Soc. Am. (32), 934A (1960).

5. Bellin, J. L. S., Westervelt, P. J., and Beyer, R. T., J. Acoust. Soc. Am. (32), 935A (1960).

6. Berktay, H. O., Journal of Sound and Vibration (2), 435 (1965).

7. Muir, T. G., Horton, C. W., Sr., and Thompson, L. A., Journal of Sound and Vibration (1979) 65 (4).

8. Rudenko, O. V., and Soluyan, S. I., Soviet Physics-Acoustics, (18), 352 (1973).

9. Barnes, R. P., Jr., and Beyer, R. T., J. Acoust. Soc. Am. (36), 1371 (1966).

10. Moffet, M. B., Westervelt, P. J., and Beyer, R. T., J. Acoust. Soc. Am. (47), 1473 (1970).

11. Moffet, M. B., Westervelt, P. J., and Beyer, R. T., J. Acoust. Soc. Am. (49), 339 (1971).

12. Tiffin, D. L., Continuous Seismic Reflection Profiling in the Straits of Georgia, British Columbia, Canada, Dec. 1969, Dept. of Geophysics, Institute of Oceanography, University of B. C. (PHD Thesis).

13. Wilson, O. B., Jr., and Helton, R. A., Acoustic Properties of Sediments at Weapons Test Ranges of the Naval Undersea Warfare Engineering Station, Keyport, Washington, p. 39, TECH RPT NPS-61-79-005, June 1979.

14. Clay, C. S., and Medwin, H., Acoustical Oceanography, p. 259, Wiley, 1977.

15. Channel Industries Incorporated, Catalog number 761-01.

16. Skowronek, L. J., LCDR, USN, Masters Thesis (title unknown), Naval Postgraduate School, Monterey, Dec. 1982.

17. Bobber, R. J., Underwater Electroacoustic Measurements, p. 145, NRL, U. S. Government Printing Office, July 1970.

18. International Transducer Corp., TECH DATA for ITC-5238, S/N 01.

19. Klein Associates Inc., Basic Towfish Schematic 402(E).

20. Naval Underwater Systems Center, New London, Verbal Communication with William Konrad.

21. Celesco Transducer Products Inc., Data Sheet for LC-10 Hydrophones.

22. Kinsler, L. E., and others, Fundamentals of Acoustics, 3rd ed., Wiley, 1982.

23. Tucker, D. G., and Gazey, B. K., Applied Underwater Acoustics, p. 143, Pergamon, 1966.

24. Naval Underwater Systems Center, New London, Handbook for the Analysis of Piezoelectric Transducers, p. 1-3, NUSC TECH DOC 6029.

25. Hunt, F. V., Electroacoustics, p. 125, American Institute of Physics, 1982 reprint of 1954 edition.

26. Strum, R. D., and Ward, J. R., Electric Circuits and Networks, p. 387, Quantum, 1973.

27. Krohn-Hite Model 3500, Specification Sheet, Dec. 1980.

28. Ithaco Model 1201, Instruction and Maintenance Manual, Nov. 1980.

29. Beyer, R. T., Nonlinear Acoustics, p. 101, NAVSEASYSCOM, U. S. Government Printing Office, 1974.

30. Socinno and Depalma, IEEE Sonics and Ultrasonics Symposium, San Diego, CA, Oct. 25-29, 1982.

31. Hamilton, M. F., and Fenlon, F. H., J. Acoust. Soc. Am. (72), p. S-41 (1982).

32. Private Communication with D. Blackstock, Nov. 12, 1982.

33. Fenlon, F. H., and MacKendree, R. S., J. Acoust. Soc. Am. (66), p. 534 (1979).

34. Morse, P. M., Vibration and Sound, p. 344, Acoustical Society of America reprint, 1976.

INITIAL DISTRIBUTION LIST

		No. Copies
1.	Defense Technical Information Center Cameron Station Alexandria, Virginia 22314	2
2.	Library, Code 0142 Naval Postgraduate School Monterey, California 93940	2
3.	George L. Sackman (Code 62Sa) Department of Electrical Engineering Naval Postgraduate School Monterey, California 93940	8
4.	Alan B. Coppens (Code 61Cz) Department of Physics Naval Postgraduate School Monterey, California 93940	3
5.	Department Chairman (Code 61) Department of Physics Naval Postgraduate School Monterey, California 93940	1
6.	Steven L. Garrett (Code 61Gx) Department of Physics Naval Postgraduate School Monterey, California 93940	2
7.	Gary D. Ewing (Code 62Ew) Department of Electrical Engineering Naval Postgraduate School Monterey, California 93940	1
8.	LCDR C. L. Burmaster (Code 61Zr) Department of Physics Naval Postgraduate School Monterey, California 93940	1
9.	Dominique Odero (Code 610d) Department of Physics Naval Postgraduate School Monterey, California 93940	1

		No. Copies
10.	LT P. J. LeStrange 302 Gideon Street, A9 Dowagiac, Michigan 49047	1
11.	LT R. L. Eyman 3736 Budd Street San Diego, California 92111	2
12.	Kapitänleutnant A. H. Seemann 2 Dankwerthstrasse 2300 Kiel West-Germany	1
13.	Technical Operations Officer (Code 80) Naval Undersea Warfare Engineering Station Keyport, Washington 98345	1
14.	Research and Engineering Department ATTN: Bob Merriman William Anderson Naval Undersea Warfare Engineering Station Keyport, Washington 98345	1 1
15.	Officer in Charge ATTN: Dr. W. Konrad Dr. M. Moffett New London Laboratory Naval Underwater Systems Center New London, Connecticut 06320	1 1
16.	Dr. T. Muir Dr. D. Blackstock Applied Research Laboratory P. O. Box 8029 Austin, Texas 78712	1 1
17.	Commander (Code 5313) ATTN: M. F. Morrison Naval Ocean Systems Center San Diego, California 92152	1
18.	Commanding Officer ATTN: D. Folds Naval Coastal Systems Center Panama City, Florida 32407	1

		No. Copies
19.	International Transducer Corporation ATTN: W. Bunker 640 McCloskey Place Goleta, California 93017	1
20.	Acoustic Systems Incorporated ATTN: Dr. J. Fish 600 Norman firestone Road Goleta, California 93017	1
21.	Klein Associates Incorporated ATTN: W. Key Klein Drive Salem, New Hampshire 03079	1
22.	O. B. Wilson (Code 61W1) Department of Physics Naval Postgraduate School Monterey, California 93940	1
23.	Commander, Naval Sea Systems Command ATTN: Code 63R3 Naval Sea Systems Command Headquarters Washington, D. C. 20362	1